UNIVERSITY OF OKLAHOMA

GRADUATE COLLEGE

THE INFLUENCE OF ORGANIC METABOLITES BINDING WITH FERRIC IRON ON CORROSION MECHANISMS IN OIL AND GAS PRODUCTION WATER

A THESIS

SUBMITTED TO THE GRADUATE FACULTY

in partial fulfillment of the requirements for the

Degree of

MASTER OF ENVIRONMENTAL SCIENCE

By

YAN LI
Norman, Oklahoma
2018

THE INFLUENCE OF ORGANIC METABOLITES BINDING WITH FERRIC IRON ON CORROSION MECHANISMS IN OIL AND GAS PRODUCTION WATER

A THESIS APPROVED FOR THE
SCHOOL OF CIVIL ENGINEERING AND ENVIRONMENTAL SCIENCE

BY

_____
Dr. Mark A. Nanny, Chair

_____
Dr. Elizabeth C. Butler

_____
Dr. Tohren C. G. Kibbey

© Copyright by YAN LI 2018
All Rights Reserved.

Acknowledgements

I would like to thank my parents, Huijing Li and Suping Chai, who supported and gave me unconditional love during my life. I also want to thank my daughter, Rena Du, who gives me all her love and stays with me without any complaints.

I would like to give my thanks to my thesis advisor, Dr. Mark Nanny, for accepting me as his graduate student and supporting me through my project as well as teaching me to be a better student and scientist.

I would also like to thank Dr. Elizabeth Butler and Dr. Tohren Kibbey for their assistance and patience as well as for serving on my committee. I also wish to express special thanks to Dr. Joseph Suflita, Dr. Kathleen Duncan and Dr. Renxing Liang for helping me in building my microbiology knowledge and assisting me with microbiology efforts.

Finally, I would like to express a very special thanks to all of the staff in the CEES office: Ms. Audre Carter, Ms. Cindy Vitt Murphy, Ms. Marlene Smith and Ms. Susan Williams. Whenever I needed help, they were always there and gave me their full support.

Table of Contents

Acknowledgements iv

Table of Contents v

List of Tables ix

List of Figures xv

Abstract xviii

Chapter 1: Introduction 1

1.1 Abiotic corrosion and microbial induced corrosion of carbon steel 1

1.2 Hypotheses and Objectives 6

1.2.1 Research questions 8

1.2.2 Hypotheses 8

1.2.3 Objectives 8

Chapter 2: Literature review 11

2.1 CO_2 corrosion 11

2.2 Corrosion driven by sulfate-reducing bacteria 13

2.3 Solubility and reduction kinetics of iron(III) oxyhydroxides 18

2.3.1 Solubility of iron oxyhydroxides 19

2.3.2 Dissolution of insoluble Fe(III) in the presence of organic ligands by forming Fe(III)-ligand complexes 20

2.4 Influence of organic ligands on the iron oxides reduction by iron-reducing bacteria 24

2.5 Influence of iron-reducing bacteria on the corrosion of steel..... 29
Chapter 3: Methodology..... 31
3.1 Site description and samples collection..... 31
3.2 Chemical analysis of nine production water samples..... 32
3.2.1 General chemical properties of nine production water samples 32
3.2.2 Total dissolved iron and manganese ion concentration measurement 35
3.2.3 Equilibrium Fe(III) concentration calculation by MINEQL+..... 37
3.3 Targeted metabolomics analysis by gas chromatography coupled with a mass selective detector for Putumayo Basin production water samples and Barnett Shale production water samples 38
3.4 Qualitative carbon steel corrosion assay under aerobic conditions with filtered Putumayo Basin production water samples 45
3.5 Scanning electron microscopy-energy dispersive X-Ray spectroscopy analysis of free-floating biofilms with embedded particulates of Barnett Shale production water samples 47
Chapter 4: Results..... 49
4.1 Chemical characteristics of production water samples..... 49
4.1.1 Water chemistry of Putumayo Basin production water 49
4.1.2 Water chemistry of Barnett Shale production water 54

4.2 Targeted metabolomics analysis by gas chromatography coupled with a mass selective detector 59
4.2.1 Targeted metabolomics results of Putumayo Basin production water samples 59
4.2.2 Targeted metabolomics results of production water samples from the Barnett Shale 68
4.3 Qualitative carbon steel corrosion assay under aerobic conditions with filtered Putumayo Basin production water samples 83
4.4 Scanning electron microscopy-energy dispersive X-Ray spectroscopy analysis of the free-floating biofilm with embedded particulates of Barnett Shale production water samples 86
Chapter 5: Discussion 92
5.1 Solubility of iron ions in the production water samples from the Putumayo Basin and Barnett Shale 92
5.2 Formation of Fe(III)-ligands complex increased the solubility of Fe(III) 97
5.3 The influence of the total dissolved iron concentration on the function of microorganisms 101
Chapter 6: Conclusions and Future work 112
6.1 Research questions 114
6.2 Hypotheses 114
6.3 Objectives 115

References 116

List of Tables

Table 1- 1 Cause of corrosion-related failure in petroleum-related industries 3

Table 2- 1 Four SRB strains accelerating corrosion rate of carbon steel when using lactate as an electron donor 14

Table 2- 2 Stability constant of Fe(III)-organic acids complexes 22

Table 2- 3 Reduction potentials and free energies of some species of..... 27

Table 3- 1 Furnace operating conditions for Fe and Mn measurement 37

Table 4- 1 Water chemistry of Putumayo Basin production water samples..... 50

Table 4- 2 Comparison of the measured dissolved iron concentration in the Putumayo Basin production water samples by GF-AAS and the calculated equilibrium iron concentration by MINEQL+ 51

Table 4- 3 Comparison of the measured dissolved Mn concentration in the Putumayo Basin production water samples by GF-AAS and the calculated equilibrium Mn concentration by MINEQL+ 53

Table 4- 4 Water chemistry of Barnett Shale gas tank production water samples 56

Table 4- 5 Comparison of the measured dissolved iron concentration in the Barnett Shale production water samples by GF-AAS and the calculated equilibrium iron concentration by MINEQL+ 57

Table 4- 6 Comparison of the measured dissolved Mn concentration in the Barnett Shale production water samples by GF-AAS and the calculated equilibrium Mn concentration by MINEQL+ 58

Table 4- 7 Peak area of compounds detected in GC/MS spectrum of Loro production water samples from the Putumayo Basin by using MTBSTFA as derivatization reagent 61

Table 4- 8 Peak area of compounds detected in GC/MS spectrum of Caribe production water samples from the Putumayo Basin by using MTBSTFA as derivatization reagent 61

Table 4- 9 Peak area of compounds detected in GC/MS spectrum of Acae production water samples from the Putumayo Basin by using MTBSTFA as derivatization reagent 62

Table 4- 10 Peak area of compounds detected in GC/MS spectrum of Sucombio production water samples from the Putumayo Basin by using MTBSTFA as derivatization reagent 63

Table 4- 11 List of compounds detected in the GC-MS spectrum of Sucombio production water sample from the Putumayo Basin by using BSTFA as derivatization reagent 65

Table 4- 12 Comparison of detectability of dicarboxylic acids, α-hydroxycarboxylic acids and PEG-carboxylic acids in the GC/MS spectra between reagent MTBSTFA and BSTFA 66

Table 4- 13 List of peak area of dicarboxylic acids, α-hydroxycarboxylic acids, and polyethylene glycol (PEG) carboxylic acids in the “Free ligands” sample and “Total ligands” sample detected in the GC-MS spectra of Sucombio production water sample from the Putumayo Basin by using BSTFA as derivatization reagent..... 68

Table 4- 14 List of all of compounds detected in the GC-MS spectra of all five Barnett Shale production water samples by using BSTFA as derivatization reagent..... 71

Table 4- 15 Peak area of compounds detected in GC-MS spectrum of SE 19 production water sample from the Barnett Shale by using BSTFA as derivatization reagent 72

Table 4- 16 Peak area of compounds detected in GC-MS spectrum of SE 18 production water sample from the Barnett Shale by using BSTFA as derivatization reagent 73

Table 4- 17 Peak area of compounds detected in GC/MS spectrum of SE 17 production water sample from the Barnett Shale by using BSTFA as derivatization reagent 74

Table 4- 18 Peak area of compounds detected in GC-MS spectrum of KJV 7 production water sample from the Barnett Shale by using BSTFA as derivatization reagent 75

Table 4- 19 Peak area of compounds detected in GC-MS spectrum of MC 5 production water sample from the Barnett Shale by using BSTFA as derivatization reagent 76
Table 4- 20 Comparison of peak area of dicarboxylic acids and α-hydroxycarboxylic acids in the GC/MS spectrum of “Free ligands” and “Total ligands” samples for SE 19 production water sample from the Barnett Shale ... 79
Table 4- 21 Comparison of peak area of dicarboxylic acids and α-hydroxycarboxylic acids in the GC/MS spectrum of “Free ligands” and “Total ligands” samples for SE 18 production water sample from the Barnett Shale ... 79
Table 4- 22 Comparison of peak area of dicarboxylic acids and α-hydroxycarboxylic acids in the GC/MS spectrum of “Free ligands” and “Total ligands” samples for SE 17 production water sample from the Barnett Shale ... 80
Table 4- 23 Comparison of peak area of dicarboxylic acids and α-hydroxycarboxylic acids in the GC/MS spectrum of “Free ligands” and “Total ligands” samples for KJV 7 production water sample from the Barnett Shale ... 80
Table 4- 24 Comparison of peak area of dicarboxylic acids and α-hydroxycarboxylic acids in the GC/MS spectrum of “Free ligands” and “Total ligands” samples for MC 5 production water sample from the Barnett Shale ... 81
Table 4- 25 Comparison of total area of dicarboxylic acids and α-hydroxycarboxylic acids and the dissolved iron concentration measured by AAS in the Barnett Shale production water samples 82

Table 4- 26 Comparison of SEM graph of corrosion feature for Putumayo Basin production water samples 84
Table 4- 27 S/Fe (atom/atom) ratio in the free-floating biofilm with embedded particulates of SE 19 production water sample from the Barnett Shale 89
Table 4- 28 S/Fe (atom/atom) ratio in the free-floating biofilm with embedded particulates of SE 18 production water sample from the Barnett Shale 89
Table 4- 29 S/Fe (atom/atom) ratio in the free-floating biofilm with embedded particulates of SE 17 production water sample from the Barnett Shale 90
Table 4- 30 S/Fe (atom/atom) ratio in the free-floating biofilm with embedded particulates of MC 5 production water sample from the Barnett Shale..... 90
Table 4- 31 S/Fe (atom/atom) ratio in the free-floating biofilm with embedded particulates of KJV 7 production water sample from the Barnett Shale..... 91
Table 5- 1 Description of average chemical properties data of the regional wells (n = 21) from the Putumayo Basin provided by EcoPetrol (EcoPetrol, 2014) 93
Table 5- 2 Influence of pH and alkalinity on the calculated equilibrium iron concentration by MINEQL+ 95
Table 5- 3 Influence of pH and alkalinity on the calculated equilibrium iron concentration by MINEQL+ 96
Table 5- 4 Comparison of total area of iron-chelating molecules and the dissolved iron concentration in the Sucombio production water sample from the Putumayo Basin and the Barnett Shale production water samples 100

Table 5- 5 Dissolved iron concentration, the atomic S/Fe ratio of the free-floating biofilm embedded with particulates, the relative abundance of microorganisms, and the sulfate reduction rate in the Sucombio production water sample from the Putumayo Basin and five production water samples from the Barnett Shale 105

List of Figures

Figure 1- 1 A typical corrosion cell under aerobic conditions 2

Figure 2- 1 An electrochemical cell for CO_2 corrosion on a steel surface 13

Figure 2- 2 Different types of iron corrosion by SRB (CMIC & EMIC) at circumneutral pH (Enning & Garrelfs, 2014) 18

Figure 2- 3 Structure of Fe(III)-oxalate$_3^{3-}$ complex 22

Figure 2- 4 Dissolved iron concentration vs. time in the presence of oxalate, malonate, succinate, glutarate, and adipate in 0.2 g/L hematite (Duckworth & Martin 2013) 24

Figure 2- 5 Model of Fe(III) reduction in Geobacter sulfurreducens. (a) The potential pathway for electrons through the membranes and periplasm. The pathway is still uncertain because many cytochromes are expressed in Geobacter under Fe(III) reducing conditions (Bird *et al*., 2011)..... 28

Figure 3- 1 Schematic illustrating the two samples of "Free-ligands" and "Total ligands" 39

Figure 4- 1 GC/MS spectra of Putumayo Basin production water samples by using MTBSTFA as derivatization reagent (from the top to the bottem: Loro, Caribe, Acae, and Sucombio). The all samples had same dilution and the spectra had same intensity..... 60

Figure 4- 2 GC/MS spectrum of Sucombio production water sample from the Putumayo Basin by using BSTFA as derivatization reagent..... 64

Figure 4- 3 GC/MS trace comparison of Free ligands (bottom spectrum) and Total ligands (top spectrum) samples for Sucombio production water sample from the Putumayo Basin by using BSTFA as derivatization reagent 67

Figure 4- 4 GC/MS spectra of Barnett Shale production water samples by using BSTFA as derivatization reagent (from the top to the bottem: SE 19, SE 18, SE 17, KJV 7 and MC 5). The all samples had same dilution and the spectra had same intensity. 70

Figure 4- 5 GC/MS trace comparison of the “Total ligands” sample (top spectrum) and “Free ligands” samples (bottom spectrum) for SE 19, SE 18, SE 19, KJV 7 and MC 5 (from the bottom to the top) production water sample from the Barnett Shale 78

Figure 4- 6 Linear relationship between the peak area of iron-chelating molecules and the dissolved iron concentration in the Barnett Shale production water samples..... 82

Figure 4- 7 SEM graphs of corrosion products on C1080 carbon steel after immersion in different Putumayo Basin water sample: (A) Control (0.7% chloride water), (B) Caribe production water, (C) Acae production water, (D) Sucombio production water under 2,000 X magnification; (A 1) Control (0.7% Nloride water), (B 1) Caribe production water, (C 1) Acae production water, (D 1) Sucombio production water under 10,000 X magnification; 85

Figure 4- 8 Free-floating biofilm with embedded particulates in the production water samples from Barnett Shale (sample SE 19) 87

Figure 4- 9 S/Fe (atom/atom) ratio of the free-floating biofilm with embedded particulates of the Barnett Shale production water samples by SEM –EDX analysis..... 88

Figure 5- 1 Linear relationship between the peak area of iron-chelating molecules and the dissolved iron concentration in the Sucombio production water sample from the Putumayo Basin and the Barnett Shale production water samples 100

Figure 5- 2 Relative abundance (%) of different genera of bacteria in the Barnett Shale production water samples* 108

Figure 5- 3 Different combinations/proportions of Deltaproteobacteria in Barnett Shale production water samples* 108

Figure 5- 4 Relative abundance* (%) of different genera of bacteria in Putumayo Basin production water samples* 111

Abstract

Corrosion of carbon steel is a potential hazard to oil and gas production infrastructure. The total annual cost of corrosion in the oil and gas production industry is estimated to be $1.372 billion in the USA (Simons, 2008). Over 20% of the total corrosion cost is caused by microbial induced corrosion (MIC) or biocorrosion (Javaherdashti, 2008). MIC of the carbon steel infrastructure in oil and gas production facilities is most often associated with the activity of sulfate-reducing bacteria (SRB). However, a different biocorrosion mechanism was presumably observed in the pipelines in the Putumayo Basin, southwest Colombia, South America and production water storage tanks in the Barnett Shale, north Texas, USA. Both sites typically experienced very specific types of corrosion and/or MIC. CO_2 corrosion was considered as the corrosion mechanism in Putumayo Basin sampling sites, while SRB induced corrosion was presumed to be the main corrosion mechanism in Barnett Shale storage tanks. However, in the Putumayo Basin production water samples, the pH of all samples was circumneutral which didn't support typical CO_2 corrosion mechanism. The total dissolved iron ions species (ferrous and ferric species) concentration was 6 to 8 orders of magnitude higher than the equilibrium iron concentration with respect to solid-phase $Fe(OH)_3$. The *Shewanella* genus, which is known to contain iron-reducing bacteria (IRB), comprised 30% of the microbes detected in Sucombio production water sample from the Putumayo

Basin. In Barnett Shale production water samples, only one sample indicated it was impacted by the typical SRB corrosion mechanisms. The four samples lacked sulfate reducing activity and had no FeS precipitate or had sulfate reducing activity but FeS was only 14% to 21% of the corrosion solid phase products. These four samples had dissolved iron ions concentrations 2 to 5 times higher than the equilibrium iron concentration of solid-phase $FeCO_3$ and contained bacteria orders with species that can act as both SRB and IRB. As such, the Putumayo and Barnett Shale results indicated that there were other microbial induced corrosion mechanisms in the sampling sites besides that facilitated by SRB. The research questions of this study are: 1) what caused the high total dissolved iron concentration in the production water samples from Putumayo Basin and Barnett Shale, and 2) can the high total dissolved iron concentration shift the function of microorganisms from sulfate respiration to ferric respiration. It is hypothesized that organic ligands chelated with Fe(III) in the ferric oxyhydroxide layer to form soluble ferric-ligands complexes, resulting in the high total dissolved iron concentration. The increased availability of dissolved ferric ions shifted the function of microorganisms from sulfate respiration to ferric respiration, thereby allowing microbes with iron reducing abilities to take advantage of the thermodynamic and kinetic gains in energy to thrive. Gas chromatography/mass spectrometry analysis showed a positive relationship between the concentration of organic metabolites and the total

dissolved iron concentration in Putumayo production water samples, and a positive linear relationship was found between iron-chelating molecules and the total dissolved iron ions concentration in Barnett Shale production water samples. These results support the hypothesis that organic ligands chelated with Fe(III) and caused the high dissolved iron concentration. Evidence supporting the hypothesis that the high concentration of the total dissolved ferric ions shifted the microbial community to favor microbes capable of respiration ferric ions was supported by the atomic ratio of S/Fe in particulates collected from biofilms, as well as sulfate reduction assays and microbial community analysis results.

Chapter 1: Introduction

1.1 Abiotic corrosion and microbial induced corrosion of carbon steel

According to the ISO 8044 standard, corrosion is a "physicochemical interaction between a metal and its environment that results in changes in the properties of the metal, and which leads to significant impairment of the function of the metal, the environment, or the technical system" (ISO-8044, 2015). Electrochemical corrosion is a redox reaction involving the transfer of electrons produced by oxidation of metal to an electron acceptor. Under aerobic conditions, electrons are transferred to molecular oxygen to produce hydroxide ions; while under anaerobic conditions, protons are reduced to produce molecular hydrogen (Beech & Sunner, 2004). Electrochemical corrosion requires 1) an anodic reaction, 2) a cathodic reaction and 3) an electrolyte (Figure 1- 1). The anodic reaction involves oxidation of zero-valent metal to produce electrons and metal cations. The cathodic reaction involves reduction of molecular oxygen or protons. Usually, the electrolyte is an aqueous phase where ions can transfer from the anode to the cathode (Popoola *et al.*, 2013).

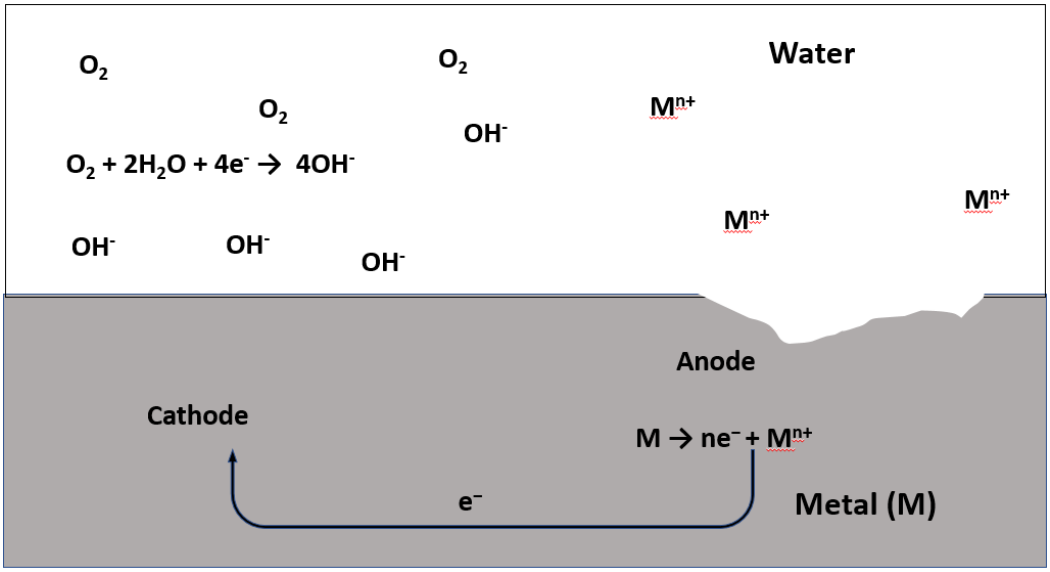

Figure 1- 1 A typical corrosion cell under aerobic conditions

Carbon steel is used extensively for pipelines and production infrastructure in the oil and gas industry because of its low cost. However, because of carbon steel's low corrosion resistance, corrosion is a major problem (Tawancy *et al.*, 2013). About 25% of all failures in the oil and gas industry are caused by corrosion (Kermani & Harrop, 1996). Table 1-1 (Kermani & Harrop, 1996) summarize the percentage distribution of corrosion-related failure during 1980's and CO_2 related failure accounts for 28% of corrosion failure.

Table 1- 1 Cause of corrosion-related failure in petroleum-related industries (Kermani & Harrop, 1996)

Type of failure	Total failure (%)
CO_2 related	28
H_2S related	18
Preferential weld	18
Pitting	12
Erosion corrosion	9
Galvanic	6
Crevice	3
Impingement	3
Stress corrosion	3

CO_2 in an aqueous environment is a corrosive species that has caused several failures related to the oil and gas pipelines as well as equipment. The dissolution of CO_2 in water forms corrosive carbonic acid, H_2CO_3, and the dissociation of H_2CO_3 increases concentration of proton (H^+), carbonate (CO_3^{2-}) and bicarbonate (HCO_3^-) ions. In CO_2 related corrosion, zero-valent iron loses two electrons to form Fe^{2+} at the anode, and at the cathode, the two electrons are transferred to adsorbed protons for reduction to H_2. Fe^{2+} then reacts with CO_3^{2-} to form siderite ($FeCO_{3(S)}$) on the corroded steel surface (Gao *et al.*, 2011). The formation of $FeCO_{3(S)}$ consumes Fe^{2+} and carbonate which not only thermodynamically

drives the oxidation reaction forward, but also leads to a low dissolved iron concentration in a typical CO_2 corrosion system. There are two major forms of CO_2 corrosion: pitting and mesa attack (Schmitt & Horstemeier, 2006). The pitting corrosion is a localized corrosion on the steel surface forming deep and narrow pits (Schmitt & Horstemeier, 2006), and the mesa attack corrosion typical forms deep and flat-bottomed corrosion morphology (Bruschi *et al.*, 2017).

The second most prominent type of corrosion failures in the oil and gas industry are H_2S related failures that account for 18% of the total corrosion failures (Table 1-1). Dissolution of H_2S in water forms hydrogen sulfide (H_2S), and the dissociation of H_2S increases concentration of proton (H^+), sulfide (S^{2-}) and bisulfide (HS^-) ions. Zero-valent iron loses two electrons at the anode to form Fe^{2+} at the anode, and at the cathode, the two electrons are transferred to adsorbed protons for reduction to H_2. Fe^{2+} then reacts with S^{2-} to form FeS precipitations on the corroded steel surface (Zheng *et al.*, 2013). The formation of $FeS_{(S)}$ precipitation consumes Fe^{2+} and S^{2-} which kinetically drives the oxidation reaction forward, and leads to a low dissolved iron concentration in a typical H_2S corrosion system.

"Corrosion resulting from the presence and activities of microbes on metals and metal alloys is generally referred to as microbiologically induced corrosion (MIC)" (Little *et al.*, 2007). Among the main types of bacteria related to metal corrosion, sulfate-reducing bacteria (SRB) are considered to be associated with

the majority of steel corrosion under anaerobic conditions (Miranda *et al.*, 2006; Beech & Sunner, 2004). For example, AlAbbas *et al.* (2013) studied the corrosion of carbon steel under anaerobic conditions for biotic and abiotic systems with an SRB consortium obtained from an oil well located in Louisiana, USA. The consortium contained *Desulfomicrobium sp*. which are sulfate-reducing bacteria. The results showed the corrosion rate of carbon steel increased from 10 mils per year (mpy) under abiotic conditions to 60 mpy under biotic conditions (AlAbbas, et al., 2013). In another example of MIC, Paula *et al.* (2016) reported that the medium with the addition of SRB mixed cultures increased the corrosion rate of carbon steel to 47.2 mpy after 35 days incubation, which is 10 times higher than the abiotic control. Likewise, Magot *et al*. (1997) demonstrated that *Dethiosulfovibrio peptidovorans* gen. nov., sp. nov. can reduce sulfate to sulfide and increased the corrosion rate of carbon steel from 20 mpy to 157 mpy. Other researchers also have demonstrated with similar experiments that SRB can promote corrosion of steel (Padilla-Viveros *et al.,* 2006; Gayosso *et al.,* 2004)

In the oil and gas industries, pipeline interiors typically contain suitable conditions for SRB to survive because of the anaerobic and/or low oxygen concentration conditions (Javaherdashti, 2008). *Desulfomicrobium* sp and *Dethiosulfovibrio peptidovorans* gen. nov., sp. nov. were found in two oil wells (AlAbbas *et al.*, 2013; Magot *et al.*, 1997); *Desulfovibrio vietnamensis* was isolated from a gas pipeline (Gayosso *et al.*, 2004); and *Desulfovibrio alaskensis*

was obtained from a water-oil separator (Padilla-Viveros *et al.*, 2006). In the referenced studies, the above four strains caused increasing of corrosion rate of carbon steel using sulfate as the terminal electron donor and lactate as the electron acceptor.

1.2 Hypotheses and Objectives

Production water tanks, oil wells, and pipelines are critical components in the oil and gas industry and are susceptible to corrosion because they are usually made of carbon steel which has low corrosion resistance (Tawancy *et al.*, 2013). Maintaining or replacing corroded carbon steel infrastructures places a significant financial strain on the industry. Hence, it is important to determine the cause(s) and the underlying mechanism(s) of MIC in order to develop and implement prevention, monitoring and remediation strategies. This study examined two sites experiencing corrosion of carbon steel, presumably CO_2 related corrosion in the Putumayo Basin, Colombia, and SRB driven corrosion in the Barnett Shale, north Texas. In both situations, the physicochemical conditions of several of the sampling sites didn't exactly fit those anticipated for traditional CO_2-related corrosion or SRB driven corrosion. Thus, it was hypothesized that other MIC mechanisms may be occurring. Therefore, an extensive characterization of the physicochemical and microbiological parameters of the production water was undertaken. This thesis presents the findings of the physicochemical parameters and uses them to address questions

about the corrosion mechanisms. These results are evaluated against microbiological data obtained by other researchers also working on this project.

In these studies, production water samples were collected from four oil wells in the Putumayo Basin, southwest Colombia, South America presumed to be experiencing CO_2 corrosion to varying extents. As well, production water samples were collected from five storage tanks located in the Barnett Shale, north Texas, USA. Three storage tanks were presumed experiencing SRB corrosion based upon bottle dilution tests for SRBs and acid producing bacteria (APBs), and two storage tanks were considered to not be experiencing corrosion. Based upon the equilibrium thermodynamics, the dissolved iron concentration in the Putumayo Basin production water samples should range from 4.8×10^{-9} to 4.3×10^{-8} ppm due to the formation of goethite under oxygen periodic input conditions when the pH ranged from 6.84 to 8.55; in the Barnett Shale production water samples, the dissolved iron concentration ranged from 9.7 to 74.8 ppm with respect to $FeCO_{3(S)}$ under anoxic conditions when the pH ranged from 6.09 to 6.92. However, in the systems experiencing corrosion, the dissolved iron concentration exceeded the thermodynamic equilibrium concentration by several times to several orders of magnitude. This thesis research specifically examined the reason for the exceptionally high dissolved iron concentration and their presumed impact on the microbiology.

1.2.1 Research questions

The research questions of this study were:

1) What facilitated the dissolved iron concentration in the production water samples to be several times to several orders of magnitude higher than equilibrium thermodynamic predicted concentration?

2) Did the high dissolved iron concentration, which was higher than the calculated equilibrium concentration, favor and promote IRB respiration?

1.2.2 Hypotheses

Based on the two research questions, the following two hypotheses were proposed:

1) The very high concentration of dissolved iron is due to the presence of organic ligands that complex ferric ions to produce soluble Fe(III)- organic ligands complexes.

2) Increasing the dissolved Fe(III) concentration made soluble Fe(III) a more kinetically favorable electron acceptor than solid phase ferric oxyhydroxides thereby favoring microorganisms capable of using ferric iron as a terminal electron acceptor.

1.2.3 Objectives

Based on the research questions and hypotheses, the first objective was to characterize the high dissolved iron concentration in production water samples.

- The dissolved iron concentration was measured by graphite furnace atomic absorption spectroscopy (AAS);
- To evaluate if the dissolved iron concentration in the production water samples were oversaturated, MINEQL+ was used to calculate the predicted thermodynamic equilibrium iron concentration based upon water chemistry of each production water sample and solubility of solid phase ferric oxyhydroxides and ferrous carbonate; MINEQL+ is computer software capable of solving chemical equilibrium problems including determination of chemical speciation, solid phase saturation states, precipitation-dissolution, and adsorption (Westall, 1976).
- To determine what caused the high dissolved iron concentration in the production water samples, targeted metabolomics using gas chromatography/ mass spectroscopy (GC/MS) was used to characterize organic ligands in the production water samples Targeted metabolomics is a quantitative approach to identify and quantify specific groups of metabolites (DeHaven *et al.*, 2010);

The second objective was to correlate the dissolved iron concentration, water chemistry, and particulates composition, with microbial community data to determine how the dissolved iron concentration impacts or favors iron-reducing bacteria over sulfate-reducing bacteria.

- The S/Fe ratio of particulates enmeshed in the free-floating biofilm was measured by scanning electron microscopy-energy dispersive X-Ray spectroscopy (SEM-EDS) to infer if sulfate reduction was the predominant reaction;
- Sulfate reduction assay was used to measure microbial sulfate reduction activity in production water samples in the aqueous phase;
- Unpublished microbial diversity was evaluated by 16S rRNA gene sequencing, and numbers of total bacteria, archaea were estimated by qPCR for Barnett Shale production water samples (Duncan et al., 2017). Data collected by Dr. Joseph Suflita's group and Dr. Kathleen Duncan's group from the Department of Microbiology and Plant Biology at the University of Oklahoma. was used to determine the main microbes in the planktonic phase.
- The function of microorganisms in the production water samples was inferred by comparing the total dissolved iron concentration with the S/Fe ratio, sulfate reduction assay, and microbial diversity results.

Chapter 2: Literature review

This literature review will describe the mechanisms of CO_2 corrosion and SRB induced corrosion in greater detail which are the two most important corrosion mechanisms in the oil and gas industry. These mechanisms are discussed in detail in order to compare with experimental results, such as pH, the total dissolved iron concentration, ferrous iron concentration, the dissolved oxygen concentration, sulfide concentration and atomic S/Fe ratio of the precipitation, to determine if the sampling sites were experiencing the presumed corrosion mechanism. Additionally, a literature review will be presented on the solubility of ferric oxides, the mechanisms of Fe(III) reduction by iron-reducing bacteria (IRB), and the influence of iron-reducing bacteria on corrosion of steel since they are important to controlling iron-cycling in the system being examined. Thermodynamically and kinetically, the formation of Fe(III)-organic ligand complexes favors a microorganism shift from sulfate reduction to iron reduction. Combined, the literature reviews help to identify chemical changes that occur during the shift microorganisms from sulfate respiration to iron respiration due to the high dissolved iron concentration in the production water samples.

2.1 CO_2 corrosion

In the oil and gas industry, CO_2 is often naturally present or is injected into reservoirs to facilitate petroleum recovery (Mathiassen, 2003). The first reported CO_2 corrosion in the oil and gas industry was in 1947 by Uhlig who illustrated

that at the same concentration (2.5 ml/L of gas (CO_2 or O_2) volume/liquid (production water) volume). CO_2 can cause 20% as much corrosion to carbon steel as O_2 at 100 ℃ (Uhlig, 1947). When CO_2 dissolves into the aqueous phase, it reacts with water to form carbonic acid (H_2CO_3). The dissociation of carbonic acid produces HCO_3^{2-}, or CO_3^- and H^+ (equation 1 and 2).

Dissociation of carbonic acid:

$H_2CO_3 \leftrightarrow H^+ + HCO_3^-$ equation 1

$HCO_3^- \leftrightarrow H^+ + CO_3^{2-}$ equation 2

A mechanism explaining how carbonic acid is corrosive to carbon steel was proposed by Schwenk, who hypothesized that the dissociation of H_2CO_3 provided H^+ that adsorbed to the steel surface. The adsorbed H^+ accepted electrons at the cathode (equation 3) (Schwenk, 1974) that were produced by the oxidation of iron at the anode.

Schwenk mechanism (Figure 2-1):

$2H^+_{ads} + 2e^- \rightarrow H_2$ equation 3

In the CO_2 related corrosion system, when the pH is less than 4, the reduction of H^+ is considered as the predominant reaction due to the high H^+ concentration. At the pH 4 to 6, the predominant carbonate species is H_2CO_3 since the dissociation constants pK_{a1} and pK_{a2} of carbonic acid are 6.3 and 10.3. Thus, besides the reduction of H^+, the reduction of H_2CO_3 can occur. (equation 4 and 5) (De Waard & Milliams, 1975);

De Waard & Milliams mechanism (Figure 2-1):

$H_2CO_{3\ ads} + e^- \rightarrow H_{ads} + HCO_3^-$ (Rate determining step) equation 4

$2H_{ads} \rightarrow H_2$ equation 5

Fe^{2+} produced from the anodic reaction can react with CO_3^{2-} or HCO_3^- to form siderite ($FeCO_{3(S)}$) on the corroded steel surface (equation 6) (Gao *et al.*, 2011).

$Fe^{2+} + CO_3^{2-} \rightarrow FeCO_{3(S)}$ equation 6

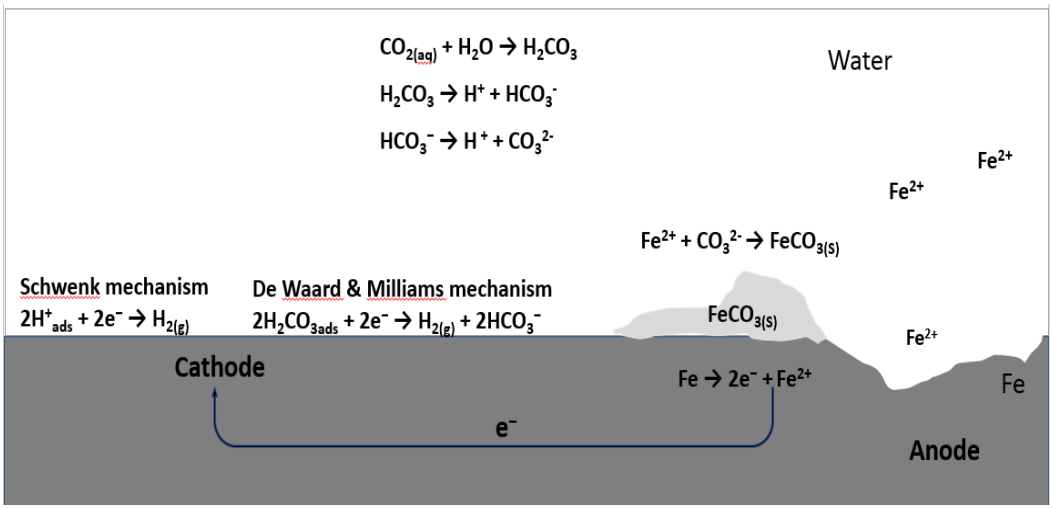

Figure 2- 1 An electrochemical cell for CO_2 corrosion on a steel surface

2.2 Corrosion driven by sulfate-reducing bacteria

Biocorrosion or microbiologically induced corrosion (MIC) occurs when microorganisms facilitate the deterioration of metal. The three main types of bacteria related to metal corrosion are sulfate-, iron- and CO_2-reducing bacteria (Beech & Sunner, 2004). Among them, sulfate-reducing bacteria (SRB) are considered to be associated with the majority of carbon steel corrosion under

anaerobic conditions (Miranda *et al.*, 2006). It has estimated that in the SRB induced more than 77% of the corrosion in the oil-producing wells in the USA (Lapointe *et al.*, 1991). Multiple studies have demonstrated that the addition of a SRB strain to anaerobic carbon steel system facilitated corrosion which caused the acceleration of corrosion rate of carbon steel (Paula *et al.,* 2016; AlAbbas *et al.*, 2013; Miranda *et al.*, 2006; Padilla-Viveros *et al.,* 2006; Beech & Sunner, 2004; Gayosso *et al.,* 2004). Table 2-1 presents four SRB species that accelerate corrosion rate of carbon steel when using lactate as an electron donor and carbon source.

Table 2- 1 Four SRB strains accelerating corrosion rate of carbon steel when using lactate as an electron donor

SRB		Corrosion rate (mpy)		Incubation time (hours)	Reference
Species	Source	biotic	abiotic		
Desulfomicrobium sp	oil well	60	10	840	(AlAbbas *et al.*, 2013)
Dethiosulfovibrio peptidovorans gen. nov., sp. nov.	oil well	157	20	168	(Magot *et al.*, 1997)
Desulfovibrio vietnamensis	gas pipeline	20	0.2	988	(Gayosso *et al.*, 2004)
Desulfovibrio alaskensis	H_2O-oil separator	8	1.2	100	(Padilla-Viveros *et al.*, 2006)

The first attempt to explain the mechanism of SRB-induced corrosion was in 1934 by von Wolzogen Kühr & van der Vlugt (1934) who illustrated that sulfate

reduction activity could cause corrosion under anaerobic conditions. They proposed the theory, “cathodic depolarization theory”, where at the cathode, protons were reduced to form molecular hydrogen adsorbed on the steel surface by accepting electrons from metallic iron oxidation. The adsorption of molecular hydrogen forms a new layer or film at the cathode and causes polarization of the surface, thereby changing the surface potential. The removal of generated molecular hydrogen at the cathode requires higher activation energy, thus the formation of molecular hydrogen will inhibit the corrosion of steel. In an SRB driven corrosion system, the molecular hydrogen could be consumed when SRB reducing sulfate to sulfide through the hydrogenase activity and the removal of molecular hydrogen promotes corrosion of steel. The cathodic depolarization theory reactions are given below (equation 7 through 12):

Anodic reaction: $Fe \rightarrow Fe^{2+} + 2e^-$ equation 7

Dissolution of water: $2H_2O \rightarrow 2H^+ + 2OH^-$ equation 8

Cathodic reaction: $2H^+_{ads} + 2e^- \rightarrow 2H_{ads}$ equation 9

Cathodic depolarization: $1/4SO_4^{2-} + 2H \rightarrow 1/4S^{2-} + H_2O$ by SRB equation 10

Corrosion product: $Fe^{2+} + S^{2-} \rightarrow FeS_{(S)}$ equation 11

Overall reaction:

$4Fe + SO_4^{2-} + 4H_2O \rightarrow FeS_{(S)} + 3Fe^{2+} + 8OH^-$ equation 12

The utilization of cathodic hydrogen by SRB was studied by Pankhania *et al.* (1986). It was demonstrated that when the hydrogenase activity and production

of cathodic hydrogen increased, the concentration of sulfate decreased and the *Desulfovibrio vulgaris* growth was observed which suggested that SRB can use cathodic hydrogen as electron donor when sulfate was reduced to sulfate (Pankhania *et al.,* 1986). However, how the utilization of cathodic hydrogen facilitating corrosion of steel was not discussed. Spruit & Wanklyn (1952) questioned the cathodic depolarization theory based upon the molar ratio of the total amount of Fe^0 that is oxidized to ferrous ions/FeS. Based on the cathodic depolarization theory and the overall reaction as shown in equation 14, if the only source of hydrogen was coming from the cathodic reaction, the molar ratio of the total amount of Fe^0 that is oxidized to ferrous ions/reduced sulfate should be 4. However, the results of Spruit & Wanklyn's (1952) study showed that when the produced cathodic hydrogen was the only electron donor, the ratio ranged from 5 to 9 which indicated that not all reduced cathodic hydrogen was used for sulfate reduction, therefore, the produced FeS was less than the expectation. It was hypothesized that the remaining hydrogen may form hydrogen gas and/or involve the reduction of CO_2 to form cellular biomass; with the addition of lactate, the ratio ranged 0.9 to 1.5 which indicated that lactate was oxidized to carbonate or bicarbonate. In the cathodic depolarization theory, the consumption of produced cathodic hydrogen promotes corrosion of steel while sulfide is presented as the products of sulfate reduction by SRB and the corrosivity of sulfide isn't involved in the theory. The mechanism of "chemical

microbially influenced corrosion" (CMIC) suggests that when SRB reduce sulfate to sulfide, SRB mainly use biodegradable organic compounds (shown as <HCOH>) as an electron donor and produce H_2S (equation 13) (Dinh *et al.*, 2004). SRB facilitate corrosion of carbon steel indirectly through biogenic H_2S which is corrosive to carbon steel. When H_2S reacts with Fe^0, hydrogen is produced (equation 14, Figure 2-2, reaction Ⓑ), and the produced hydrogen can also be used by SRB when reducing sulfate to sulfide. The overall reaction of CMIC is showed as equation 15 (Figure 2-2, reaction Ⓒ). Therefore, the availability of organic matter controls the CMIC.

$2\text{<HCOH>} + 4SO_4^{2-} \rightarrow 2HCO_3^- + H_2S$ equation 13

$H_2S + Fe^0 \rightarrow FeS + H_2$ equation 14

$3\text{<HCOH>} + SO_4^{2-} + 2Fe + 8H^+ \rightarrow 3\ HCO_3^- + 2FeS_{(S)} + 2H_2O$ equation 15

In 2012, Enning et al. demonstrated that *Desulfovibrio ferrophilus* strain IS5 accelerated corrosion of steel 71 times higher than the sterile control when no biodegradable organic matter present. Thus, the "electrical microbially influenced corrosion" (EMIC) mechanism is proposed that metallic iron loss electrons at the anode and electrons are transferred to the cathode where SRB reduce sulfate to sulfide by direct contact with steel surface or through the semi-conductive corrosion products, FeS, as equation 16, and the overall reaction is shown in equation 17.

$8e^- + SO_4^{2-} + 9H^+ \rightarrow HS^- + 4H_2O$ equation 16

$4Fe + SO_4^{2-} + 4H_2O \rightarrow FeS_{(S)} + 3Fe^{2+} + 8OH^-$ equation 17

The molar ratio of oxidation product (Fe^{2+}) and reduction products (S^{2-}) is 4:1, and the excess Fe^{2+} reacts with carbonate (CO_3^{2-}) to form $FeCO_{3(S)}$ in the system, the overall EMIC reaction is shown in equation 18 (Figure 2-2, reaction Ⓐ):

$4Fe + SO_4^{2-} + 3HCO_3^- + H_2O \rightarrow FeS_{(S)} + 3FeCO_{3(S)} + 5OH^-$ equation 18

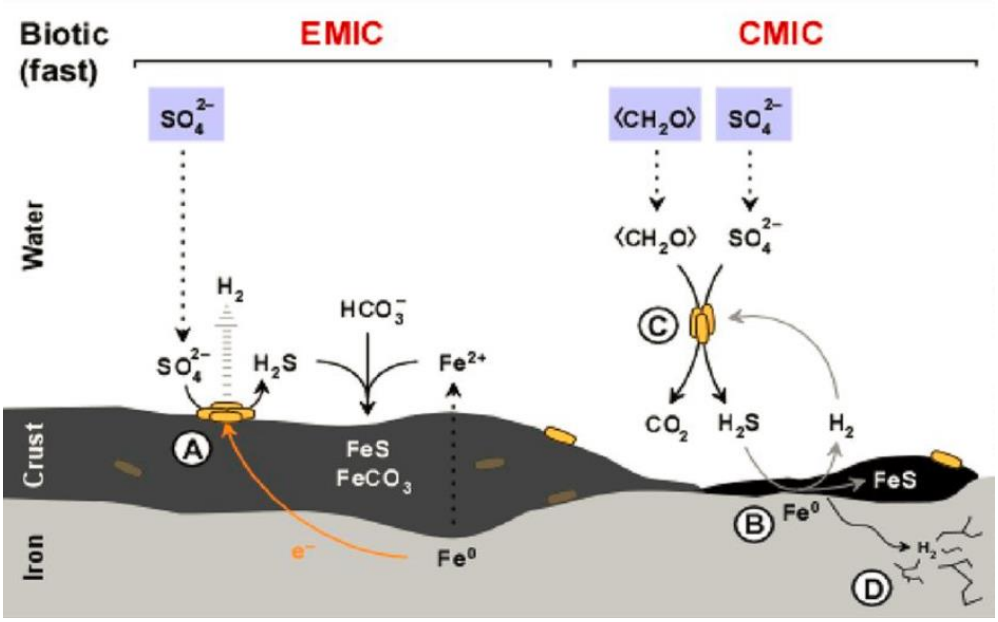

Figure 2- 2 Different types of iron corrosion by SRB (CMIC & EMIC) at circumneutral pH (Enning & Garrelfs, 2014)

2.3 Solubility and reduction kinetics of iron(III) oxyhydroxides

Iron is the fourth most abundant element on Earth, and the oxidation state of Fe(III) occurs predominantly in insoluble forms (e.g. oxides, hydroxides and oxyhydroxides). The solubility and dissolution kinetics of iron oxides limit the iron activity and availability (Kraemer, 2004). In order to compare the dissolved iron concentration we measured in samples to the thermodynamic equilibrium iron

concentration, the solubility of iron oxyhydroxides is reviewed since the main corrosion products formed on the steel surface in aerobic conditions is iron oxyhydroxides (α-FeOOH, y-FeOOH and β-FeOOH,) (Yamashita *et al*., 1994a, Yamashita *et al*., 1994b; Brown *et al.*, 1983; Misawa *et al*., 1974).

2.3.1 Solubility of iron oxyhydroxides

The solubility of different Fe(III) oxides depends on the pH of the solution, the crystalline form of iron oxides, and crystal size (Kraemer, 2004; Trolard & Tardy, 1987; Byrne & Kester, 1976). Byrne & Kester (1976) reported that in seawater (at 36.22‰ salinity and 25°C) at the pH range from 3.30 to 9.39, the solubility of new precipitate $Fe(OH)_{3(S)}$ decreased as the pH increased. In the pH range from 6.82 to 8.57, the dissolved Fe(III) concentration was from 3.16 $\times 10^{-4}$ ppm to 1.89 $\times$ 10^{-5} ppm (Byrne & Kester, 1976). Schwertmann (1991) reported that the solubility of iron oxides was variable based on the different oxides forms. The dissolved Fe(III) concentration of lepidocrocite (γ-FeOOH) and goethite (α-FeOOH) was 3.52×10^{-7} ppm and 7.82×10^{-6} ppm at pH = 7 and 25℃, respectively. The solubility of α-FeOOH also depends on the crystal size. At pH = 8 and 25℃, when the crystal size increased from 8 nm to 100 nm, the solubility decreased three orders of magnitude from 1.90×10^{-4} ppm to 3.97×10^{-7} ppm (Kraemer, 2004). Overall, regardless of the iron oxyhydroxide species and crystal size, the highest solubility of iron oxyhydroxides is around 1 $\times 10^{-4}$ ppm at

neutral pH. This value will be used as the thermodynamic equilibrium concentration of iron oxyhydroxides and compared to the measured dissolved iron concentration in the production water samples.

2.3.2 Dissolution of insoluble Fe(III) in the presence of organic ligands by forming Fe(III)-ligand complexes

Since the very low solubility of iron oxides limits the iron activity and availability, the dissolution of iron oxides is a very important process for microorganisms. Through the reduction of Fe(III), microorganisms can incorporate iron into proteins or generate energy by using Fe(III) as a terminal electron acceptor and organic matter as the electron donor (Lee & Newman, 2003; Banfield & Nealson, 1997; Lovley & Phillips, 1988). Many studies of dissolution of insoluble Fe(III) by organic acids due to the formation of Fe(III)-organic ligands complexes has been reported (Wang *et al.*, 2017; Paris & Desboeufs, 2013; Okochi & Brimblecombe, 2002; Drever & Stillings, 1997; Panias *et al*., 1995). In the production water samples obtained from oil wells, dicarboxylic acids, mainly oxalic acid (C_2), malonic acid (C_3), succinic acid (C_4), methyl succinic acid (C_5) and glutaric acid (C_s), have been found (Kharaka *et al*., 1993). The concentration of those reported dicarboxylic acids have been reported up to 494 mg/L oxalic acid, 2541 mg/L malonic acid, 63 mg/L succinic acid, 22mg/L methyl succinic acid and 95 mg/L glutaric acid in oil well production water samples (Kharaka *et al*., 1993).

Terminal dicarboxylic acids, such as oxalic acid (C_2), malonic acid (C_3) and succinic acid (C_4) can form complexes with Fe(III) which play an important role in the dissolution of insoluble ferric iron from the ferric oxyhydroxide (Okochi & Brimblecombe, 2002). Oxalic acid has been added to commercial solvent formulations devised for the hydrometallurgical process to remove iron oxides, owing to its excellent dissolving capability on rust (Panias *et al*., 1995). At neutral pH, dicarboxylic acids exist as de-protonated state (salt) due to their pKa value, such as oxalic acid (pK_{a1} = 1.23, pK_{a2} = 4.19), malonic acid (pK_{a1} = 2.83, pK_{a2} = 5.69) and succinic acid (pK_{a1} = 4.16, pK_{a2} = 5.61). In addition, dicarboxylic acids can form strong complexes with Fe(III) with high stability constant. The stability constant (binding constant) of the Fe(III)-oxalate complexes reaction is shown in equation 20 when oxalate chelates with Fe(III) in a ratio of 3:1 to form three 5-membered rings around Fe(III) (Figure 2-3) with high stability constant of log K_{so} = 18.6. The stability constants of dicarboxylic acids, α-hydroxycarboxylic acids, and mono-PEG carboxylic acid are two to several orders of magnitude higher than monocarboxylic acids (Table 2-2) which suggests that those organic acids bond strongly enough to displace oxide and hydroxide and thus form the Fe(III)-ligand complexes and facilitate dissolution of Fe(III).

$$Fe^{3+} + 3oxalate^{2-} \leftrightarrow (Fe\text{-}oxalate_3)^{3-} \qquad \text{equation 20}$$

$$\beta_3 = \{(Fe\text{-}oxalate_3)^{3-}\}/\{Fe^{3+}\}\{oxalate^{2-}\}^3 = 10^{18.6}$$

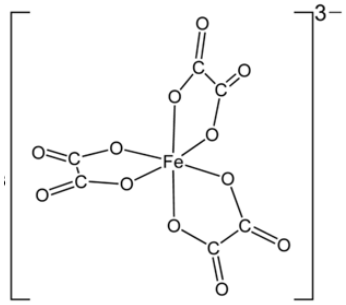

Figure 2- 3 Structure of Fe(III)-oxalate$_3^{3-}$ complex

Table 2- 2 Stability constant of Fe(III)-organic acids complexes

Fe(III)-complexes		Stability constant		Reference
monocarboxylic acid	Fe(III)-formate	log β_1	3.1	(Perrin, 1959)
	Fe(III)-acetate	log β_1	3.2	(Perrin, 1959)
	Fe(III)-propionate	log β_1	3.45	(Perrin, 1959)
	Fe(III)-butyrate	log β_1	3.0	(Perrin, 1959)
dicarboxylic acid	Fe(III)-oxalate	log β_1	9.4	(Perrin, 1959)
	Fe(III)-oxalate	log β_3	18.6	(Martell & Smith, 1974)
	Fe(III)-malonate	log β_1	9.4	(Perrin, 1959)
	Fe(III)-malonate	log β_3	16.6	(Martell & Smith, 1974)
	Fe(III)-succinate	log β_1	8.8	(Perrin, 1959)
	Fe(III)-succinate	log β_3	10.6	(Martell & Smith, 1974)
α-hydroxycarboxylic acids	Fe(III)-glycolate	log β_3	8.11	(Portanova *et al.,* 2003)
	Fe(III)-malate	log β_3	7.1	(Martell & Smith, 1974)
PEG-carboxylic acid	Fe(III)-diglycolate*	log β_3	6.56	(Napoli, 1972)

"*": Diglycolate is the salt form of PEG carboxylic acids with 1 ethylene group.

The influence of the formation of Fe(III)-ligands complexes on the dissolution of insoluble Fe(III) from solid iron oxides was reported by Duckworth & Martin (2013). After stirring 72 hours and at pH =5, the dissolved iron concentration of 0.2 g/L hematite was 110, 19 and 35 µM with the addition of 10 mM oxalic acid, malonic acid, and glutaric acid respectively, and no significant dissolved iron concentration change was found in the addition of 10 mM succinic acid and the dissolved iron concentration in the control sample was undetectable (Duckworth & Martin 2013). The concentration of 10 mM dicarboxylic acids was 100 to 500 times higher than the measured final dissolved iron concentration at 72 hours, however, Duckworth & Martin (2013) demonstrated that at all sampling time points (n=10) within the 72 hours, the samples were far from equilibrium and a linear relationship between the incubation time and dissolved iron concentration was found which suggested that the longer duration of incubation time, the more dissolved iron were detected until the system was at equilibrium (Figure 2-4).

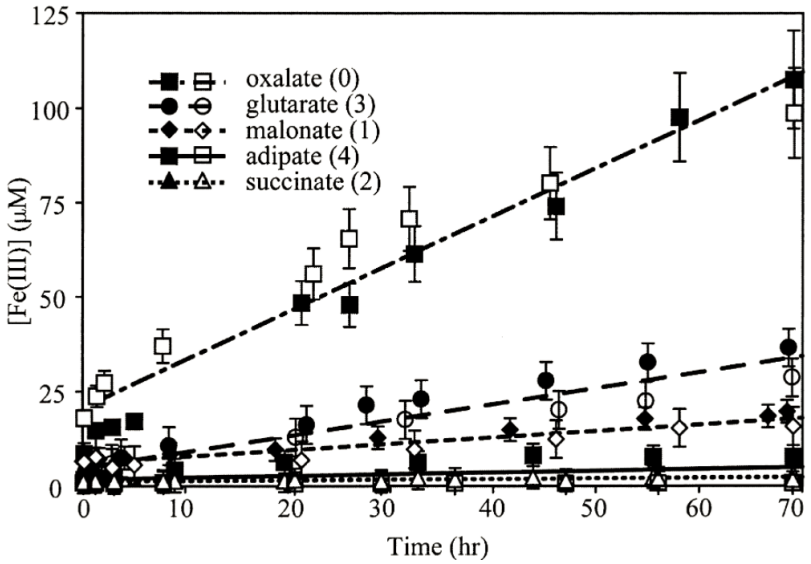

Figure 2- 4 Dissolved iron concentration vs. time in the presence of oxalate, malonate, succinate, glutarate, and adipate in 0.2 g/L hematite (Duckworth & Martin 2013)

In summary, dicarboxylic acids can form complexes with Fe(III) and the formation of complexes can facilitate the dissolution of ferric iron from solid iron oxides. However, the monocarboxylic acid (acetic acid, formic acid) didn't form Fe(III)-ligand complexes by adsorbing to ferric oxyhydroxide and facilitating dissolution under atmospheric conditions and solubilize the insoluble iron oxides (Okochi & Brimblecombe, 2002). In the production water samples, mono-carboxylic acid will not be considered to be the effective parameters in the solubilization of insoluble ferric iron.

2.4 Influence of organic ligands on the iron oxides reduction by iron-reducing bacteria

Iron-reducing bacteria (IRB) are the microorganisms that have the ability to use Fe(III) as an electron acceptor and can be grouped into two groups: assimilatory

and dissimilatory. The assimilatory IRB reduce Fe(III) for incorporation into proteins, while the dissimilatory IRB reduce Fe(III) for energy generation (Lee & Newman, 2003). Dissimilatory IRB, such as from the genus *Shewanella* and *Geobacter*, can generate energy by using organic compounds as an electron donor and Fe(III) as a terminal electron acceptor under anaerobic conditions (Banfield & Nealson, 1997; Winkelmann, 1997; Nealson & Saffarini, 1994; Lovley & Phillips, 1988).

At circumneutral pH, due to the very low solubility in water, solid phase iron oxides are not readily bioavailable for IRB utilization. As discussed in section 2.3.2, formation Fe(III)-organic ligand complexes can facilitate the dissolution of insoluble Fe(III) which increases the bioavailability of Fe(III). Organic ligands, such as nitrilotriacetic acid (NTA), EDTA, oxalate and malate, can form strong complexes with Fe(III) and promote the reduction of insoluble Fe(III) by IRB (Maurice *et al.,* 2001; Kostka *et al.*, 1999; Holmén *et al.,* 1999). Holmén *et al.* (1999) reported that when the amorphous $Fe(OH)_3$ was incubated with *G. metallireducens,* the Fe(II) concentration in the addition of NTA sample was 3 times higher than the without NTA sample (Holmén *et al.*, 1999). Similar results were observed when iron oxides incubated with *S. oneidensis* MR-1 that the addition of NTA sample had 2 times higher reduction rate than the without NTA sample (Kostka *et al.*, 1999). Arnold *et al.*, (1988) demonstrated that the reduction rate of goethite (α-FeOOH) by *Pseudomonas* sp. 200 increased 10 and

15 times with addition of NTA and EDTA respectively, compared with the no ligand addition sample. The addition of oxalate and malate also increases the microbial reduction rate of insoluble Fe(III) (Kostka *et al.*, 1999). Kostka *et al.* (1999) reported for the reduction of Fe(III) from Smectite by *S. oneidensis* MR-1, the addition of 2 mM oxalate and malate, respectively, caused the reduced Fe(II) concentration to increase 1.5 and 1.3 times higher respectively than without ligands over a 50 days incubation period.

As shown in Table 2-3, because of the difference redox potential of the solid iron oxides forms/Fe(II), when microbes use solid ferric iron as a terminal electron acceptor and reduce it to ferrous iron, the amount of available free energy ranges from -9 to + 60 kJ/mole which demonstrates that microbes using solid-phase ferric oxides as electron acceptor is a highly variable mechanism for providing energy through the respiration of ferric iron (Bird *et al.*, 2011). However, when ferric iron chelates with NTA or citrate, the redox potential of Fe(III)-ligand/Fe(II)-ligand increases, thereby the amount of available free energy for ferric iron respiration increases to -35.9 and -37.1 kJ/mole respectively (Bird *et al.*, 2011). The Fe(III) chelating ligands can cause dissolution of Fe(III) from the insoluble iron oxides and increase the solubility of dissolved ferric ion.

Table 2- 3 Reduction potentials and free energies of some species of Fe(III)/Fe(II) (Bird et al., 2011)

Reduction pair	E_{env}* (volts)[a]	ΔG (kJ/mol)[b]
Fe^{3+}/Fe^{2+} (pH 2)	0.77	–74.2
$Ferrihydrite_{solid}/Fe^{2+}$	+0.1 to –0.1	–9.6 to 9.6
$\alpha\text{-}FeOOH_{solid}/Fe^{2+}$	–0.274	26.4
$\alpha\text{-}Fe_2O_{3solid}/Fe^{2+}$	–0.287	55.4
Fe_3O_{4solid}/Fe^{2+}	–0.314	60.6
Fe(III)-citrate/Fe(II)-citrate	0.385	–37.1
Fe(III)-NTA/Fe(II)-NTA	0.372	–35.9

[a]: E_{env}* indicates environmentally relevant midpoint potentials: pH 7 except where noted, standard concentrations except for solid Fe minerals, for which Fe^{2+} is 100 μM.
[b]: ΔG calculations assume standard conditions and pH 7, except in the case of iron minerals where $[Fe^{2+}]$ is assumed to be 100 μM.

Despite a gain in energy upon reducing soluble ferric iron bound by organic ligands compared to solid phase ferric oxides, attention must be given to the actual amount of energy the microbe will obtain during ferric respiration. Bird *et al.* (2011) illustrated that the microbial energy gain occurs during electron transfer from the NAD+/NADH in the cellular cytoplasm to the menaquinones (MQ/MQH_2) couple in the inner membrane. Electron transfer beyond this point through the periplasm, outer membrane and to the final ferric electron acceptor does not contribute to the microbial energy gain, despite the difference in free energy associated with these different ferric species, both dissolved and solid

phase. However, increasing the concentration of available ferric ions as soluble ferric-ligands complexes increases the kinetic rates of ferric respiration relative to solid-phase ferric respiration, thereby making ferric respiration a feasible respiration process for microbes capable of iron (Figure 2-7) (Bird *et al.*, 2011).

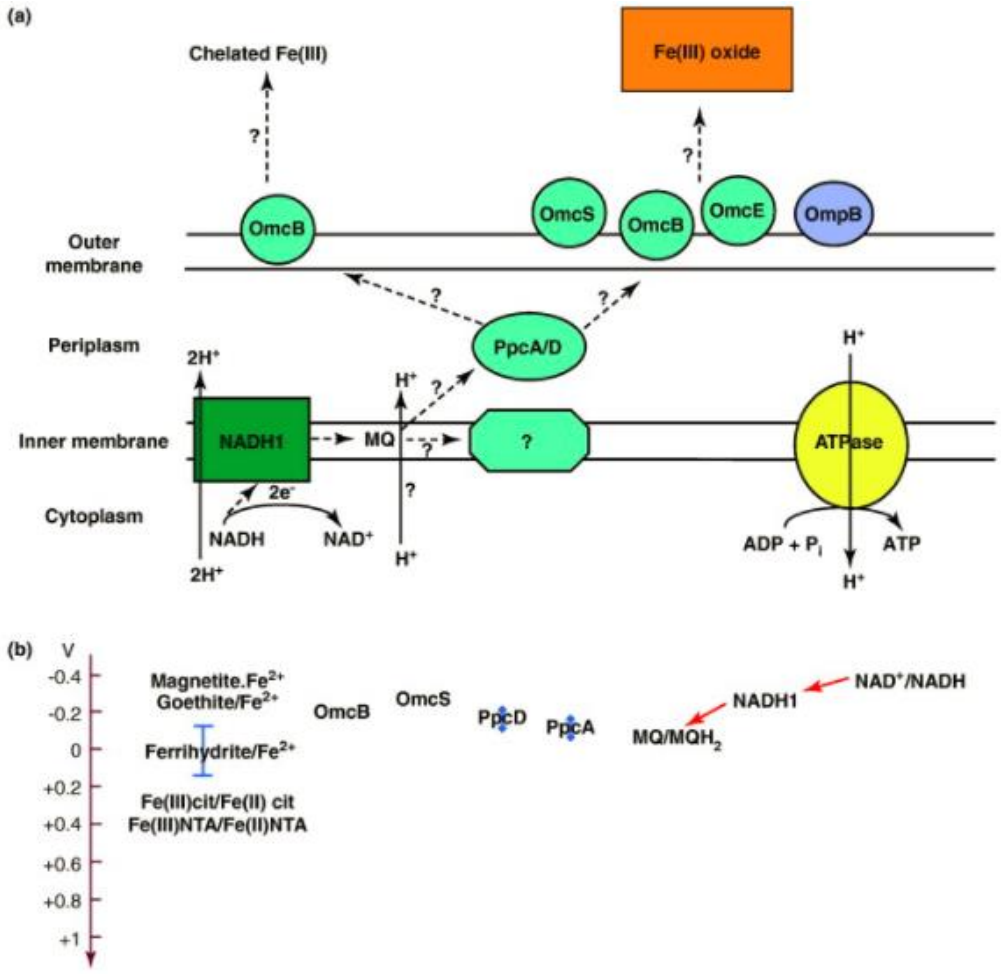

Figure 2- 5 Model of Fe(III) reduction in Geobacter sulfurreducens. (a) The potential pathway for electrons through the membranes and periplasm. The pathway is still uncertain because many cytochromes are expressed in Geobacter under Fe(III) reducing conditions (Bird *et al*., 2011)

2.5 Influence of iron-reducing bacteria on the corrosion of steel

Among the three main types of bacteria related to metal corrosion, sulfate-, iron- and CO_2-reducing bacteria (Beech & Sunner, 2004), iron-reducing bacteria (IRB) can use ferric iron as a terminal electron acceptor under anaerobic conditions and facilitate or promote the deterioration of metal by reducing Fe(III) from the iron oxyhydroxide, consequently removing the passivating iron oxyhydroxide layer and exposure the metallic steel to cause further oxidation reactions (Little *et al.*, 2007).

Corrosion of carbon steel can form a solid layered structure including iron oxyhydroxide, magnetite, ferric hydroxide, siderite, ferrous sulfide, and iron oxide which may passivate the steel surface and inhibit the corrosion of carbon steel (Cornell & Schwertmann, 2003; de Moraes *et al.*, 2000; Refait *et al.*, 1998; McNeil & Little, 1990). Obuekwe *et al.* (1981) demonstrated that the presence of IRB, *Pseudomonas sp.* no. 200 isolated from corroded oil pipelines, extensively removed the iron oxides layer from the steel coupon under anaerobic conditions and exposed the metallic metal to environment, while the steel coupon incubated under abiotic conditions formed a crystalline-amorphous layer on the coupon surface. Starosvetsky (2016) reported that under anaerobic conditions, *S. oneidensis* removed the corrosion products layer completely from steel surface under anaerobic conditions, and *G. sulfurreducens* removed most oxidized products on steel coupon compared with sterile control. The removal of the

corrosion products layer led to metallic iron exposed to oxygen for further oxidization. Thus, the literature review indicates that the mechanisms of IRB facilitated corrosion appears to be the removal of passivating iron oxides layer from steel surface and the exposure of the metallic iron to oxidants causes further oxidation of steel.

Chapter 3: Methodology

3.1 Site description and samples collection.

Site 1-- Putumayo Basin, southwest Colombia, South America

The Putumayo Basin is located in the Putumayo-Oriente-Maranon province in eastern Colombia, Ecuador, and Peru. Reservoirs with CO_2 exceeding 20 vol. % have been found in this area (Thrasher & Fleet, 1995). Production water samples were directly collected from four oil wellheads: Acae, Caribe, Loro, and Sucombio by EcoPetrol in December 2013 and stored in 5-liter polypropylene container. Then samples were shipped with ice packs to the University of Oklahoma and stored at 4 ℃.

Site 2-- Barnett Shale, north Texas, USA.

The Barnett Shale is near Arlington, north Texas, USA which is overlying on the Ellenburger Group carbonates (Pollastro, 2007). Samples were collected from five gas production water storage tanks in June 2015: Krum Joint Venture #7 (KJV 7), Steward-Enis 17 (SE 17), Steward-Enis 18 (SE 18), Steward-Enis 19 (SE 19) and Miller-Cuffman unit 5 (MC 5). Production water was obtained by lowering sterile 1 L glass bottles through the thief hatch. Sampling bottle was full of production water without headspace and sealed as soon as possible to prevent from oxidizing. The production water samples were stored at 4 ℃ before use. In addition, for each tank, around 100 mL production water sample was immediately filtered with 0.2 μm polyethersulfone (PES) membrane (Whatman,

Puradisc 25 mm, Cat. No.: 6780-2502), added concentrated HNO_3 (Fluka, TraceSELECT) 0.5 ml with plastic pipette and sealed in a 150 mL serum bottle for the total dissolved metal ions measurement. Samples were kept in the refrigerator at 4 ℃ before use. All glassware was cleaned with 10% HNO_3 (Fluka, TraceSELECT); washed with a resistivity of 18.2 MΩ (nanopure) water and autoclaved for 30 minutes before brought to the field.

3.2 Chemical analysis of nine production water samples

3.2.1 General chemical properties of nine production water samples

For Putumayo Basin production water samples, all experiments were performed after samples were shipped to the University of Oklahoma, Norman, OK. A 100 ml production water sample was taken out from the 5-liter polypropylene container with a glass pipette and filtered with a paper filter (Whatman. Grade GF/F glass microfiber filter. Cat. No.: 1001150) for pH, alkalinity, and ferrous iron concentration measurement.

For Barnett Shale production water samples, pH and alkalinity, dissolved oxygen and sulfide were measured immediately in-field with filtered samples using a 0.45 μm PES membrane (Whatman, Puradisc 25 mm, Cat. No.: 6781-2504).

pH: The pH value was measured with a pH meter (SympHony B10P pH meter) coupled with a glass electrode and calibrated with pH 4.00, pH 7.00 & pH 10.00 buffer (AquaPhoenix Scientific, Cat. No.: S25849A, S25849B & S25849).

Alkalinity: The alkalinity of Putumayo Basin production water samples was determined in our lab according to "Standard Test Methods for Acidity or Alkalinity of Water" (ASTM Standard D1067-16, 2016) with the following modifications: a 50 mL filtered sample was taken out with a class A glass pipette and titrated with 0.01 M sulfuric acid to reach pH of 4.3 with a pH meter (SympHony B10P pH meter).

The alkalinity titration of Barnett Shale samples was measured in the field using a Hach Digital Titrator (Hach, Mod. 16900-01) with 25 mL filtered (0.20 μm PES membrane, Waterman, Puradisc 25 mm, Cat. No.: 67802502) production water samples. The measurement was performed according to "Hach digital titration (Model 16900-01) manual: Alkalinity (10 to 4000 mg/L as $CaCO_3$), Method 8203" with Hach Digital Titration Cartridge (Hach, Cat. 14389-01) (Hach, 1993). The cartridge contained 0.800 mol/L sulfuric acid. Production water samples were titrated to pink (pH = 4.3) using methyl red as indicator.

Ferrous iron: The measurement using filtered 25 ml Putumayo Basin production water samples was performed according to "DR/700 colorimeter procedures manual: Iron, Ferrous (0 to 5.00 mg/L) for water, wastewater and seawater, method No. 8146" by using the 1,10-phenanthroline method that

1,10-Phenanthroline can forms a complex with ferrous ion and the complex has absorption at 510 nm (Hach, 1997).

Sulfide: The measurement was performed in the lab for the two sites' samples using Chemetrics kits (Chemetrics, Cat. K- 9510D) according to the manufacturer's instructions (Chemetrics, 2016). In an acidic solution, sulfide reacts with N, N-dimethyl-p-phenylenediamine and ferric chloride to produce methylene blue.

Dissolved oxygen: The dissolved oxygen concentration of Barnett Shale production water samples was measured using a FireSting O_2 probe (PyroScience, OXROB10) in-field.

Inorganic anions (chloride, sulfate, nitrate, and nitrite) (data collected by colleagues from OU Department of Microbiology and Plant Biology): All samples were measured in Dr. Suflita's lab in the University of Oklahoma, Norman campus. Samples were filtered through a 0.20 µm PES membrane (Waterman, Puradisc 25 mm, Cat. No.: 67802502). Inorganic anions (chloride, sulfate, nitrate, and nitrite) were quantified by suppressed ion-chromatography on a Dionex ICS-3000 system (Dionex; Sunnyvale, CA) equipped with Dionex AS4A-SC guard (4 mm x 50 mm) and analytical (4 mm x 250 mm) columns. Separations were performed at the mobile phase of carbonate buffer (1.7 mM HCO_3^-; 1.8 mM CO_3^{2-}; 2.0 ml/min) and a suppression current of 35 mA. Samples

for nitrate and sulfate analysis were pretreated with Dionex OnGuardII Ag and Na cartridges to remove interfering halides (Liang, 2015; O'Grady, 1980).

3.2.2 Total dissolved iron and manganese ion concentration measurement

The total dissolved iron and manganese were measured with atomic absorption spectrometer (AAS) (Varian AA 240 with graphite furnace) with the D_2-lamp background corrector. HNO_3 is produced by Fluka (TraceSELECT) and diluted with a resistivity of 18.2 MΩ water (nanopure water). All glassware was cleaned with 10% HNO_3 (Fluka, TraceSELECT) and washed with nanopure water. A 40 ppb standard Fe solution was diluted from 1mg/L iron standard solution (Hach, Cat. 139-49) with class A glass pipettes and volumetric flasks. A standard curve was formed by diluting the 40 ppb standard stock solution to 0, 4, 8, 16, 24, 32, 40 ppb with 1% HNO_3 (Fluka, TraceSELECT) solution auto-sampler on the Varian AA240. A 20 ppb standard Mn solution was diluted from 1,000 mg/L Manganese standard solution (Ricca, Cat. No.: AMN1KH-100). A standard curve was formed by diluting the 20 ppb standard stock solution to 0, 2, 4, 8, 12, 16, 20 ppb with 1% HNO_3 solution by auto-sampler on the Varian AA240.

A 5 mL aliquot of Putumayo Basin production water sample was removed from the original 5 liter polypropylene container with a glass pipette and filtered with 0.20 µm PES membrane (Whatman, Puradisc 25 mm, Cat. No.: 67802502), acidified with HNO_3 (Fluka, TraceSELECT) and diluted to 100, 10,000 and

1,000,000 fold so that the diluted sample could fit into the linear regression range of the instrument. The 1% HNO_3 solution, class A glass pipettes and volumetric flasks were used to do the dilution.

A 1 mL aliquot of Barnett Shale production water sample was taken out from serum bottles which were filtered and acidified in the field with a 1 mL class A glass pipettes. The 1 mL aliquot was put into 100 mL class A volumetric flask and diluted with 1% HNO_3 solution. Further dilution, if needed, was performed with 1% HNO_3 solution, class A glass pipettes and volumetric flasks.

The measurement was performed using Fe hollow cathode lamp (Agilent technologies, coded Fe/Co/Mn/Cu/Cr HC-lamp, part No.: 5610107600), Mn hollow cathode lamp (Agilent technologies, coded Mn HC-lamp, part No.: 561003300). Ultra high purity argon (Airgas, Part #: AR UHP300) was used as carrier gas. Standards and samples were injected in triplicate. Nanopure water and 1% HNO_3 solution was used as blank. Instrumental parameters and operational conditions for the determination of Fe and Mn followed the instrumental recommendations parameters are shown in Table 3-1. Peak height was selected to quantify the dissolved Fe and Mn concentration because the atomization temperature of Fe and Mn is at 2400 ℃. At this temperature, the peak is broad and peak height is more sensitive than peak area (Rothery, 1998).

Table 3- 1 Furnace operating conditions for Fe and Mn measurement

Wavelength: 248.3 nm[1], 279.5 nm[2]; Current: 10.0 mA[1], 5.0 mA[2]; Slit Width: 0.2 nm; Mode: Peak Height					
Step No.	Temp (℃)	Time (sec.)	Gas Flow (L/min)	Read	Store
1	85	5.0	0.3	No	No
2	95	40.0	0.3	No	No
3	120	10.0	0.3	No	No
4	700	5.0	0.3	No	No
5	700	1.0	0.3	No	No
6	700	2.0	0.3	No	Yes
7	2400	0.8[1], 0.9[2]	0.3	Yes	Yes
8	2400	2.0	0.3	Yes	Yes
9	2500	2.0	0.3	No	Yes

[1]: Fe measurement, [2]: Mn measurement

3.2.3 Equilibrium Fe(III) concentration calculation by MINEQL+

MINEQL+ is capable of solving chemical equilibrium problems including determination of chemical speciation, solid phase saturation states, precipitation-dissolution, and adsorption. An extensive thermodynamic database is included in the model (Westall, 1976). The valent of iron ions of the solid iron phase was determined by the ferrous iron concentration and the dissolved oxygen concentration. Based on the physical and geochemical background of the

sampling sites, the concentration of sulfide, pH and alkalinity, and the solubility of the $Fe(OH)_{3(S)}$, $FeS_{(S)}$, $FeCO_{3(S)}$, and $Fe(OH)_{2(S)}$, the presented solid iron minerals were selected which was used to predict thermodynamic equilibrium dissolved iron concentration by the MINEQL+. The total carbonate concentration of the production water samples was estimated by pH and alkalinity value assuming the sampling site was closed to the atmosphere.

3.3 Targeted metabolomics analysis by gas chromatography coupled with a mass selective detector for Putumayo Basin production water samples and Barnett Shale production water samples

Targeted metabolomics measured the solubilized, low molecular weight organic acids. Because the stability constants of dicarboxylic acids, α-hydroxycarboxylic acids, and PEG carboxylic acid are two to several orders of magnitude higher than monocarboxylic acids, this suggests that those organic acids bond strongly enough to displace oxide and hydroxide and thus form the Fe(III)-ligand complexes and facilitate dissolution of Fe(III). The defined groups of organic ligands which bound with Fe(III) and facilitated dissolution of insoluble iron were dicarboxylic acids, α-hydroxycarboxylic acids, and PEG carboxylic acid in our research. In the production water samples, ligands existed as two forms: “Free ligands” and “Fe-bound ligands”. The “Free ligands” were the ligands which didn’t bind with Fe(III) at neutral pH in the production water samples, and the

“Fe-bound ligands” were the ligands bound to Fe(III) at neutral pH in the production water sample. “Total ligands” included “Free ligands” and “Fe-bound ligands”. In order to extract the “Free ligands”, production water sample was acidified to pH =2 so that organic ligands were under the protonated states, and could be extracted by organic solvent—ethyl acetate (EtOAc). In order to extract the “Total ligands”, including “Fe-bound ligands” and “Free ligands”, production water sample was raised pH to 12 so that Fe(III) precipitated as Fe(OH)3(S) and the “Fe-bound ligands” became free. After filtration to remove the Fe(OH)3(S) precipitate, production water sample was acidify to pH =2 so that the “Free-ligands” and “Fe-bound” ligands both could be extracted with EtOAc (Figure 3-1).

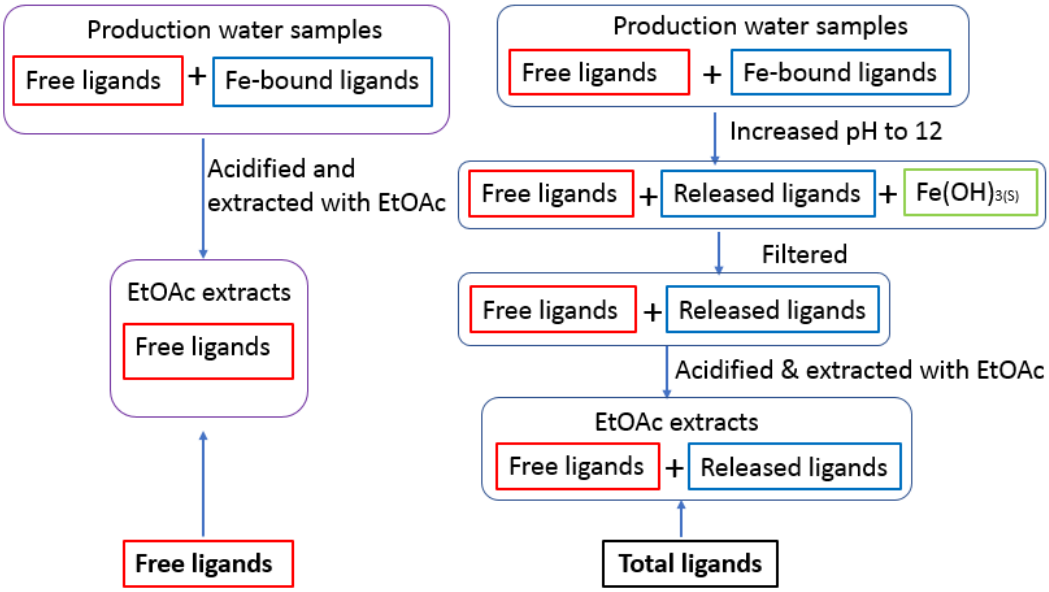

Figure 3- 1 Schematic illustrating the two samples of "Free-ligands" and "Total ligands"

The optimal pH which has the most $Fe(OH)_{3(S)}$ precipitation was determined by observing the formation of precipitation at different pH. A 20 ml Sucombio production water sample from the Putumayo Basin was filtered with a 0.20 µm PES membrane (Whatman, Puradisc 25 mm, Cat. No.: 6781-2504). The filtered sample was increased pH to 8 with 1 M NaOH to observe the formation of precipitation. If precipitation formed, sample was filtered with a 0.20 µm PES membrane (Whatman, Puradisc 25 mm, Cat. No.: 6781-2504), increased pH to 9 and observe the formation of precipitation. If new precipitation formed, sample was filtered with a 0.20 µm PES membrane (Whatman, Puradisc 25 mm, Cat. No.: 6781-2504), continued increasing pH to 10, 11, 12, 13 step by step and observe the formation of precipitation until no precipitate formed to determine the optimal pH value which has the most $Fe(OH)_{3(S)}$ precipitate. The results showed that after pH 12 no more precipitate formed as pH increased and pH 12 was selected.

The internal standard, 9-fluorenecarboxylic acid (9-FCA), was used to measure relative retention time of sample peaks. Utilizing this relative retention time and comparing against MS fragmentation patterns, it was possible to correctly identify mono- and di-aromatic acids, as well as, mono- and dicarboxylic acids (Westbrook & Nanny, 2013).

To characterize the Fe-bound compounds in the production water, this study used derivatization method which made compounds more volatile, detectable at

reasonable temperature and avoided decomposition at high temperature (Mohd, 2012). N-methyl-N-(tert-butyldimethylsilyl) trifluoroacetamide (MTBSTFA) with 1% *tert*-butyldimethylsilylchloride (Aldrich, Lot#: BCBC8901) which substitutes the active hydrogen (in -OH, -COOH, -NH, -NH_2, and -SH groups) with a dimethylsilyl group was used first (John et al., 1998).

Y: O, S, NH, NR, COO;

This derivatization step was conducted in an anaerobic chamber filled with N_2 to prevent the reaction of oxygen with the derivatization reagent (Westbrook & Nanny, 2013). The methodology of derivatized with MTBSTFA is described below:

A 30 mL aliquot from each Putumayo Basin production water samples was removed with a glass pipette and filtered with a paper filter (Whatman, Grade 802, 24 cm diameter) to remove large particulates. Then the filtered sample was filtered with a 0.45 µm nitrocellulose membrane (Fisher, 47 mm, Cat. No.: 097192E) to remove microbial cells and very fine particulates. A 20 mL membrane filtered aliquot of Putumayo Basin production water samples was acidified to pH 2 with 1 M hydrochloric acid (HCl) so that all organic acids were in the protonated states and extracted three times with 15 mL of EtOAc in a separatory funnel. The EtOAc extracts were combined and dried with anhydrous sodium sulfate (Na_2SO_4) and filtered with a paper filter (Whatman, Grade 802, 24

cm diameter), and then concentrated to around 10 mL using a rotary evaporator. This residual was placed into a 20 mL amber vial and flushed with N_2 until dry. After addition of the internal standard (100 µL of 0.01 M 9-FCA), the amber vial was sealed with a tert-butyl septa screw top and flushed with N_2 for approximately 10 minutes. Then the vial was placed into an anaerobic chamber with an N_2 atmosphere. 400 µL of dichloromethane (DCM) was added with a 500 µL syringe and 100 µl of MTBSTFA with a 250 µL syringe as derivatization reagent was added to the 20 mL amber vial. The vial was removed from the anaerobic chamber and placed in a water bath for 20 minutes at 60 ℃ and stored in the freezer until needed for GC/MS analysis. Vails should not be stored longer than 72 hours due to decomposition of the derivatized products (Westbrook & Nanny, 2013).

A value of 1 µL of the derivatized sample was injected with a 10 µL glass syringe into the Agilent 6980 gas chromatography coupled with a model 5973 mass selective detector (GC/MS). The gas chromatograph utilizes an Agilent ZB5-MSi capillary column, L=30m x I.D.= 0.25mm. Ultra high purity helium (Airgas, Part #: HE UHP300) was used as the carrier gas at a constant flow rate of 1 mL/min. The split flow is at a 20:1 ratio. The GC temperature gradient was set initially at 60 ˚C and held for 3 minutes, then ramping by 3˚C/min to 280˚C and then ramping by 15˚C/min to 300˚C (Westbrook & Nanny, 2013).

However, in the GC/MS spectra using MTBSTFA as the derivatization reagent, only one dicarboxylic acid, succinic acids, were detected in the Putumayo Basin production water sample. In order to detect more dicarboxylic acids, α-hydroxycarboxylic acids, PEG carboxylic acids, a new derivatization reagent, N, O-Bis(trimethylsilyl)trifluoroacetamide (BSTFA, Aldrich, Lot#: 1388081-30709122), was used to replace MTBSTFA. BSTFA introduced a trimethylsilyl group to substitute the active hydrogen (in -OH, -COOH, -NH, $-NH_2$, and -SH groups) with a trimethylsilyl group (Aktas *et al*., 2010).

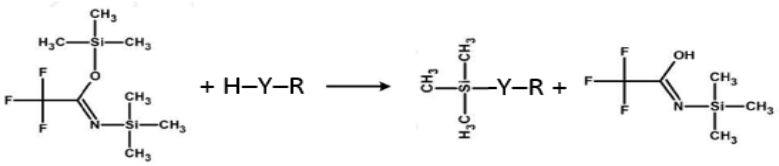

Y: O, S, NH, NR, COO;

Pietrogrande *et al*. (2002) suggested in GC/MS spectra, when using BSTFA as derivatization reagent, C_3–C_9 dicarboxylic acids had low detection limits (≤2 ng/m^3) and high reproducibility (RSD% ≤ 10%) and the results showed that 8 other Fe-bound compounds were detected in the BSTFA derivatized GC/MS spectra of the Putumayo Basin production water samples.

Because of the pH adjustment step and the changing of derivatization reagent, the new methodology was shown below: A 50 mL aliquot of the Sucombio production water sample from the Putumayo Basin and Barnett Shale production water samples were taken out with a glass pipette and filtered with a paper filter

(Whatman, Grade 802, 24 cm diameter) and a 0.45 µm nitrocellulose membrane (Fisher, 47 mm, Cat. No.: 097192E).

A 20 mL aliquot of above filtered 50 mL production water sample was acidified to pH 2 with 1 M HCl and extracted three times with 15 mL of EtOAc in a separatory funnel. This sample was defined as “Free ligands”.

The remaining 30 mL filtered production water sample was adjusted pH to 12 with 1 M NaOH so that organic ligands released from Fe(III)-organic ligands complexes as $Fe(OH)_3$ precipitate formation. $Fe(OH)_{3(S)}$ precipitate was removed by filtration with a 0.20 µm PES membrane (Whatman, Puradisc 25 mm, Cat. No.: 6781-2504) to avoid dissolution of $Fe(OH)_{3(S)}$. A 20 mL aliquot of pH increased and filtered sample was acidified to pH 2 with 1 M HCl and extracted three times with 15 mL of EtOAc in a separatory funnel. This sample was defined as “Total ligands” which includes “Free ligands” and “Fe-bound ligands”.

The EtOAc extracts of the “Free ligands” and “Total ligands” samples were dried with anhydrous sodium sulfate (Na_2SO_4) and filtered with a paper filter (Whatman, Grade 802, 24 cm diameter), the following steps were according to the methodology of derivatization with MTBSTFA with the following modification: changing the MTBSTFA to BSTFA.

3.4 Qualitative carbon steel corrosion assay under aerobic conditions with filtered Putumayo Basin production water samples

The C1018 carbon steel circular coupons used in this study was composed of 0.14–0.2% C, 0.6–0.9% Mn, 0.035% maximum S, 0.03% maximum P, and the remainder was Fe (Alabama Specialty Products, Inc). The composition of C1018 steel coupon was examined with X-ray diffraction (XRD) by Dr. Recep Avci's group from the Montana State University, Bozeman, MT. Round C1018 carbon-steel coupons (9.53 mm in diameter by 1 mm in thickness) were put in a thin steel plate with 1cm diameter holes drilled in and the steel plate was locked on a magnetized platform while polishing the coupons.

The C1018 carbon coupons were polished using a Dremel 4000 High-Performance Rotary Tool (Dremel) coupled with following accessories.

The steps and accessories were listed below with their speeds used for polishing: ①. 503 3/8" Flapwheel (Dremel), 120 grits (rotary speed: 30 - 35); ②. 511E EZ Lock Finishing Abrasive Buffs (Dremel), 180 and 280 grits (rotary speed: 5 - 12); ③. 512E EZ Lock Finishing Abrasive Buffs (Dremel), 320 grits (rotary speed: 5 - 12); ④. 423E EZ Lock Cloth Polishing Wheel (Dremel), coupled with grey polishing compound (used to prevent light scratches and restore the natural look of metal) and then green polishing compound (used for a high polish finish) (rotary speed: 5 - 7).

After polishing, coupons were cleaned with acetone, physically wiped with a cotton swab and Kimwipe tissues, and dried with N_2. Coupons were kept in a sealed serum bottle under 100% N_2 conditions and put into an anaerobic chamber with an N_2 atmosphere (Garimella, 2014).

To remove the microbes and particulates in the production water samples, a 10 mL aliquot from each sample was taken out with a glass pipette and filtered with a 0.20 µm PES membrane (Whatman, Puradisc 25 mm, Cat. No.: 67802502). C1018 carbon steel coupon was immersed for 48 hours in 15 ml Falcon tube with 5 mL of each filtered production water sample. The control solution was 0.7% NaCl solution in nanopure water which represented the average chloride concentration of the four Putumayo Basin production water samples. All sample were sealed with the cap of Falcon tubes. After 48 hours, coupons were taken out, cleaned with 10 mL nanopure water, and flushed with N_2 until dry.

Scanning electron microscope (SEM) was performed using a Zeiss NEON 40 EsB (Carl Zeiss, Oberkochen, Germany) scanning electron microscope and energy dispersive X-Ray spectroscopy (EDS) was performed using OXFORD Link Pentafet X-ray analyzer with IXRF software. SEM images were obtained under 2,000 X magnifications using an acceleration voltage of 15 kV and a working distance of 9 mm. The entire surface of each coupon was examined under low magnification (300 X) and between 20 to 30 image areas (0.064 mm× 0.048 mm) were selected to characterize the typical corrosion products such as pits and crevices. EDS was

used to detect the composition of corrosion products on the carbon steel surface since the EDS can provide not only element identification but also the concentration of each element (Newbury, 2009). The EDS data obtained under 10,000 X magnifications and each EDS scan area was 0.08 µm × 0.08 µm.

After examined with SEM-EDS for uncleaned coupon; these coupons were cleaned by following the "Standard practice for preparing, cleaning, and evaluating corrosion test specimens " (ASTM Standard G1-03, 2003) with additional modifications: coupon was put into 10 mL acid cleaning solution for 5 minutes and rinsed sequentially with nanopure water and ethanol, dried with N_2 and examined with SEM (Garimella, 2014) under 2000 X magnifications.

3.5 Scanning electron microscopy-energy dispersive X-Ray spectroscopy analysis of free-floating biofilms with embedded particulates of Barnett Shale production water samples

The 1 liter Schott bottles containing Barnett Shale production water samples with no headspace were put into an anaerobic chamber with a gas composition of a mix of 5% H_2 and 95% N_2 (Airgas, Part #: X02NI95C3000092). A 100 mL production water was filtered with 0.45 µm nitrocellulose membrane (Fisher, 47 mm, Cat. No.: 097192E). The free-floating biofilm and embedded particulates were collected from the filter with conductive tape (Pelco, Double-Sided Carbon Tape). The conductive tape is electrically conductive and can establish an electrical connection to conduct the specimen current to ground to eliminate the

charge accumulation (Yang, 2013). In addition, the conductive tape can fix the biofilm and the embedded particulates. The conductive tape (8 mm x 8 mm) with samples was put on a standard SEM pin stub mount and the mount was put on an SEM holder. The SEM holder was sealed in a Qorpak bottle with a polyethylene-lined metal cap, moved out of the anaerobic chamber and transferred to the SEM lab. The holder with particulates and biofilm samples were immediately transferred to the SEM-EDS chamber to ensure that the time of exposure to the atmosphere was less than 2 minutes.

SEM was performed using a Zeiss NEON 40 EsB (Carl Zeiss, Oberkochen, Germany) scanning electron microscope and EDS was performed using OXFORD Link Pentafet X-ray analyzer with IXRF software. Images of the biofilm and particulates were obtained under 1,000 kX magnifications using an acceleration voltage of 15 kV and a working distance of 9 mm. The entire surface of the sample was examined under low magnification (300 kX). Then the selected typical area was examined with EDS under 1,000 kX magnification and each EDS scan area was 1 μm × 1 μm. By using EDS to obtained the element composition and the concentration of each element, the atomic ratio of S/Fe of the particulates embedded in the free-floating biofilm was calculated.

Chapter 4: Results

4.1 Chemical characteristics of production water samples

4.1.1 Water chemistry of Putumayo Basin production water

Putumayo Basin, southwest Colombia, South America

In a typical CO_2 related corrosion system, the pH value should be low due to the dissolution of CO_2 to form H_2CO_3 and the dissociation of H_2CO_3 to produce protons. However, the pH value of the four production water samples ranged from 6.84 to 8.55 which didn't fit the presumed CO_2 related corrosion system. The alkalinity ranged from 656 to 2242 (ppm, $CaCO_3$) presumably resulting from porous sandstones and limestones found in the Putumayo Basin (Table 4-1) (Handford & Kairuz, 2000).

The total dissolved iron concentrations ranged from 0.3 ppm to 1452.5 ppm and the ferrous iron was not detected in any of the samples indicating that all dissolved iron was ferric iron (Table 4-1). The dissolved ferric ion concentration in all four samples was oversaturated compared to the highest equilibrium ferric ion concentration of α-FeOOH (goethite) which is around 1×10^{-4} ppm at neutral pH illustrated in Section 2.4.1, and the equilibrium iron concentration of goethite calculated with MINEQL+ is shown in Table 4-2. The oversaturated ferric ion in the production water samples indicated that corrosion occurred within these sampling sites.

Table 4- 1 Water chemistry of Putumayo Basin production water samples

	Loro	Caribe	Acae	Sucombio
pH	8.55	7.84	6.84	7.16
Alkalinity (ppm, $CaCO_3$)	1600	656	1043	2242
Dissolved iron(ppm)	0.3	1.4	9.3	1452.5
Dissolved Mn (ppm)	0.145	0.094	0.272	5.918
Fe(II) (ppm)	0	0	0	0
Sulfate (ppm)	696	318	448	281
Chloride (%, w/v)	0.1	0.01	1.5	1.2
Sulfide (mM)	0	0	0	0
Dissolved O_2 (ppm)	-	-	-	-
Temp. (℃)	-	-	-	-

"¬": not provided;

Nitrate and nitrite were not found in any sample

Unpublished chloride, sulfate, sulfide, nitrate, nitrite and dissolved oxygen data in Table 4-1 was collected by Dr. Joseph Suflita's group from the Department of Microbiology and Plant Biology, University of Oklahoma, Norman campus.

Table 4- 2 Comparison of the measured dissolved iron concentration in the Putumayo Basin production water samples by GF-AAS and the calculated equilibrium iron concentration by MINEQL+

Samples	Loro	Caribe	Acae	Sucombio
pH	8.55	7.84	6.84	7.16
Measured dissolved iron concentration by GF-AAS (ppm)	0.3	1.4	9.3	1452.5
Calculated equilibrium iron concentration by MINEQL+ (ppm)	4.3×10^{-8}	7.2×10^{-9}	4.8×10^{-9}	2.2×10^{-8}
Ratio of measured iron concentration/calculated iron concentration	2.2×10^{8}	1.9×10^{7}	6.3×10^{7}	6.5×10^{10}
Presented solid phase in MINEQL+	goethite	goethite	goethite	goethite
Oxidation state of iron	3	3	3	3
Reason for selecting solid phase in MINEQL+	No ferrous was detected and the only iron ions were ferric ions, therefore, the solid phase was presumably to be α-FeOOH			

Manganese (Mn) is added to the carbon steel during the smelting process. Mn reacts with sulfur to form MnS inclusions and counter the brittleness caused by sulfur (Kopač & Bahor, 1999). In oxic conditions, Mn(IV) is the oxidation state and MnO_2 is the main solid phase (Butterfield *et al*., 2013). The solubility of MnO_2 ranged from 0.1 to 0.3 ppm when the pH ranged from 6.9 to 8.4 (Swain *et al*., 1975). The measured dissolved Mn concentration in the Putumayo Basin production water samples were 0.094 to 5.918 ppm (Table 4-3). Compared with the Swain et al (1975) reported data, the dissolved Mn concentration of Acae and Sucombio were oversaturated, and Caribe and Loro were undersaturated. Smith *et al.* (1987) reported that the average dissolved manganese concentration of 286 U. S. rivers and streams was 24 ppb and USEPA (1984) reported a natural manganese concentration in seawater ranged from 0.4 to 10 ppb. For the Mn concentration in the subsurface water, Ayotte *et al.* (2015) demonstrated that Mn was detected at concentration of 0.03 ppm in the wells of New England Coastal Basin. The results of the measured manganese concentration in the production water samples from the Putumayo Basin ranged from 0.094 ppm to 5.918 ppm as shown in Table 4-3 which was much higher than the natural manganese concentration in the river, steam, and seawater and subsurface water. These MnS inclusions can be susceptible to corrosion (Wranglen, 1974). Therefore, manganese concentration can be used as corrosion monitoring parameter (Bostic *et al.*, 1992; Liang *et al.*, 2015). The dissolved manganese

concentration in these production water samples was presumably coming from the carbon steel corrosion, which supported the claim that corrosion was presented at those sampling sites.

Table 4- 3 Comparison of the measured dissolved Mn concentration in the Putumayo Basin production water samples by GF-AAS and the calculated equilibrium Mn concentration by MINEQL+

Samples	Loro	Caribe	Acae	Sucombio
pH	8.55	7.84	6.84	7.16
Measured dissolved Mn concentration by GF-AAS (ppm)	0.145	0.094	0.272	5.918
Calculated equilibrium Mn concentration by MINEQL+ (ppm)	0.3	0.1 to 0.3	0.1	0.1
Presented solid phase in MINEQL+	MnO_2	MnO_2	MnO_2	MnO_2
Oxidation state of Mn	4	4	4	4
Reason for selecting solid phase in MINEQL+	Under oxic conditions, the solid phase was presumably to be MnO_2			

4.1.2 Water chemistry of Barnett Shale production water

Barnett Shale, north Texas, USA.

Pollastro *et al.* (2007) reported that the overlying of Barnett Shale on Ellenburger Group carbonates results in high-salinity waters and supports the presence of carbonate. All samples had chloride concentration from 2.1 to 2.7%, which was consistent with the geological properties of Barnett Shale as Pollastro et al. reported in 2007. The total dissolved iron concentration was from 2.2 to 160.1 ppm (Table 4-4). Due to low dissolved oxygen concentration (0.000 to 0.082 ppm) (Table 4-4), those production water tanks were under anoxic conditions. Because there was no ferrous ion concentration data, it was postulated that the total dissolved iron was a combination of ferric and ferrous ions, and therefore the presented solid phase could be FeS, $FeCO_3$, $Fe(OH)_2$ and $Fe(OH)_3$. Since no sulfide was found in all five samples, FeS was presumed not to be the solid phase. The solubility constants of $FeCO_{3(S)}$, $Fe(OH)_{2(S)}$ and $Fe(OH)_{3(S)}$ are 2.1×10^{-11}, 8.0×10^{-16} (Davison, 1979) and 7.8×10^{-38} (Blais *et al.*, 2008) respectively. If the production water sample was oversaturated with respect to $FeCO_3$, it was oversaturated compared to $Fe(OH)_2$ and $Fe(OH)_3$. Therefore, $FeCO_3$ was selected as the solid phase. Based on the pH and alkalinity value of those samples, the predicted thermodynamic equilibrium concentration of $FeCO_{3(S)}$ was calculated with MINEQL+ (Table 4-5). The results showed that dissolved iron was oversaturated except SE 19 production water sample which had the lowest

dissolved iron concentration (2.2 ppm). The high dissolved iron concentration indicated that those sampling storage tanks were experienced corrosion. Under anoxic conditions, the dissolved manganese was Mn^{2+}. Because no sulfide was detected, MnS was not considered as solid phase. $MnCO_{3(s)}$ was selected as precipitate to calculate the equilibrium manganese concentration by MINEQL+. The results showed that the dissolved manganese concentration ranged from 0.524 to 3.064 ppm which was lower than the equilibrium manganese concentration of $MnCO_{3(s)}$ (Table 4-5). However, the dissolved manganese concentration was higher than the natural manganese concentration in the river, steam, seawater and subsurface water. The high dissolved manganese concentration in the production water samples supported that corrosion presented in those production water tanks.

Table 4- 4 Water chemistry of Barnett Shale gas tank production water samples

	SE 19	SE 18	SE 17	KJV 7	MC 5
pH	6.92	6.76	6.09	6.45	6.58
Alkalinity (ppm, $CaCO_3$)	185	220	116	70	114
Dissolved iron(ppm)	2.2	58.1	90.4	125.7	160.1
Dissolved Mn (ppb)	526	840	644	3321	2264
Fe(II) (ppm)	-	-	-	-	-
Sulfate (ppm)	6.7	5.5	127	8	15
Chloride (%, w/v)	2.7	2.7	2.7	2.1	2.1
Sulfide (mM)	0	0	0	0	0
Dissolved O_2 (ppm)	0	0	0.082	0	0
Temp. (℃)	30.15	28.56	28.51	30.75	30.19

"-": not provided;

Nitrate and nitrite were not found in any sample

Unpublished chloride, sulfate, sulfide, nitrate, nitrite and dissolved oxygen data collected by Dr. Joseph Suflita's group and Dr. Kathleen Duncan's group from the Department of Microbiology and Plant Biology, University of Oklahoma.

Table 4- 5 Comparison of the measured dissolved iron concentration in the Barnett Shale production water samples by GF-AAS and the calculated equilibrium iron concentration by MINEQL+

Samples	SE 19	SE 18	SE 17	MC 5	KJV 7
pH	6.92	6.76	6.09	6.45	6.58
Measured dissolved iron concentration by GF-AAS (ppm)	2.2	58.1	90.4	160.1	125.7
Calculated equilibrium iron concentration by MINEQL+ (ppm)	9.7	11.6	74.8	28.9	48.6
Ratio of measured iron concentration/calculated iron concentration	0.23	5.0	1.2	5.5	2.6
Presented solid phase in MINEQL+	$FeCO_3$	$FeCO_3$	$FeCO_3$	$FeCO_3$	$FeCO_3$
Oxidation state of iron	+2 & +3	+2 & +3	+2 & +3	+2 & +3	+2 & +3
Reason for selecting solid phase in MINEQL+	Under anoxic conditions, no ferrous concentration data provided, therefore iron ions may present as ferrous and ferric. No sulfide was detected, so FeS wasn't the precipitation. $FeCO_3$ was considered to be the precipitate since the solubility constant of $FeCO_3$ is higher than $Fe(OH)_2$ and $Fe(OH)_3$.				

Table 4- 6 Comparison of the measured dissolved Mn concentration in the Barnett Shale production water samples by GF-AAS and the calculated equilibrium Mn concentration by MINEQL+

	SE 19	SE 18	SE 17	MC 5	KJV 7
pH	6.92	6.76	6.09	6.45	6.58
Measured dissolved Mn concentration by GF-AAS (ppm)	0.526	0.84	0.644	3.321	2.264
Calculated equilibrium Mn concentration by MINEQL+ (ppm)	4.8	36.8	5.7	23.9	14.2
Ratio of measured Mn concentration/calculated Mn concentration	0.11	0.20	0.14	0.13	0.15
Presented solid phase in MINEQL+	$MnCO_3$	$MnCO_3$	$MnCO_3$	$MnCO_3$	$MnCO_3$
Oxidation state of Mn	2	2	2	2	2
Reason for selecting solid phase in MINEQL+	Under anoxic conditions, Mn mostly present as Mn^{2+}. Since no sulfide was detected, MnS was not the precipitate. Therefore, $MnCO_3$ was considered to be the precipitate.				

4.2 Targeted metabolomics analysis by gas chromatography coupled with a mass selective detector

To explain whether Fe(III) was chelating with organic ligands in the production water samples and the formation of Fe(III)-organic ligands caused Fe(III) dissolution, targeted metabolomics was used to measure the organic ligands concentration by Gas Chromatography/Mass Spectroscopy (GC/MS).

4.2.1 Targeted metabolomics results of Putumayo Basin production water samples

As shown in Figure 4-1 and Table 4-7 and 4-8, in Loro and Caribe, three linear monocarboxylic acids (C_4, C_{16}, C_{18}), one hydroxycarboxylic acid (C_7) and one catechol (C_{10}) were identified; in Acae production water samples, four linear and branched monocarboxylic acids (C_4, C_{12}, C_{16}, C_{18}), one hydroxycarboxylic acid (C_7), two aromatic monocarboxylic acids (C_7, C_9) and one catechol (C_{10}) were detected (Figure4-1 and Table 4-9); in Sucombio which had the most peak numbers and highest total peak area, thirteen linear and branched monocarboxylic acids (C_5 - C_8, C_{12}, C_{14}, C_{16} - C_{18}), one linear dicarboxylic acid (C_4), two hydroxycarboxylic acids (C_3, C_7), seven aromatic monocarboxylic acids (C_7 - C_9), one aromatic dicarboxylic acids (C_8), ten linear and cyclic alcohol (C_6 - C_9) and one catechol (C_{10}) were found (Figure 4-1 and Table 4-10). In the metabolites, the peak area of monocarboxylic acids and aromatic monocarboxylic acids, hexanoic acid, heptanoic acid, 4-hydroxybutanoic acid, 2-ethylcyclohexanol, benzoic acid and 4-methyl benzoic

acid, accounted for 63.1% of the total peak area. All sample spectra have same scale in Figure 4-1.

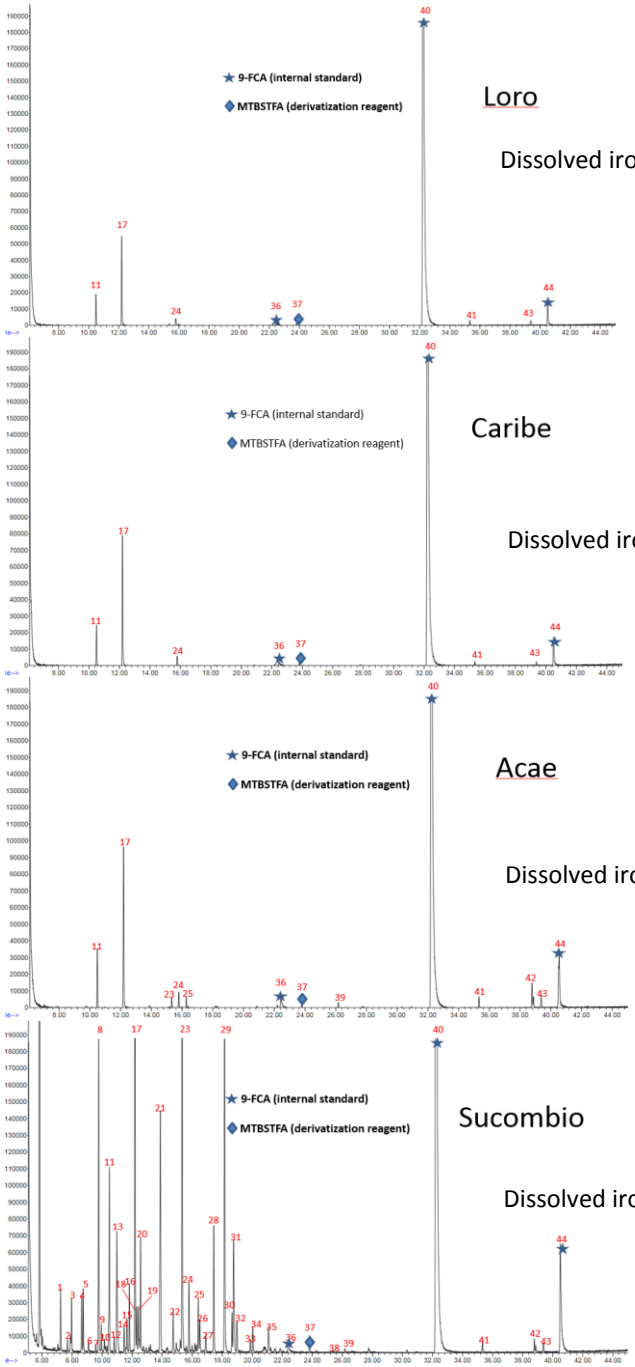

Figure 4- 1 GC/MS spectra of Putumayo Basin production water samples by using MTBSTFA as derivatization reagent (from the top to the bottem: Loro, Caribe, Acae, and Sucombio). The all samples had same dilution and the spectra had same intensity.

Table 4- 7 Peak area of compounds detected in GC/MS spectrum of Loro production water samples from the Putumayo Basin by using MTBSTFA as derivatization reagent

#	R. T. * (min)	Compounds	Peak area
11	10.439	heptanoic acid	47566
17	12.203	4-hydroxybutanoic acid	150702
24	15.792	4-tert-butylcatechol	12668
41	35.327	hexadecanoic acid	9768
43	39.396	octadecanoic acid	10830

"*" R.T. : Retention time

Table 4- 8 Peak area of compounds detected in GC/MS spectrum of Caribe production water samples from the Putumayo Basin by using MTBSTFA as derivatization reagent

#	R. T. (min)	Compounds	Peak area
11	10.439	heptanoic acid	65116
17	12.203	4-hydroxybutanoic acid	224903
24	15.792	4-tert-butylcatechol	17649
41	35.327	hexadecanoic acid	7176
43	39.396	octadecanoic acid	11299

Table 4- 9 Peak area of compounds detected in GC/MS spectrum of Acae production water samples from the Putumayo Basin by using MTBSTFA as derivatization reagent

#	R. T. (min)	Compounds	Peak area
11	10.439	heptanoic acid	61235
17	12.203	4-hydroxybutanoic acid	201015
23	15.340	benzoic acid	11741
24	15.792	4-tert-butylcatechol	17279
25	16.278	benzeneacetic acid	10380
39	26.165	dodecanoic acid	7005
41	35.327	hexadecanoic acid	16166
42	38.887	13-octadecenoic acid	33213
43	39.396	octadecanoic acid	19224

Table 4- 10 Peak area of compounds detected in GC/MS spectrum of Sucombio production water samples from the Putumayo Basin by using MTBSTFA as derivatization reagent

#	R.T. (min)	Compound	Peak area	#	R.T. (min)	Compound	Peak area
1	7.265	pentanoic acid	155920	22	14.729	1-methylcyclohexane carboxylic acid	164245
2	7.716	3-hydroxypropanoic acid	28800	23	15.340	benzoic acid	2524845
3	7.916	3-heptanol	189365	24	15.792	4-tert-butylcatechol	242785
4	8.653	3-methylpentanoic acid	140361	25	16.278	benzeneacetic acid	175803
5	8.762	4-methylvaleric acid	164008	26	16.518	cyclohexanol	104645
6	9.111	2-propyl-1-pentanol	24474	27	16.906	2-phenylethanol	70802
7	9.585	1-octanol	23375	28	17.449	3-methyl benzoic acid	454049
8	9.779	hexanoic acid	980809	29	18.158	4-methyl benzoic acid	1706298
9	9.962	2-ethyl-1-hexanol	76881	30	18.65	benzenepropanoic acid	110316
10	10.185	6-methyl-2-heptanol	51289	31	18.775	2-methyl benzoic acid	505113
11	10.439	heptanoic acid	675521	32	18.981	2-phenylbutyric acid	135183
12	10.808	3-methylphenol	46998	33	19.878	3,4-dimethylbenzoic acid	63380
13	10.997	cycloheptanol	484033	34	20.050	benzenepropanoic acid	116080
14	11.471	heptanoic acid	75567	35	21.090	3,4-dimethylbenzoic acid	124969
15	11.603	levulinic acid	121788	37	23.816	derivatization reagent	87398
16	11.825	2-ethylcyclohexanol	205283	38	25.359	succinic acid	10458
17	12.203	4-hydroxybutanoic acid	1719061	39	26.165	dodecanoic acid	18268
18	12.426	1-cyclohexylethanol	153815	41	35.327	hexadecanoic acid	30681
19	12.483	2-octenoic acid	387710	42	38.887	13-octadecenoic acid	31173
20	12.568	heptanoic acid	387710	43	39.396	octadecanoic acid	27228
21	13.883	2-ethylcyclohexanol	1105291				

The stability constants of dicarboxylic acids, α-hydroxycarboxylic acids, and PEG carboxylic acids are two to several orders of magnitude higher than monocarboxylic acids which suggests that those organic acids bond strongly enough to displace oxide and hydroxide and thus form the Fe(III)-ligand complexes and facilitate dissolution of Fe(III). However, in the GC/MS spectra of using MTBSTFA as the derivatization reagent, only succinic acid was detected. BSTFA was used to replace MTBSTFA as the derivatization reagent because Pietrogrande *et al*. (2002) suggested in GC/MS, C_3–C_9 dicarboxylic acids had low detection limits (≤2 ng/m^3) and high reproducibility (RSD% ≤ 10%) when using BSTFA as derivatization reagent; BSTFA reacts quickly, and the stable products are leading to low detector noise (Aktas *et al*., 2010); and the high volatility of BSTFA (boiling point: 45-50 °C) results in earlier eluting peaks and easier separation from organic metabolites than MTBSTFA which has a higher boiling point at 175°C. Figure 4-2 and Table 4-11 showed peaks detected in the GC/MS spectrum of Sucombio production water sample with BSTFA as derivatization reagent.

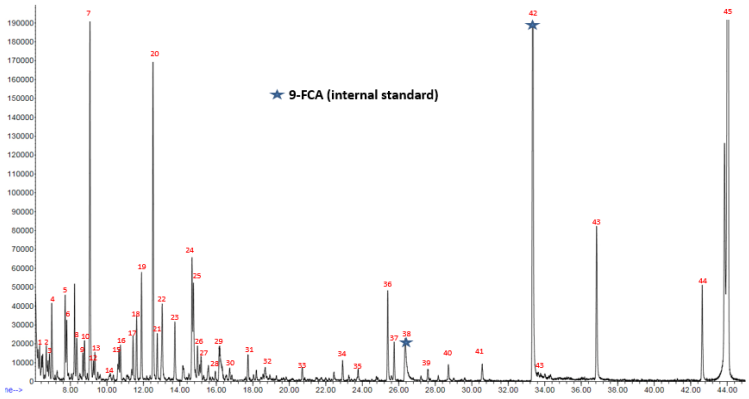

Figure 4- 2 GC/MS spectrum of Sucombio production water sample from the Putumayo Basin by using BSTFA as derivatization reagent

Table 4- 11 List of compounds detected in the GC-MS spectrum of Sucombio production water sample from the Putumayo Basin by using BSTFA as derivatization reagent

#	R.T. (min)	Compounds	#	R.T. (min)	Compounds
1	6.202	propanoic acid	24	14.735	diglycolic acid
2	6.407	H_3BO_3	25	14.946	benzenepropanoic acid
3	6.665	2-hydroxybutanoic acid	26	15.129	2-methyl-pentanedioic acid
4	6.745	heptanoic acid	27	15.520	3-methyl pentanedioic acid
5	7.705	4-methylvaleric acid	28	15.775	2-[2-(2-hydroxyethoxy)ethoxy]-acetic acid
6	7.790	glycolic acid	29	16.289	3,4-dimethylbenzoic acid
7	8.042	2-hexanol	30	16.695	hexanoic acid
8	8.322	4-oxohexanoic acid	31	18.225	2-[2-[2-(2-hydroxyethoxy)ethoxy]ethoxy]-acetic acid
9	8.665	3-octenoic acid	32	18.524	hexanedioic acid
10	8.762	hexanoic acid	33	20.701	3-hydroxybenzoic acid
11	9.048	Benzoic acid	34	22.896	4-hydroxybenzoic acid
12	9.328	cyclohexaneacetic acid	35	23.742	dodecanoic acid
13	9.608	octanoic acid	36	25.382	1,2-benzenedicarboxylic acid
14	10.174	4-oxohexanoic acid	37	25.731	3-methyl-4-hydroxybenzoic acid
15	10.637	cyclohexaneacetic acid	38	26.354	internal standard
16	10.722	benzeneacetic acid	39	27.583	1,3-benzenedicarboxylic acid
17	11.425	succinic acid	40	28.703	1,4-benzenedicarboxylic acid
18	11.631	2-methylbenzoic acid	41	30.520	tetradecanoic acid
19	11.877	methylsuccinic acid	42	33.361	internal standard
20	12.506	3-methylbenzoic acid	43	33.696	pentadecanoic acid
21	12.751	diethylene glycol	44	36.864	hexadecanoic acid
22	12.991	4-methylbenzoic acid	45	42.614	octadecanoic acid
23	13.706	phenylethanol	46	43.831	unidentified

Table 4-12 compared the high binding constant compounds, such as dicarboxylic acids, α-hydroxycarboxylic acids, and PEG carboxylic acids detected in the BSTFA and MTBSTFA derivatized GC/MS spectra. The identification results showed that

only succinic acid was detected in the MTBSTFA derivatized GC/MS spectrum while seven more dicarboxylic acids, α-hydroxycarboxylic acids, and polyethylene glycol (PEG) carboxylic acids were detected in the BSTFA derivatized GC/MS spectrum of Sucombio production water sample which supported the change of derivatization reagent.

Table 4- 12 Comparison of detectability of dicarboxylic acids, α-hydroxycarboxylic acids and PEG-carboxylic acids in the GC/MS spectra between reagent MTBSTFA and BSTFA

	Area of targeted compounds/internal standard	
Compounds	MTBSTFA	BSTFA
2-hydroxybutanoic acid	Not detected	Detected
succinic acid	Detected	Detected
methylsuccinic acid	Not detected	Detected
diglycolic acid	Not detected	Detected
2-methyl-pentanedioic acid	Not detected	Detected
3-methyl pentanedioic acid	Not detected	Detected
2-[2-[2-(2-hydroxyethoxy)ethoxy]ethoxy]-acetic acid	Not detected	Detected
hexanedioic acid	Not detected	Detected

In the production water samples, organic ligands existed as free ligands which didn't bind with Fe(III) and Fe-bound ligands. When samples were acidified to pH

= 2 and extracted with EtOAc, only free ligands were extracted. When the production water samples were increased pH to 12, Fe(III) precipitated as $Fe(OH)_{3(S)}$ and Fe-bound ligands were released. Samples were filtered to remove $Fe(OH)_{3(S)}$, acidified to pH =2 and extracted with EtOAc, the EtOAc extracts had the total ligands including free ligands and Fe-bound ligands. Therefore, if the dissolved iron was binding with organic ligands in the production water samples, the pH increase should lead to the increase of peak area of organic ligands. As shown in Figure 4-3 and Table 4-13, after increase pH to 12 in the "Total ligands" sample, the total peak area of dicarboxylic acids, α-hydroxycarboxylic acids, and polyethylene glycol (PEG) carboxylic acids was 460.1% increase of peak area compared to the "Free ligands" sample which supported our hypothesis that the formation of complexes of Fe(III) and organic ligands facilitated the high dissolved iron concentration in the production water samples.

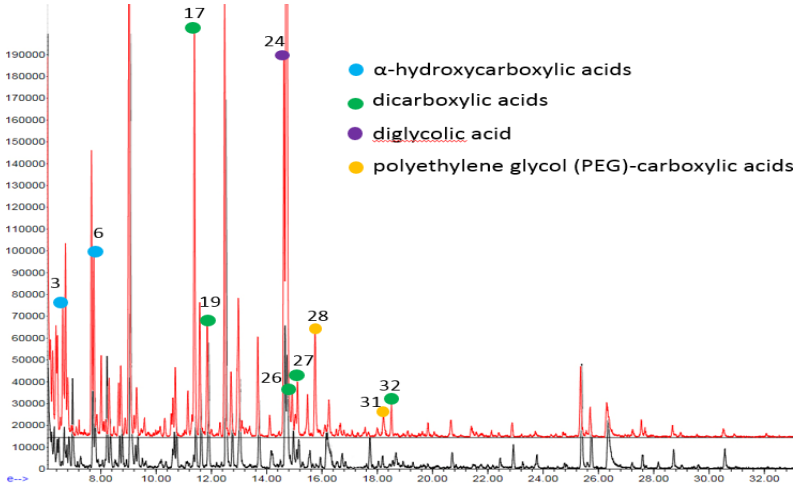

Figure 4- 3 GC/MS trace comparison of Free ligands (bottom spectrum) and Total ligands (top spectrum) samples for Sucombio production water sample from the Putumayo Basin by using BSTFA as derivatization reagent

Table 4- 13 List of peak area of dicarboxylic acids, α-hydroxycarboxylic acids, and polyethylene glycol (PEG) carboxylic acids in the "Free ligands" sample and "Total ligands" sample detected in the GC-MS spectra of Sucombio production water sample from the Putumayo Basin by using BSTFA as derivatization reagent

#	R.T. (min)	Compounds	Free ligands	Total ligands	Increase of area (%)
3	6.665	2-hydroxybutanoic acid	40317	136683	239.0
6	7.79	glycolic acid	--	143729	--
17	11.425	succinic acid	90877	612230	573.7
24	14.735	diglycolic acid	406510	2270814	458.6
26	15.129	2-methyl-pentanedioic acid	54449	85290	56.6
28	15.775	2-[2-(2-hydroxyethoxy)ethoxy] acetic acid	--	191727	--
31	18.225	2-[2-[2-(2-hydroxyethoxy)ethoxy]ethoxy] acetic acid	20952	26577	26.8
32	18.524	hexanedioic acid	13705	43497	217.4
Total peak area			804027	3677254	460.1

"--": not detected

4.2.2 Targeted metabolomics results of production water samples from the Barnett Shale

For the Barnett Shale production water samples, BSTFA was used as derivatization reagent. As shown in Figure 4-4, Table 4-14 through 4-19, in the SE 19 sample, linear and branched monocarboxylic acids (C_6, C_8, C_{16}, C_{22}), hydroxycarboxylic acids (C_2, C_4 - C_5, C_8), linear and branched dicarboxylic acids (C_2, C_5), aromatic monocarboxylic acids (C_7, C_8), linear and branched alcohols (C_2, C_5,

C_6, C_{28}), two cyclic alcohols (C_5, C_6) and three phenols (C_6, C_8, C_{14}) were detected. In the SE 18 sample, linear and branched monocarboxylic acids (C_6, C_8, C_{16}), hydroxycarboxylic acids (C_2, C_5), linear and branched dicarboxylic acids (C_2, C_4 - C_7), aromatic monocarboxylic acids (C_7, C_8), linear and branched alcohol (C_2, C_3), cyclic alcohol (C_6) and phenol (C_7, C_8) were found. In the SE 17 sample, linear and branched monocarboxylic acids (C_6 - C_8, C_{14}, C_{16}, C_{20}, C_{22}), hydroxycarboxylic acids (C_2, C_4), cyclic aliphatic acids (C_8), linear and branched dicarboxylic acids (C_5 - C_6), aromatic monocarboxylic acids (C_7 - C_9), linear and branched alcohol (C_3, C_5), cyclic alcohol (C_6, C_7) and phenol (C_7 - C_8) were found. In the KJV 7 sample, linear and branched monocarboxylic acids (C_6 - C_8, C_{22}), hydroxycarboxylic acids (C_2, C_4 - C_5, C_7), cyclic aliphatic acids (C_7), linear and branched dicarboxylic acids (C_2, C_5, C_7), aromatic monocarboxylic acids (C_7 - C_{10}), linear and branched alcohol (C_3, C_5, C_8, C_{12}, C_{14}), cyclic alcohol (C_5 - C_7, C_{10}) and phenol (C_7 - C_8) were found. In the MC 5 water sample, linear and branched monocarboxylic acids (C_6, C_8, C_{20}, C_{22}), hydroxycarboxylic acids (C_2), linear and branched dicarboxylic acids (C_5, C_7), aromatic monocarboxylic acids (C_7 – C_8), linear and branched alcohol (C_2 - C_3, C_5, C_{24}, C_{28}), cyclic alcohol (C_4) and phenol (C_7 - C_8) were found.

The peak identification information and peak area of the GC/MS spectra of Barnett Shale production water samples were shown in Figure 4-4 and Table 4-14 to 4-19. All sample dilution factors and the scale of the sample spectra were same.

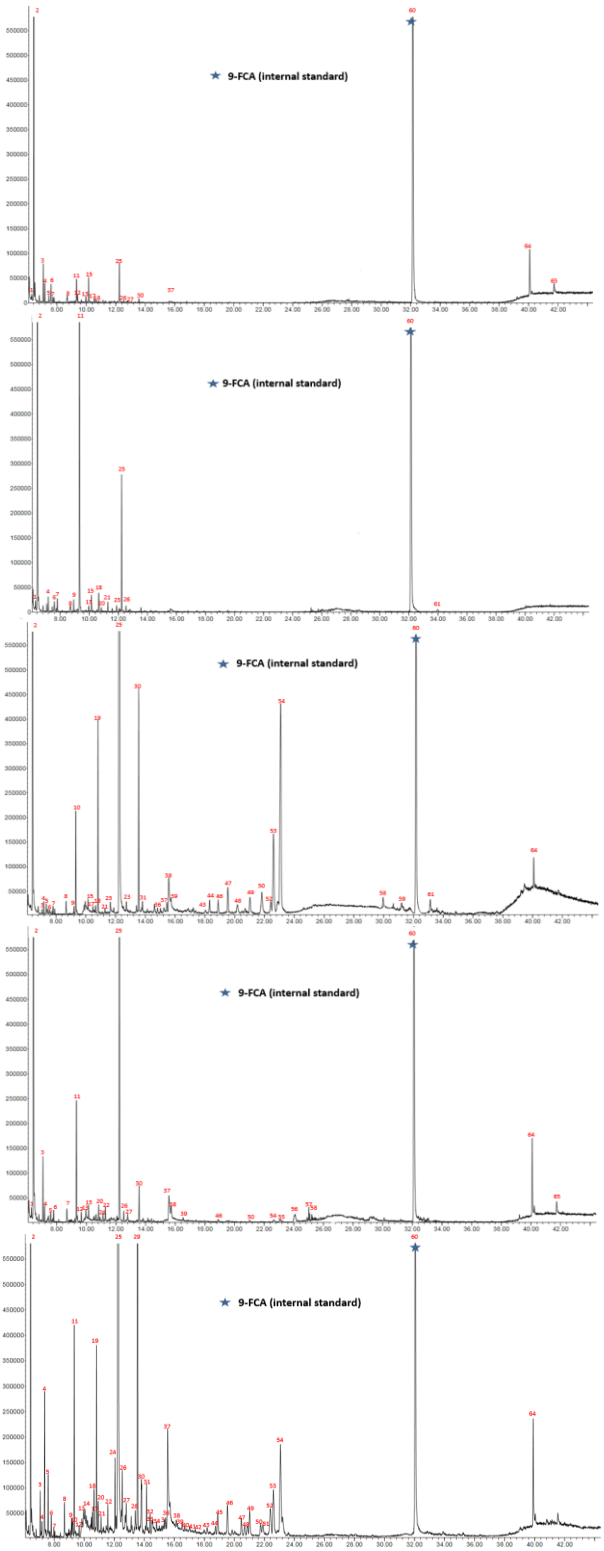

Figure 4- 4 GC/MS spectra of Barnett Shale production water samples by using BSTFA as derivatization reagent (from the top to the bottem: SE 19, SE 18, SE 17, KJV 7 and MC 5). The all samples had same dilution and the spectra had same intensity.

Table 4- 14 List of all of compounds detected in the GC-MS spectra of all five Barnett Shale production water samples by using BSTFA as derivatization reagent

#	R.T. (min)	Compounds	#	R.T. (min)	Compounds
1	6.310	ethylene glycol	34	14.809	1,8-octanediol
2	6.430	H_3BO_3	35	15.346	3,4-dimethylbenzoic acid
3	7.071	cyclopentanolide	36	15.432	methyltris(trimethylsiloxy)silane
4	7.173	2-cyclohexenol	37	15.575	N,N-dimethyl-1-dodecanamine
5	7.356	tetrahydro-2H-pyran-2-one	38	15.723	hexanedioic acid
6	7.597	2-ethylhexanoic acid	39	16.518	3-methylhexanedioic acid
7	7.802	glycolic acid	40	16.792	2,6-ditert-butylphenol
8	8.682	2-methyl phenol	41	17.032	2,4,6-trimethylbenzoic acid
9	8.922	oxalic acid	42	17.387	1-dodecanol
10	9.162	2-hydroxybutanoic acid	43	18.181	1,2-cyclohexanedicarboxylic acid
11	9.328	2-butoxyacetic acid	44	18.753	methylphosphorous acid
12	9.665	2-chlorocyclohexanol	45	18.896	unidentified
13	9.854	4-hydroxyvaleric acid	46	19.547	3-methyxoyphenol
14	10.048	1-ethylphenol	47	20.479	4-methyxoyphenol
15	10.071	2,4-dimethylphenol	48	20.856	2-cyclodecenol
16	10.240	1-butanamine	49	21.016	2-heptenoic acid
17	10.425	cyclopentanol	50	21.753	3-cyclodecenol
18	10.661	benzoic acid	51	21.822	9,12-tetradecadienol
19	10.823	1,5-pentanediol	52	22.422	3-methylbenzoic acid
20	10.928	octanoic acid	53	22.593	3-(2-oxocyclohexyl)propionaladehyde
21	11.294	glycerol	54	23.210	4-methylbenzoic acid
22	11.580	benzeneacetic acid	55	24.102	N-mehtyl-N-octyl-1-octanamine
23	11.889	succinic acid	56	25.08	13-cis-retinoic acid
24	12.066	2-methylbenzoic acid	57	25.457	5,8,11-eicosatriynoic acid
25	12.289	4-methylbenzoic acid	58	30.075	tetradecanoic acid
26	12.529	6-Chlorohexanol	59	31.189	cis-5,8,11-eicosatrienoic acid
27	13.123	7-oxo-octanoic acid	60	32.096	internal standard
28	13.405	cyclohexanone-3-carboxylic acid	61	34.024	hexadecanoic acid
29	13.552	pentanedioic acid	62	35.75	octadecanoic acid
30	13.837	phthalimidine	63	36.956	tetracosan-1-ol
31	14.14	3,4-dimethylbenzoic acid	64	40.071	docosanoic acid
32	14.392	2-deoxytetronoic acid	65	41.722	1-octacosanol
33	14.557	2-hydroxyclohexane-1-carboxylic acid			

Table 4- 15 Peak area of compounds detected in GC-MS spectrum of SE 19 production water sample from the Barnett Shale by using BSTFA as derivatization reagent

#	Compounds	Peak area	#	Compounds	Peak area
1	ethylene glycol	25460	15	2,4-dimethylphenol	93134
2	H3BO3	4508764	17	2-hydroxyocatnoic acid	16054
3	cyclopentanol	114678	18	benzoic acid	13988
4	2-cyclohexenol	54789	25	4-methylbenzoic acid	145470
5	phenol	22668	26	methylsuccinic acid	8496
6	glycolic acid	62519	29	pentanedioic acid	21740
7	2-ethylhexanoic acid	22715	40	2,6-ditert-butylphenol	9174
8	oxalic acid	39055	61	hexadecanoic acid	9047
10	3-hydroxybutanoic acid	11274	64	docosanoic acid	244111
11	2-butoxyacetic acid	104605	65	1-octacosanol	99370
13	4-hydroxyvaleric acid	20191			

Table 4- 16 Peak area of compounds detected in GC-MS spectrum of SE 18 production water sample from the Barnett Shale by using BSTFA as derivatization reagent

#	Compounds	Peak area	#	Compounds	Peak area
1	ethylene-glycol	34316	15	2,4-dimethylphenol	58666
2	H_3BO_3	2952670	18	benzoic acid	68459
4	2-cyclohexenol	45596	20	octanoic acid	16620
6	glycolic acid	42244	21	glycerol	33461
7	2-ethylhexanoic acid	54264	23	succinic acid	26668
8	oxalic acid	35326	25	4-methylbenzoic acid	488941
9	3-hydroxypropanoic acid	35611	26	methylsuccinic acid	27404
11	2-butoxyacetic acid	1383928	61	hexadecanoic acid	28094
13	4-hydroxyvaleric acid	19505			

Table 4- 17 Peak area of compounds detected in GC/MS spectrum of SE 17 production water sample from the Barnett Shale by using BSTFA as derivatization reagent

#	Compounds	Peak area	#	Compounds	Peak area
2	H_3BO_3	3960108	35	3,4-dimethylbenzoic acid	34525
4	2-cyclohexenol	60972	37	N,N-dimethyl-1-dodecanamine	524083
5	phenol	52334	38	hexanedioic acid	24566
6	glycolic acid	46785	43	1,2-cyclohexanedicarboxylic acid	94800
7	2-ethylhexanoic acid	27747	45	unidentified	93748
8	oxalic acid	59468	46	3-methyxoyphenol	215249
10	3-hydroxybutanoic acid	25003	47	4-methyxoyphenol	112206
11	2-butoxyacetic acid	372522	49	2-heptenoic acid	175474
15	2,4-dimethylphenol	24530	50	3-cyclodecenol	311437
18	benzoic acid	27667	52	3-methylbenzoic acid	92813
19	1,5-pentanediol	671239	53	3-(2-oxocyclohexyl) propionaladehyde	842354
21	glycerol	87161	54	4-methylbenzoic acid	2256363
23	succinic acid	42355	58	tetradecanoic acid	86075
25	4-methylbenzoic acid	43707795	59	cis-5,8,11-eicosatrienoic acid	140635
26	methylsuccinic acid	66324	61	hexadecanoic acid	57158
29	pentanedioic acid	827628	64	docosanoic acid	207550
30	phthalimidine	64853			

Table 4- 18 Peak area of compounds detected in GC-MS spectrum of KJV 7 production water sample from the Barnett Shale by using BSTFA as derivatization reagent

#	Compounds	Peak area	#	Compounds	Peak area
2	H_3BO_3	2034260	29	pentanedioic acid	4136358
3	cyclopentanol	144498	30	phthalimidine	463820
4	2-cyclohexenol	56270	31	3,4-dimethylbenzoic acid	287176
5	tetrahydro-2H-pyran-2-one	585035	32	2-deoxytetronoic acid	91741
6	2-ethylhexanoic acid	102400	33	2-hydroxyclohexane-1-carboxylic acid	169232
7	glycolic acid	82317	34	1,8-octanediol	58805
8	2-methyl phenol	111018	35	3,4-dimethylbenzoic acid	75706
9	oxalic acid	89874	36	unidentified	60310
10	2-hydroxybutanoic acid	120413	37	N,N-dimethyl-1-dodecanamine	1E+06
11	2-butoxyacetic acid	679099	39	3-methylhexanedioic acid	51649
12	2-chlorocyclohexanol	103377	41	2,4,6-trimethylbenzoic acid	43351
13	4-hydroxyvaleric acid	53984	43	1,2-cyclohexanedicarboxylic acid	44837
14	1-ethylphenol	77094	44	methylphosphorous acid	70479
17	cyclopentanol	43623	46	3-methyxoyphenol	244839
18	benzoic acid	147082	47	4-methyxoyphenol	79061
19	1,5-pentanediol	667450	48	2-cyclodecenol	75019
20	octanoic acid	120706	49	2-heptenoic acid	203351
21	glycerol	54386	50	3-cyclodecenol	83264
22	benzeneacetic acid	172199	51	9,12-tetradecadienol	73247
24	2-methylbenzoic acid	282112	52	3-methylbenzoic acid	302512
25	4-methylbenzoic acid	67404090	53	3-(2-oxocyclohexyl)propionaladehyde	458311
26	6-Chlorohexanol	268990	54	4-methylbenzoic acid	1157080
27	7-oxo-octanoic acid	109998	64	docosanoic acid	549422
28	cyclohexanone-3-carboxylic acid	109092			

Table 4- 19 Peak area of compounds detected in GC-MS spectrum of MC 5 production water sample from the Barnett Shale by using BSTFA as derivatization reagent

#	Compounds	Peak area	#	Compounds	Peak area
1	ethylene glycol	35293	21	glycerol	66199
2	H_3BO_3	5459861	25	4-methylbenzoic acid	2514679
3	cyclopentanol	203411	26	6-Chlorohexanol	41360
4	2-cyclohexenol	49582	29	pentanedioic acid	134572
5	tetrahydro-2H-pyran-2-one	44995	30	phthalimidine	22442
6	2-ethylhexanoic acid	54113	37	N,N-dimethyl-1-dodecanamine	190656
7	glycolic acid	45695	39	3-methylhexanedioic acid	36067
8	2-methyl phenol	68077	53	3-(2-oxocyclohexyl) propionaladehyde	29220
11	2-butoxyacetic acid	421935	54	4-methylbenzoic acid	25879
12	2-chlorocyclohexanol	70668	55	N-mehtyl-N-octyl-1-octanamine	121577
15	2,4-dimethylphenol	40389	56	13-cis-retinoic acid	66858
18	benzoic acid	25593	63	tetracosan-1-ol	37396
19	1,5-pentanediol	58227	64	docosanoic acid	397134
20	octanoic acid	19467	65	1-octacosanol	41.734

As described in the results of targeted metabolomics by GC/MS analysis of Sucombio production water, with pH increase, the Fe(III)-organic ligand complexes dissociated. Fe(III) precipitated as $Fe(OH)_{3(S)}$ and organic ligands released which caused the peak area of organic ligands increased as shown in Figure 4-5. This data supported our hypothesis that the formation of Fe(III) and organic ligand complexes caused the high dissolved iron concentration in the production water samples.

Since the stability constants of dicarboxylic acids and α-hydroxycarboxylic acids are two to several orders of magnitude higher than monocarboxylic acids which suggests that those organic acids bond strongly enough to displace oxide and hydroxide and thus form the Fe(III)-ligand complexes and facilitate dissolution of Fe(III). The relationship between Fe(III) and those organic ligands was investigated by comparing the total peak area of dicarboxylic acids and α-hydroxycarboxylic acids in the "Total ligands" sample and the concentration of dissolved iron. After a retention time of 20 minutes, there were no dicarboxylic acids and α-hydroxycarboxylic acids were detected in all five samples. In order to show the details of dicarboxylic acids and α-hydroxycarboxylic acids, the GC/MS spectra of Barnett Shale production water samples were enlarged, and the retention time was from 6 to 20 minutes as shown in Figure 4-5 and Table 4-20 to 4-24. All sample spectra have the same scale as shown in Figure 4-5.

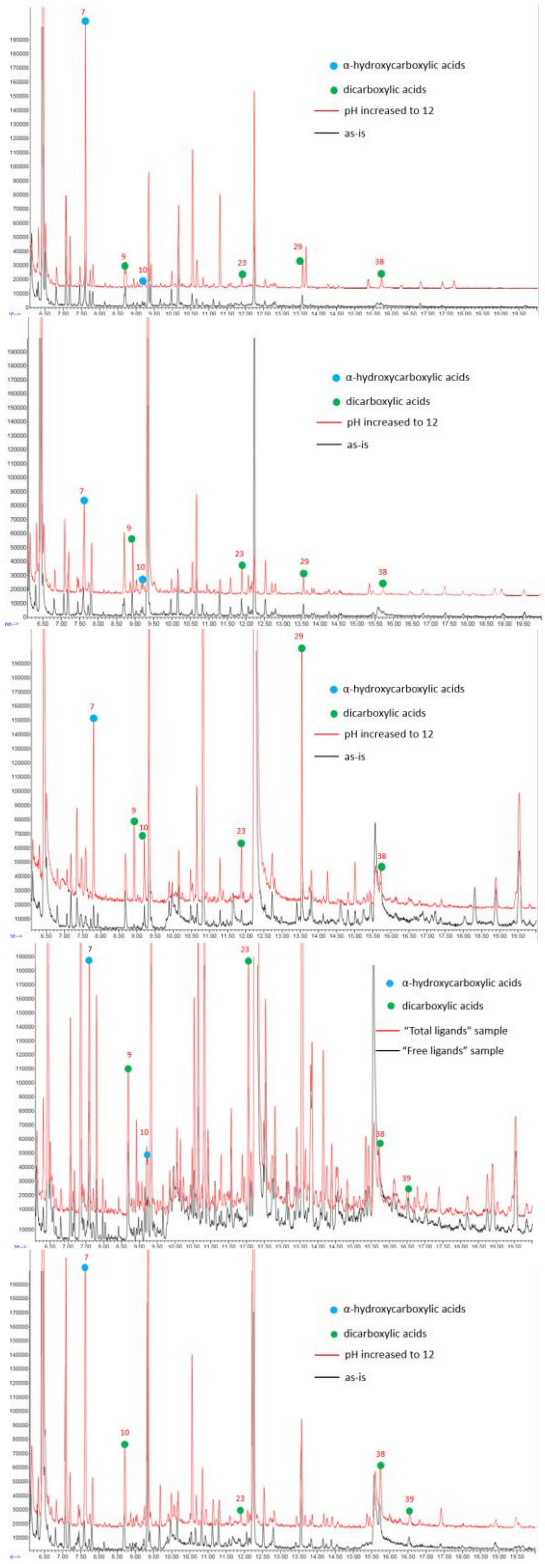

Figure 4- 5 GC/MS trace comparison of the "Total ligands" sample (top spectrum) and "Free ligands" samples (bottom spectrum) for SE 19, SE 18, SE 19, KJV 7 and MC 5 (from the bottom to the top) production water sample from the Barnett Shale

Table 4- 20 Comparison of peak area of dicarboxylic acids and α-hydroxycarboxylic acids in the GC/MS spectrum of "Free ligands" and "Total ligands" samples for SE 19 production water sample from the Barnett Shale

#	R.T. (min)	Compounds	Peak area		Increase of area (%)
			Free ligands	Total ligands	
7	7.802	glycolic acid	22715	37366	64.5
9	8.922	oxalic acid	Not detected	16552	Not calculated
10	9.162	2-hydroxybutanoic acid	11274	17381	54.2
23	11.889	succinic acid	Not detected	18746	Not calculated
29	13.552	pentanedioic acid	21740	33114	52.3
38	15.723	hexanedioic acid	Not detected	23572	Not calculated
Total area			55729	146731	163.3

Table 4- 21 Comparison of peak area of dicarboxylic acids and α-hydroxycarboxylic acids in the GC/MS spectrum of "Free ligands" and "Total ligands" samples for SE 18 production water sample from the Barnett Shale

#	R.T. (min)	Compounds	Peak area		Increase of area (%)
			Free ligands	Total ligands	
7	7.802	glycolic acid	54264	64935	19.7
9	8.922	oxalic acid	35611	53332	49.8
10	9.162	2-hydroxybutanoic acid	17815	33512	88.1
23	11.889	succinic acid	26668	30017	12.6
29	13.552	pentanedioic acid	16159	20989	29.9
38	15.723	hexanedioic acid	Not detected	19745	Not calculated
Total area			150517	222530	47.8

Table 4- 22 Comparison of peak area of dicarboxylic acids and α-hydroxycarboxylic acids in the GC/MS spectrum of "Free ligands" and "Total ligands" samples for SE 17 production water sample from the Barnett Shale

#	R.T. (min)	Compounds	Peak area		Increase of area (%)
			Free ligands	Total ligands	
7	7.802	glycolic acid	46785	102400	118.9
9	8.922	oxalic acid	59468	91018	53.1
10	9.162	2-hydroxybutanoic acid	42355	85589	102.1
23	11.889	succinic acid	66324	86192	30.0
29	13.552	pentanedioic acid	82762	112493	35.9
38	15.723	hexanedioic acid	24566	46979	91.2
Total area			322260	638375	98.1

Table 4- 23 Comparison of peak area of dicarboxylic acids and α-hydroxycarboxylic acids in the GC/MS spectrum of "Free ligands" and "Total ligands" samples for KJV 7 production water sample from the Barnett Shale

#	R.T. (min)	Compounds	Peak area		Increase of area (%)
			Free ligands	Total ligands	
7	7.802	glycolic acid	82317	243194	195.4
9	8.922	oxalic acid	89874	131661	46.5
10	9.162	2-hydroxybutanoic acid	120413	128063	6.35
23	11.889	succinic acid	Not detected	113335	Not calculated
29	13.552	pentanedioic acid	Not detected	62046	Not calculated
38	15.723	hexanedioic acid	51649	90511	75.2
Total area			344253	768810	123.3

Table 4- 24 Comparison of peak area of dicarboxylic acids and α-hydroxycarboxylic acids in the GC/MS spectrum of "Free ligands" and "Total ligands" samples for MC 5 production water sample from the Barnett Shale

#	R.T. (min)	Compounds	Peak area		Increase of area (%)
			Free ligands	Total ligands	
7	7.802	glycolic acid	45695	569077	1145.4
10	9.162	2-hydroxybutanoic acid	Not detected	24219	Not calculated
23	11.889	succinic acid	133866	134572	5.2
38	15.723	hexanedioic acid	Not detected	83077	Not calculated
39	16.518	3-methylhexanedioic acid	36067	36115	0.13
Total area			216334	846354	291.2

Moreover, after increase pH to 12, the Fe(III)-organic ligands complexes dissociated, a linear relationship between the total peak area of dicarboxylic acids & α-hydroxycarboxylic acids and the dissolved iron was found, which suggests that the dissolved iron concentration was controlled by organic ligands concentration as shown in Table 4-25 and Figure 4-6.

Table 4- 25 Comparison of the ratio of total area of dicarboxylic acids and α-hydroxycarboxylic acids and the dissolved iron concentration measured by AAS in the Barnett Shale production water samples

Samples	Ratio of total peak area of dicarboxylic acids and α-hydroxy carboxylic acids/internal standard	Measured dissolved iron concentration (ppm)
SE 17	0.1008	2.2
SE 18	0.1428	58.1
SE 19	0.4240	90.4
KJV 7	0.4794	125.7
MC 5	0.5972	160.1

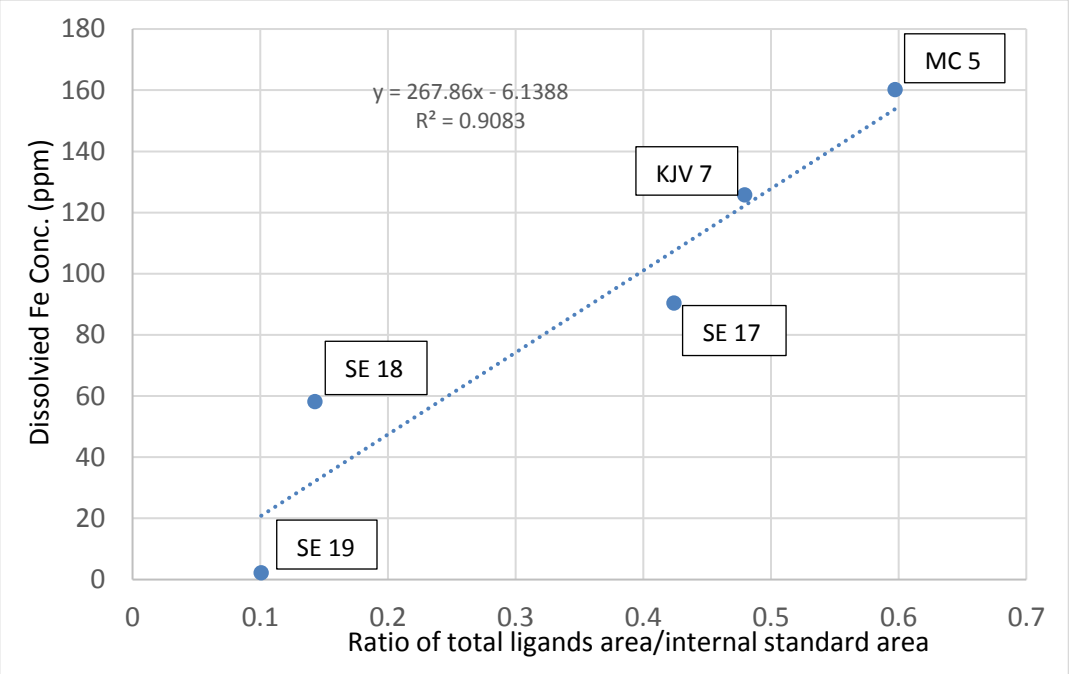

Figure 4- 6 Linear relationship between the ratio of total organic ligands peak area/internal standard area and the dissolved iron concentration in the Barnett Shale production water samples

4.3 Qualitative carbon steel corrosion assay under aerobic conditions with filtered Putumayo Basin production water samples

As illustrated in Section 2.3.2, organic acids facilitate dissolution of iron oxides by forming Fe(III)-organic ligand complexes. The goal of the carbon steel corrosion assay was to test the ability of dissolution of iron oxyhydroxides, the corrosion products on the steel surface by Putumayo Basin production water samples.

Production water samples were filtered with 0.20 μm PES membrane to sterilize the sample and eliminate the influence of microorganisms on the corrosion morphology of the steel coupon. Therefore, the concentration of organic ligands was the main parameter that contributed to the characteristics of corrosion products. The production water samples and coupons were incubated under aerobic conditions so that the oxidation products, ferrous iron was further oxidized to ferric iron and formed iron oxyhydroxide precipitate on the steel surface (Yamashita *et al*., 1994a, Yamashita *et al*., 1994b). Yumoto *et al*. (2002) illustrated that the cementite (Fe_3C) accumulates on the steel coupon surface during the corrosion process. After incubated with production water samples, carbon steel coupon was removed and examined with SEM-EDS to characterize composition and features of the corrosion products.

The results showed that no ferric oxyhydroxide corrosion products were found on the steel surface incubated with the Sucombio sample which had the most organic acids. However, the corrosion products of the control, Acae, and Caribe all have iron oxyhydroxides. The results indicated that the iron oxyhydroxide was

removed by organic ligands (Table 4-26 and Figure 4-7). By showing such corrosivity as a function of the concentration of the dissolved ligands, it could be inferred that the ligands were helping to facilitate steel corrosion under aerobic conditions by dissolution of the corrosion products --iron oxyhydroxides.

Table 4- 26 Comparison of SEM graph of corrosion feature for Putumayo Basin production water samples

	Total peak area of organic ligands	Description of corrosion products on the steel surface before cleaning
Control	0	Only one feature observed – crevice iron oxyhydroxide crystalline structures
Caribe	0	cementite bands (Fe3C) and iron oxyhydroxide structures were found
Acae	0	Etched pearlite observed in corroded areas; cementite bands (Fe_3C) Amorphous ferric oxyhydroxide structures were found
Sucombio	10458	Etched pearlite observed in corroded areas Cementite bands (Fe_3C) Much less of ferric oxyhydroxide corrosion products than Control, Caribe, and Acae were found, which indicates dissolution by organic ligands

*Loro: Insufficient sample volume for experiments

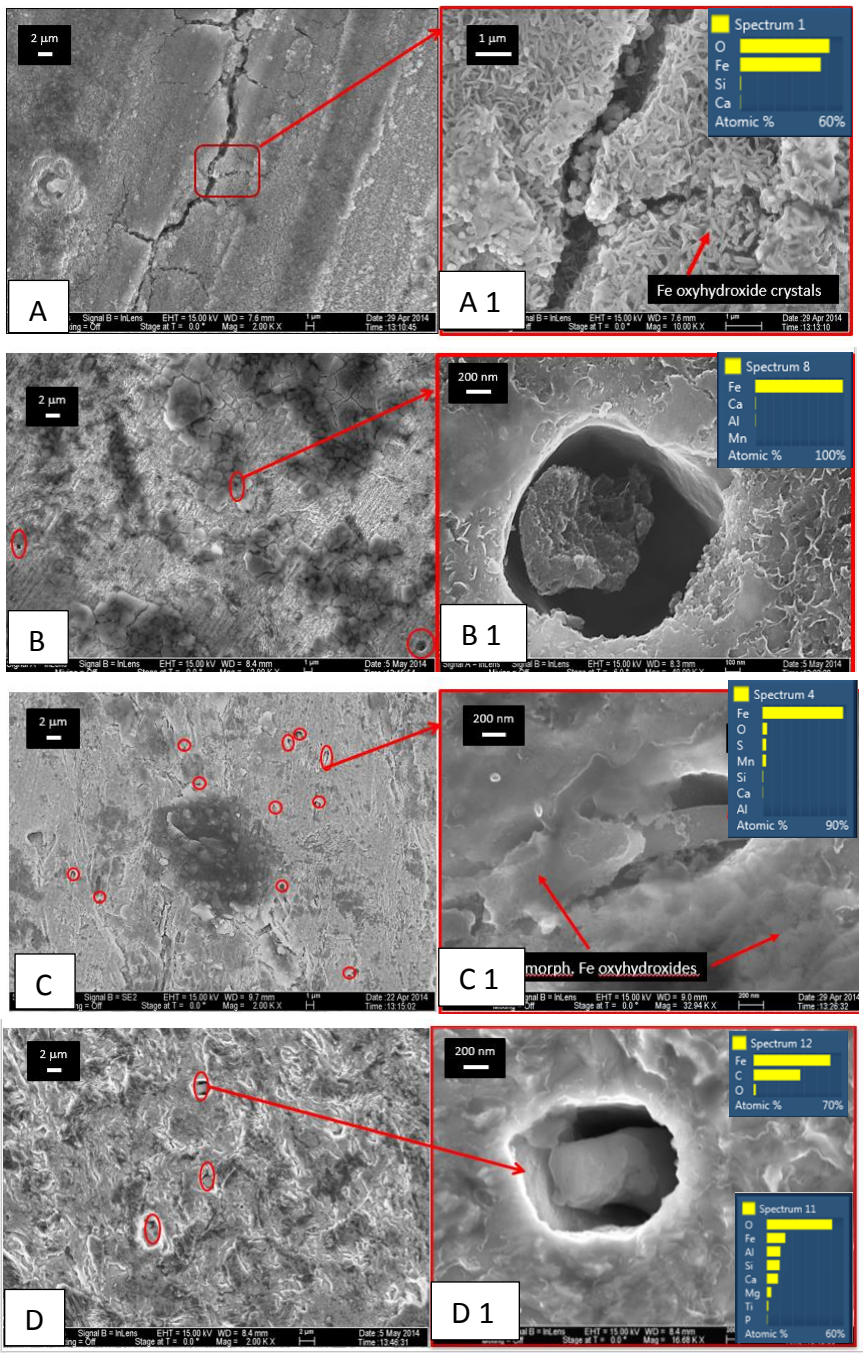

Figure 4- 7 SEM graphs of corrosion products on C1080 carbon steel after immersion in different Putumayo Basin water sample: (A) Control (0.7% chloride water), (B) Caribe production water, (C) Acae production water, (D) Sucombio production water under 2,000 X magnification; (A 1) Control (0.7% Nloride water), (B 1) Caribe production water, (C 1) Acae production water, (D 1) Sucombio production water under 10,000 X magnification;

4.4 Scanning electron microscopy-energy dispersive X-Ray spectroscopy analysis of the free-floating biofilm with embedded particulates of Barnett Shale production water samples

The communities of microorganisms which attach to a surface form biofilm. Extracellular polymetric substance (EPS) is defined as "organic polymers of microbial origin which in biofilm systems are frequently responsible for binding cells and other particulate materials together (cohesion) and to the substratum (adhesion)" (Wingender *et al*., 1999). Carbohydrates and proteins are the main component of EPS (Wingender *et al*., 1999). Therefore, in the SEM- EDX spectrum of the particulates embedded in the free-floating biofilm, carbon is contributed by cell mass of the EPS and nitrogen is from proteinaceous EPS (Bitton, 2005). In a typical SRB induced corrosion system because the biogenic sulfide reacts with anodic ferrous ions to form $FeS_{(S)}$ (McNeil & Little, 1990), $FeS_{(S)}$ precipitate should present in the solid phase as a characteristic parameter. Therefore, it is hypothesized that if SRB induced corrosion occurred in those sampling tanks. $FeS_{(S)}$ should be present in the particulates which embedded in the free-floating biofilm. All steps before putting into the SEM chamber were performed under anaerobic conditions and the exposure time to atmosphere of filtered biofilm and particulates should be kept less than 2 minutes to prevent samples from being oxidized. The elemental compositions were measured with SEM-EDS, the ratio of S/Fe was calculated to deduce the solid composition. Figure 4-8 showed the production water samples with free-floating biofilm embedded with particulates.

Figure 4- 8 Free-floating biofilm with embedded particulates in the production water samples from Barnett Shale (sample SE 19)

Figure 4-9 concluded the atomic S/Fe ratio of the biofilm with embedded particulates of Barnett Shale production water samples. Table 4-27 through 4-31 showed the EDS results of the composition of sulfur and iron of the particulates embedded in the free-floating biofilm of Barnett Shale production water samples. The SEM-EDS results showed that

1) in the free-floating biofilm with embedded particulates of SE 19 production water sample, iron was presented as FeS, FeS_2, and/or Fe_3S_4 since the S/Fe (atom/atom) ratio was 1.56 ± 0.20 (Figure 4-9 and Table 4-27) which indicated that sulfate reduction occurred and SRB induced corrosion was the main corrosion mechanism;

2) in the free-floating biofilm with embedded particulates of SE 18, SE 17 and MC 5 production water samples, iron was presented as carbonate and/or oxides and only 14 to 21% as FeS because the S/Fe (atom/atom) was from 0.14 to 0.21 (Figure 4-9 and Table 4-28 through 4-30) which indicated that sulfate reduction occurred but not the main corrosion mechanism in the three tanks;

3) in the free-floating biofilm with embedded particulates of KJV 7 production water sample, iron particulates were mostly presented as oxides and/or carbonates (Figure 4-9 and Table 4-31) due to the low S/Fe (atom/atom) of 0.04 ±0.04 which indicated that sulfate reduction was not occurred and SRB induced corrosion was not the corrosion mechanism in the KJV 7 tank.

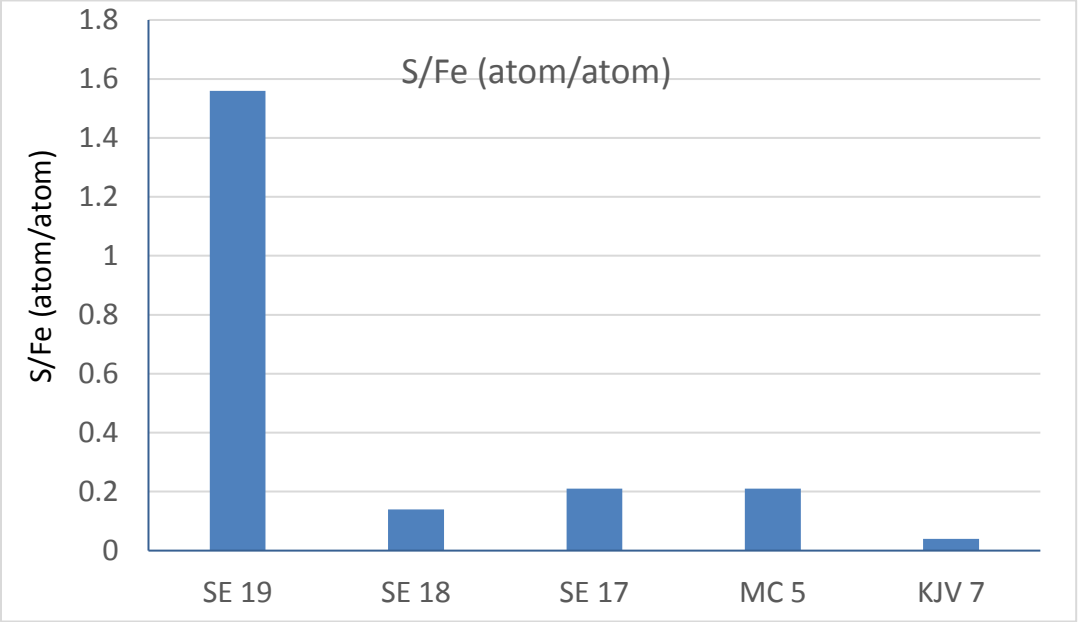

Figure 4- 9 S/Fe (atom/atom) ratio of the free-floating biofilm with embedded particulates of the Barnett Shale production water samples by SEM –EDX analysis

Table 4- 27 S/Fe (atom/atom) ratio in the free-floating biofilm with embedded particulates of SE 19 production water sample from the Barnett Shale

Fe (Wt%)	S (Wt%)	S/Fe (atom/atom)	Average S/Fe (atom/atom)
5.23	6.00	2.00	1.56 ± 0.26
18.23	16.36	1.56	
11.26	7.53	1.16	
8.49	7.17	1.47	
11.40	8.97	1.37	
9.97	9.46	1.65	
4.72	4.57	1.69	

Table 4- 28 S/Fe (atom/atom) ratio in the free-floating biofilm with embedded particulates of SE 18 production water sample from the Barnett Shale

Fe (Wt%)	S (Wt%)	S/Fe (atom/atom)	Average S/Fe (atom/atom)
21.26	1.33	0.11	0.14 ± 0.13
26.13	1.72	0.11	
18.14	1.68	0.16	
31.68	8.40	0.46	
42.93	2.85	0.12	
31.06	2.59	0.15	
50.11	0.96	0.03	
30.70	0.30	0.02	

Table 4- 29 S/Fe (atom/atom) ratio in the free-floating biofilm with embedded particulates of SE 17 production water sample from the Barnett Shale

Fe (Wt%)	S (Wt%)	S/Fe (atom/atom)	Average S/Fe (atom/atom)
20.08	0.53	0.05	0.21 ± 0.10
17.53	2.51	0.25	
13.24	2.30	0.30	
15.13	1.60	0.18	
17.71	2.34	0.23	
8.56	1.65	0.34	
19.62	1.54	0.14	

Table 4- 30 S/Fe (atom/atom) ratio in the free-floating biofilm with embedded particulates of MC 5 production water sample from the Barnett Shale

Fe (Wt%)	S (Wt%)	S/Fe (atom/atom)	Average S/Fe (atom/atom)
43.49	1.25	0.05	0.21 ± 0.22
39.82	16.94	0.74	
36.68	0.74	0.04	
32.16	2.75	0.15	
39.14	0.18	0.01	
21.75	2.99	0.24	
31.18	7.65	0.43	
36.74	1.48	0.07	
46.00	1.01	0.04	
41.79	4.13	0.17	
29.84	6.44	0.38	

Table 4- 31 S/Fe (atom/atom) ratio in the free-floating biofilm with embedded particulates of KJV 7 production water sample from the Barnett Shale

Fe (Wt%)	S (Wt%)	S/Fe (atom/atom)	Average S/Fe (atom/atom)
25.18	0.15	0.010	0.04 ± 0.04
34.56	0.14	0.007	
23.04	0.12	0.009	
29.60	0.29	0.017	
31.39	0.22	0.012	
56.45	0.00	0.000	
35.64	0.15	0.007	
25.87	2.05	0.138	
32.87	1.74	0.092	
31.95	0.54	0.029	
28.56	1.20	0.073	
30.01	1.29	0.075	

Only the atomic ratio of S/Fe of the free-floating biofilm with embedded particulates of SE 19 was over than 1 which indicated that sulfate reduction was the main corrosion mechanism. In the SE 18, SE 17 and MC 5, the S/Fe (atom/atom) ratio ranged from 0.14 to 0.22 which suggested that in those samples, sulfate reduction was presented but not the major corrosion mechanisms and there were other corrosion mechanisms occurring. In the KJV 7 samples, the atomic ratio of S/Fe was 0.04 which didn't support SRB driven corrosion mechanism.

Chapter 5: Discussion

The overall goal of this research was to test two hypotheses: 1) the concentration of dissolved iron that exceeds thermodynamic equilibrium calculated iron concentration is due to organic ligands that complex iron ions to produce soluble Fe(III)- organic ligands complexes; 2) and that increasing the dissolved iron concentration increased the kinetics of iron reduction respiration, thereby favoring microorganisms capable of using ferric iron as a terminal electron acceptor over microbes that respire sulfate to sulfide.

5.1 Solubility of iron ions in the production water samples from the Putumayo Basin and Barnett Shale

The first proposed research question addressed the dissolved iron concentration that was higher than the equilibrium iron concentration. In the Putumayo Basin samples, no ferrous ion was detected in any of the Putumayo Basin production water samples indicating that all dissolved iron were ferric ions (Table 4-1). When the crystal size increased from 8 nm to 100 nm, the solubility decreased three orders of magnitude from 1.90×10^{-4} ppm to 3.97×10^{-7} ppm at neutral pH illustrated in Section 2.4.1 and the equilibrium iron concentration with respect to goethite calculated with MINEQL+ ranged from 4.8×10^{-9} ppm to 4.3×10^{-8} ppm as shown in Table 4-2.

EcoPetrol provided unpublished industrial records containing chemical properties data of regional wells (n=21) from the Putumayo Basin, and the average data of the 21 wells is shown in Table 5-1 (EcoPetrol, 2014).

Table 5- 1 Description of average chemical properties data of the regional wells (n = 21) from the Putumayo Basin provided by EcoPetrol (EcoPetrol, 2014)

Gas phase	
CO_2 (% Vol.)	20.57 ± 10.00
O_2 (% Vol.)	15.09 ± 4.75
H_2S (% Vol.)	0
Aqueous phase	
pH	6.97 ± 0.54
Alkalinity (ppm, $CaCO_3$)	426.16 ± 368.37
Dissolved Fe (ppm)	2.14 ± 3.15
Sulfate (ppm)	369 ± 347
sulfide (ppm)	0

Reservoirs in the Putumayo Basin with CO_2 exceeding 20 vol. % have been found (Thrasher & Fleet, 1995). The high CO_2 concentrations in the gas phase (Table 5-1) was the reason that EcoPetrol postulated that CO_2-related corrosion was the primary corrosion mechanism. The oxygen concentration in the gas phase was consistent with the variable oxygen inputs and indicated that SRB driven corrosion shouldn't be the main corrosion mechanisms since SRB corrosion occurs only under anaerobic conditions (Miranda *et al.*, 2006; Beech & Sunner, 2004) (Table 5-1). It is assumed that the measured dissolved iron of the regional wells was ferric

iron due to the high O_2 concentration. The presence of sulfate and the absence of detectable $H_2S(g)$ in the gas phase and dissolved sulfide in the aqueous phase supported that SRB driven corrosion was not the main corrosion mechanism in the 21 regional wells.

In Putumayo Basin production water samples, the ferrozine assay results showed ferrous iron was absent in all four samples indicating that the dissolved iron existed as ferric iron. Comparison of the calculated equilibrium iron concentration using MINEQL+ based on the solubility of goethite, and at the pH and alkalinity of the Putumayo Basin production water samples, ranged from 7.22×10^{-9} to 4.32×10^{-8} ppm while the measured dissolved iron concentrations measured by GF-AAS ranged from 0.3 ppm to 1452.5 ppm which are 7 to 10 orders of magnitude higher than the predicted dissolved iron (Table 4-2).

Manganese (Mn) is adding to the carbon steel during the melting process to react with sulfur to form MnS inclusions and counter the brittleness of steel caused by sulfur (Sauveur, 1916). The results of the measured manganese concentrations ranged from 94 ppb to 5918 ppb as shown in Table 4-1 which was higher than the natural manganese concentration in the river, steam and seawater (0.4 ppb to 24 ppb) (Smith *et al.,* 1987; USEPA, 1984) which supported that corrosion occurred in the four sampling wells.

The total carbonate concentration was calculated with the pH and alkalinity by MINEQL+. Table 5-2 showed that the calculated equilibrium iron concentration of goethite was controlled by the H^+ concentration and alkalinity.

Table 5- 2 Influence of pH and alkalinity on the calculated equilibrium iron concentration by MINEQL+

Samples		pH	$[H^+]$ concentration (mol/L)	Alkalinity (ppm, $CaCO_3$)	Solid precipitate	Calculated equilibrium iron concentration by MINEQL+ (ppm)
Putumayo Basin	Loro	8.55	2.82×10^{-9}	1600	$Fe(OH)_{3(S)}$	4.79×10^{-9}
	Caribe	7.84	1.45×10^{-8}	656	$Fe(OH)_{3(S)}$	7.22×10^{-9}
	Acae	6.84	1.45×10^{-7}	1043	$Fe(OH)_{3(S)}$	4.32×10^{-8}
	Sucombio	7.16	6.92×10^{-8}	2242	$Fe(OH)_{3(S)}$	2.23×10^{-8}

In the Barnett Shale production water samples, because of no ferrous ions concentration data, the total dissolved iron might be ferric ion and ferrous ion both, ferric ion only or ferrous ion only. The presented solid phase could be $FeCO_{3(S)}$, $FeS_{(S)}$, $Fe(OH)_{2(S)}$ and $Fe(OH)_{3(S)}$. No sulfide was detected in those samples, therefore, $FeS_{(S)}$ was not considered as the solid Fe(III) form (Table 4-1). The solubility constants of $FeCO_{3(S)}$, $Fe(OH)_{2(S)}$ and $Fe(OH)_{3(S)}$ are 2.1×10^{-11}, 8.0×10^{-16} (Davison, 1979) and 7.8×10^{-38} (Blais *et al.*, 2008) respectively. Since the solubility constant of $FeCO_{3(S)}$ is higher than $Fe(OH)_{2(S)}$ and $Fe(OH)_{3(S)}$ and the Barnett Shale is overlying on the Ellenburger Group carbonates (Pollastro, 2007) which supported the presence of carbonate, the equilibrium concentration of $FeCO_{3(S)}$ was calculated with MINEQL+ to evaluate if the dissolved iron were oversaturated in those tanks.

The total carbonate concentration was calculated with the pH and alkalinity by MINEQL+. The results showed that the equilibrium iron concentration of $FeCO_{3(S)}$

calculated by MINEQL+ was 9.7, 11.6, 74.8, 28.9 and 48.6 ppm while the measured dissolved iron concentration by AAS was 2.2, 59.1, 97.2, 160.1 and 125.6 ppm which was 22%, 502%, 121%, 553% and 259% oversaturated compared with the predicted $FeCO_{3(S)}$ concentration calculated by MINEQL+ for SE 19, SE 18, SE 17, MC 5 and KJV 7 respectively (Table 4-5). Table 5-3 showed that the calculated equilibrium iron concentration of $FeCO_{3(S)}$ was controlled by the H^+ concentration, but it was not proportional to the H^+ concentration which indicated that the alkalinity of production water samples also contributed to the solubility of $FeCO_{3(S)}$ since the total carbonate concentration was calculated based on the pH and alkalinity.

Table 5- 3 Influence of pH and alkalinity on the calculated equilibrium iron concentration by MINEQL+

Samples		pH	$[H^+]$ concentration (mol/L)	Alkalinity (ppm, $CaCO_3$)	Solid precipitate	Calculated equilibrium iron concentration by MINEQL+ (ppm)
Barnett Shale	SE 19	6.92	1.20×10^{-7}	185	$FeCO_{3(S)}$	9.7
	SE 18	6.76	1.74×10^{-7}	220	$FeCO_{3(S)}$	11.6
	SE 17	6.09	8.13×10^{-7}	116	$FeCO_{3(S)}$	74.8
	MC 5	6.58	2.63×10^{-7}	114	$FeCO_{3(S)}$	28.9
	KJV 7	6.45	3.55×10^{-7}	70	$FeCO_{3(S)}$	48.6

The dissolved manganese concentration ranged from 526 ppb to 3321 ppb which was higher than the reported manganese concentration in the natural river, steam and seawater (0.4 to 24 ppb) (Smith *et al.,* 1987; USEPA, 1984). The high

dissolved iron and dissolved manganese indicated corrosion occurred in those sampling tanks.

5.2 Formation of Fe(III)-ligands complex increased the solubility of Fe(III)

The dissolved iron concentration in the production water samples from the Putumayo Basin was over 7 orders of magnitude higher than the equilibrium iron concentration of goethite calculated by MINEQL+ and the dissolved iron concentration in the production water sample from in the Barnett Shale was 2 to 5 times higher than the equilibrium $FeCO_{3(S)}$ concentration calculated by MINEQL+, except SE 19 which was undersaturated. It was hypothesized that the high dissolved iron concentration caused by the formation of Fe(III)-organic ligands complexes.

The production water samples were adjusted pH to 2 so that all organic acids were at protonated states and could be extracted with EtOAc. In order to release organic ligands from the Fe(III)-ligands complexes, production water samples were increased pH so that Fe(III) precipitated as $Fe(OH)_{3(S)}$ and organic ligand released. Using oxalic acid as an example which has larger binding constant than C_3 and C_4 dicarboxylic acid when binding with Fe(III) ($\beta_3 = 10^{18.6}$). When increasing pH, Fe^{3+} prefers to react with OH^- and form $Fe(OH)_{3(S)}$ precipitate due to the low solubility constant (K_{s0}) (Blais *et al.*, 2008) (equation 25).

$$Fe(OH)_{3(S)} \leftrightarrow Fe^{3+} + 3OH^- \qquad \text{equation 25}$$

$K_{s0} = \{Fe^{3+}\}\{OH^-\}^3 = 10^{-37.11}$

Snoeyink & Jenkins (1980) demonstrated that the lowest dissolved Fe(III) concentration is 1×10^{-11} mol/L at pH = 8, the further pH increase will form $Fe(OH)_4^-$ and increase dissolved iron concentration (equation 26).

$Fe^{3+} + 4OH^- \leftrightarrow Fe(OH)_4^-$ equation 26

$\beta_4 = Fe(OH)_4^-/\{Fe^{3+}\}\{OH^-\}^4 = 10^{22.32}$

However, compared the β_4 of $Fe(OH)_4^-$ and K_{s0} of $Fe(OH)_{3(S)}$, Fe^{3+} will preferentially precipitate as $Fe(OH)_{3(S)}$ rather than form $Fe(OH)_4^-$. In addition, Macalady *et al*. (1990) illustrated that the formation of $Fe(OH)_{3(S)}$ needs several hours to reach completely precipitation. After pH 8, the addition of OH^- provides excess OH^- and kinetically moved the precipitate reaction forward. When using 1 M NaOH to increase the pH of 20 ml Sucombio production water sample from the Putumayo Basin, at pH 9, 10, and 11, new precipitation was observed while only after pH 12, no new precipitate was found. Therefore, the production water samples were increased pH to 12 rather than pH = 8 to get the maximum amount of precipitation and un-chelated ligands concentration. The sample was filtered to remove $Fe(OH)_{3(S)}$ precipitate and decreased pH to 2 so that all organic acids were at protonated state.

Targeted metabolomics results of our production water samples showed α - hydroxy acids (e.g. glycolic acid, 2-hydroxybutanoic acid), dicarboxylic acids (e.g. oxalic acid, succinic acid, methyl succinic acid, pentanedioic acid and heptanedioic acid) and PEG carboxylic acids (e. g. diglycolic acid (PEG-carboxylic acid with one

PEG group), and PEG-carboxylic acids with two and three PEG groups) which could chelate with Fe(III) to complex and cause dissolution of Fe(III) from the solid iron oxides. The stability constants of dicarboxylic acids, α-hydroxycarboxylic acids, and PEG carboxylic acids are two to several orders of magnitude higher than monocarboxylic acids which suggests that those organic acids bond strongly enough to displace oxide and hydroxide and thus form the Fe(III)-ligand complexes and facilitate dissolution of Fe(III).

The relationship between dissolved Fe(III) concentration and the peak area of dicarboxylic acids, α-hydroxycarboxylic acids, and PEG-carboxylic acids was investigated in this research. Because the Barnett Shale production water samples and Sucombio production water sample from Putumayo Basin were analyzed at the different times, the relative concentration of total organic ligands was determined by using the ratio of the total area of organic ligands peak areas/internal standard (9-FCA) peak area. Even those samples had different water came from the different resources with different water chemistry properties, when compared the relative concentration of the Fe chelating molecules and the dissolved iron concentration, a good linear relationship was found as shown in Table 5-4 and Figure 5-1. The linear relationship supported the first hypothesis that the organic ligands caused the high dissolved iron concentration due to the formation of Fe(III)-ligands complexes. Meanwhile, this linear relationship also suggested that the organic ligands concentration controlled the dissolved iron concentration.

Table 5- 4 Comparison of total area of iron-chelating molecules and the dissolved iron concentration in the Sucombio production water sample from the Putumayo Basin and the Barnett Shale production water samples

Sampling sites		Ratio of total peak area of organic ligands /9-FCA	Dissolved iron concentration (ppm)
Barnett Shale	SE 19	0.1008	2.2
	SE 18	0.1428	58.1
	SE 17	0.424	90.4
	KJV 7	0.4794	125.7
	MC 5	0.5972	160.1
Putumayo Basin	Sucombio	2.5798	1452.5

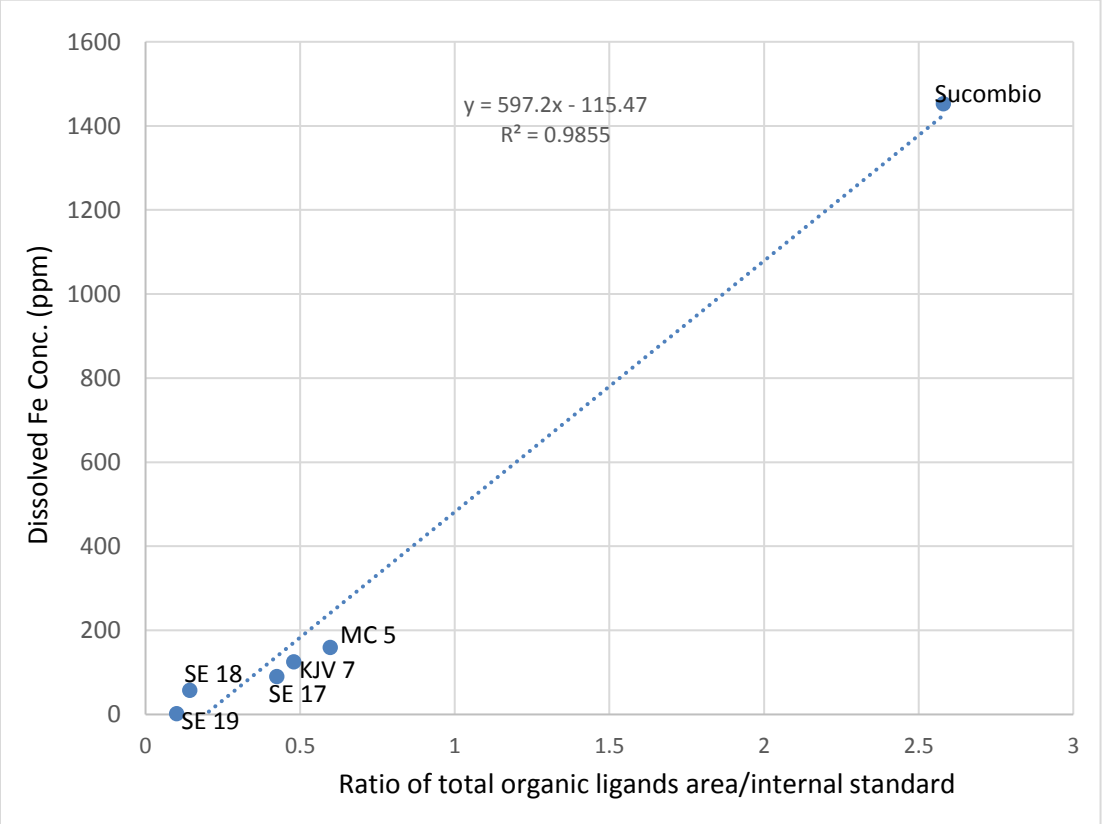

Figure 5- 1 Linear relationship between the ratio of total organic ligands peak area/internal standard area and the dissolved iron concentration in the Sucombio production water sample from the Putumayo Basin and the Barnett Shale production water samples

5.3 The influence of the total dissolved iron concentration on the function of microorganisms

The linear relationship between the total peak area of Fe(III) chelating molecules and the dissolved iron concentration strongly suggest that the high dissolved iron concentration was due to the formation of Fe(III)-organic ligand complexes (Table 5-3 and Figure 5-3). The influence of increased dissolved iron concentration on the function of microorganisms was discussion below. Stumm & Morgan (1970) illustrated that the standard redox potential of Fe(III)/Fe(II) and SO_4^{2-}/ H_2S

	E^0(V)
$Fe^{3+} + e^- \leftrightarrow Fe^{2+}$	+0.77
$SO_4^{2-} + 9H^+ + 8e^- \leftrightarrow H_2S + 4H_2O$	+0.34

Fe(III)/Fe(II) redox relative to sulfate reduction is much more energetically favorable. However, most ferric irons are in solid phase forms in nature, therefore thermodynamic gain decreases due to the energy required for dissolution, and formation of dissolved ferric iron. Thus, the free energy available using ferric oxides in ferric respiration decreases. However, when ferric ions are complexed by organic ligands to form soluble ferric-ligand complexes, there is much more energy available for iron respiration. Bird *et al.* (2011) illustrated that when microbes use ferric iron as a terminal electron acceptor and reduce to ferrous iron, the amount of available free energy varies from -9 to + 60 kJ/mole, depending on the solubility of the ferric oxide phase being reduced. Alternatively, if ferric iron is chelated by an organic ligand, NTA and citrate thereby increasing

the solubility of ferric iron, the amount of available free energy for ferric iron respiration increases to -35.9 and -37.1 kJ/mole respectively (Bird *et al.*, 2011).

In comparison to energy obtained by microbial respiration of ferric iron, SRBs produce H_2S through the reduction of sulfate at pH 7 with a free energy gain of -169.8 kJ/mol, as shown below (Kato, 2016):

$SO_4^{2-} + 9H^+ + 8e^- \leftrightarrow H_2S + 4H_2O \quad E^{0\prime} = 0.22\ V \quad \Delta G = -169.8\ kJ/mol\ (for\ 8e^-)$

In order to compare the free energy gain per electron between Fe(III) reduction and sulfate reduction, the free energy of sulfate reduction is calculated for one electron transfer at pH 7 is -21.2 kJ/mol.

Thermodynamically, microorganisms can get more energy from reducing Fe(III) from the Fe(III)-ligand complexes to Fe(II) (-37.1 to -35.9 kJ/mol) than sulfate reduction (-21.22 kJ/mol) per mole electron transfer which potentially makes Fe(III) more favorable electron acceptor than sulfate when ferric iron is soluble and complexed by ligands.

Despite a gain in energy upon reducing soluble ferric iron bound by organic ligands compared to solid phase ferric oxides, attention must be given to the actual amount of energy the microbe will obtain during ferric respiration. Bird *et al.* (2011) illustrated that the microbial energy gain occurs during electron transfer from the NAD+/NADH in the cellular cytoplasm to the menaquinones (MQ/MQH_2) couple in the inner membrane. Electron transfer beyond this point through the periplasm, outer membrane and to the final ferric electron acceptor does not contribute to the microbial energy gain. Despite the difference in free energy

associated with these different ferric species, both dissolved and solid phase. However, increasing the concentration of available ferric ions as soluble ferric-ligands complexes increase the kinetic rates of ferric respiration relative to solid-phase ferric respiration, thereby making ferric respiration a feasible respiration process for microbes capable of iron (Bird *et al.*, 2011).

In the Barnett Shale, the standard approach industry uses to monitor MIC in the production water storage tanks is NACE international standard test method by using Modified Postgate's B (MPB) media (TM0194-94, 1994). By setting up different dilution series (1:10, 1:100, 1:1,000, 1: 10,000, 1:100,000 and 1:1,000,000) and incubating under anaerobic conditions, the diluted bottles which showed black due to the formation of $FeS_{(S)}$ within 28 days was considered positive of SRB. High SRB was found in the tanks of SE 18, SE 19 and MC 5, while low SRB was found in SE 17 and KJV 7. It was presumed that those tanks experienced SRB induced corrosion.

Because the solubility constant of $FeS_{(S)}$ is 6.3×10^{-18} (Blais *et al.*, 2008), Fe^{2+} will react with the sulfate reduction products and form precipitate as long as S^{2-} is produced. In a typical SRB induced corrosion system, due to the formation FeS_X precipitates (e.g. FeS, FeS_2, Fe_3S_4) (McNeil & Little, 1990), the characteristic parameters of SRB driven corrosion system are concluded as below: 1) SRB are active, 2) the dissolved iron concentration should be low in the aqueous phase, and 3) the atomic S/Fe ratio of precipitation should equal or higher than 1 in the solid phase of corrosion products. However, data collected from the Barnett Shale

production water samples (e.g. pH, alkalinity, dissolved iron concentration (Table 4-1), the atomic ratio of the particulates embedded in the free-floating biofilm, the sulfate reduction activity and the relative abundance of deltaproteobacteria and gammaproteobacteria) indicated that despite the presence of SRB, other MIC mechanisms may be occurring other than these driven by sulfate-reduction MIC mechanisms. The data also indicated that the MPB method routinely used by industry may not be accurately assessing MIC in production water tanks.

The relative abundance of two classes, deltaproteobacteria (%) and gammaproteobacteria (%), were evaluated by 16S rRNA gene sequencing, and numbers of total bacteria, archaea were estimated by qPCR (Duncan et al., 2017). Data collected by Dr. Bradley Stevenson's group, Dr. Joseph Suflita's group and Dr. Kathleen Duncan's group from the Department of Microbiology and Plant Biology at the University of Oklahoma, Norman campus. *Desulfobacter, Desulfovibrionales,* and *Desulfuromonadales* which have species that can use both Fe(III) and sulfate as terminal electron acceptor were found in the Deltaproteobacteria. Gammaproteobacteria include genera that are facultative aerobes and iron reducers. Furthermore, *Shewanella,* a genus of Gammaproteobacteria, is known as IRB which can use Fe(III) as a terminal electron acceptor. The sulfate reduction activity used a radiotracer technique (Ulrich et al., 1997) to evaluate the SRB activity in the production water samples. Data collected by Dr. Joseph Suflita's group from the Department of Microbiology and Plant Biology at the University of Oklahoma, Norman campus.

Table 5- 5 Dissolved iron concentration, the atomic S/Fe ratio of the free-floating biofilm embedded with particulates, the relative abundance of microorganisms, and the sulfate reduction rate in the Sucombio production water sample from the Putumayo Basin and five production water samples from the Barnett Shale

		Barnett Shale					Putumayo Basin
		SE 19	SE 18	SE 17	MC 5	KJV 7	Sucombio
pH		6.92	6.76	6.09	6.58	6.45	7.16
Dissolved iron concentration (ppm)		2.2	58.1	90.4	160.1	125.7	1452.5
Ratio of measured iron concentration by AAS/calculated iron concentration by MINEQL+		0.23	5.0	1.2	5.5	2.6	6.5×10^{10}
Atomic S/Fe ratio of the free-floating biofilm embedded with particulates		1.56 ± 0.20	0.14 ± 0.14	0.21 ± 0.07	0.21 ± 0.23	0.04 ± 0.04	Not available
Native sulfate reduction rate (μmol S/ml/day) *		0.203	0.065	0.001	0.158	0.001	0.007
Relative abundance (%)**	Gammaproteobacteria	10.5	13.5	43.1	30.7	51.5	⩾30.0
	Deltaproteobacteria	41.0	10.7	14.4	27.6	4.7	Not available

*: Unpublished sulfate reduction rate measurement using a radiotracer technique (Ulrich et al., 1997). Data collected by Dr. Joseph Suflita's group from the Department of Microbiology and Plant Biology at the University of Oklahoma, Norman campus.
**: Unpublished microbial diversity was evaluated by 16S rRNA gene sequencing, and numbers of total bacteria, archaea were estimated by qPCR (Duncan et al., 2017). Data collected by Dr. Bradley Stevenson's group, Dr. Joseph Suflita's group and Dr. Kathleen Duncan's group from the Department of Microbiology and Plant Biology at the University of Oklahoma, Norman campus.

In order to address the influence of dissolved iron concentration on microbial respiration and preference for terminal electron acceptors, the relationship among the dissolved iron concentration, the atomic S/Fe ratio of the particulates embedded in the free-floating biofilm, the sulfate reduction rate and the relative

abundance (%) of deltaproteobacteria and gammaproteobacteria of the Sucombio production water sample from the Putumayo Basin and five production water samples from the Barnett Shale.

In an SRB driven corrosion system, sulfate is reduced to sulfide, and ferrous iron reacts with sulfide to form $FeS_{(S)}$ precipitate and H^+ (equation 27). No ligands are involved in the reduction reaction of sulfate to sulfide. For each mole of ferrous iron precipitation as $FeS_{(S)}$, 1 mole of H^+ is produced which leads to modest pH and alkalinity change.

$$Fe^{2+} + HS^- \leftrightarrow FeS_{(S)} + H^+ \qquad \text{equation 27}$$

Due to the formation of $FeS_{(S)}$ precipitate, dissolved iron concentration in the aqueous phase should be low, but the atomic ratio of S/Fe in the solid phase should be high.

When the organic ligands concentration in the production water samples increases, the formation of Fe(III)-ligand complexes facilitates the dissolution of solid ferric iron and causes high dissolved iron concentration in the production water samples. In an IRB driven system, ferric iron from the Fe(III)-ligand complex is reduced to ferrous iron, and ligands are released. When ferrous iron is oxidized and forms iron oxyhydroxide precipitation and H^+ (equation 28), for each mole of ferrous iron precipitation as FeOOH precipitate formation, 2 moles of H^+ is produced which decrease pH and alkalinity.

$$4Fe^{2+} + O_2 + 6H_2O \leftrightarrow 4FeOOH_{(S)} + 8H^+ \qquad \text{equation 28}$$

Due to the formation of Fe(III)-ligands, in the aqueous phase, dissolved iron centration is high and Fe(III) is bioavailable for IRB using; S/Fe (atom/atom) is low since no FeS precipitate in the solid phase. The released organic ligands react with iron oxyhydroxide, form Fe(III)-ligand complexes and increase dissolved iron concentration (equation 29)

$FeOOH_{(S)} + 3\ HL \leftrightarrow Fe^{3+}L_3 + 2H_2O$ equation 29

In the Barnett Shale production water samples, the SE 19 sample had the highest pH and lowest dissolved iron concentration which was undersaturated compared with the equilibrium $FeCO_{3(S)}$ concentration. The main composition of the particulates embedded in the free-floating biofilm was FeS, FeS_2 and/or Fe_3S_4 based on the atomic S/Fe ratio (Table 5-5). The SE 19 sample had the highest sulfate reduction rate of SRB (Table 5-5), the relative abundance (%) of Deltaproteobacteria was 40.9% which was the highest proportion compared with other four Barnett Shale production water samples, and around 30% of the Deltaproteobacteria was *Desulfobacter* which have species can use both sulfate and Fe(III) as a terminal electron acceptor (Table 5-5, Figure 5-2 and 5-3) (Lovley, 1993). The above results indicated that SRB presented and sulfate reduction favored in the SE 19. Due to the undersaturated Fe(III) concentration, the Fe(III) respiration was not kinetically feasible and sulfate reduction was more favorable than Fe(III) reduction in the SE 19.

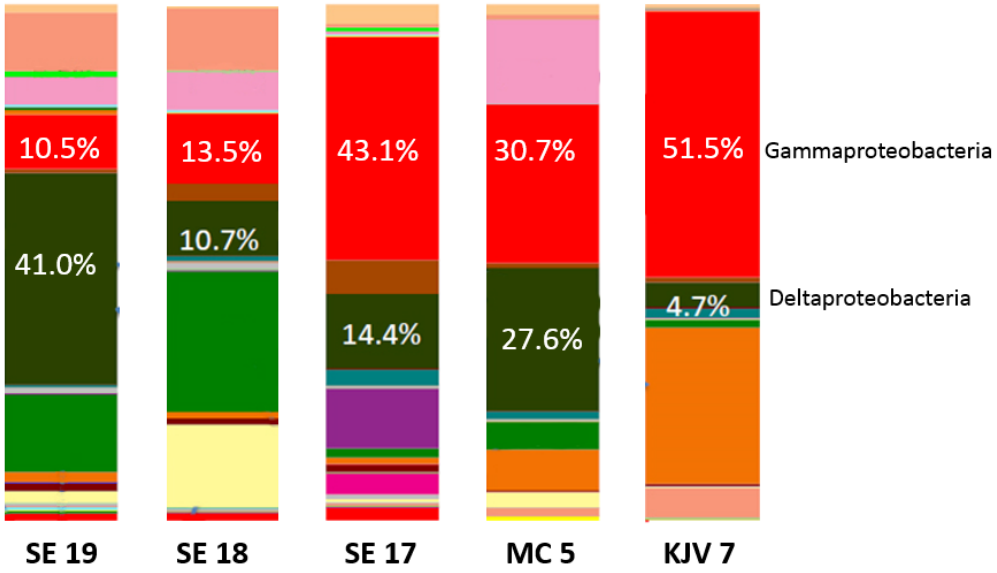

Figure 5- 2 Relative abundance (%) of different genera of bacteria in the Barnett Shale production water samples*

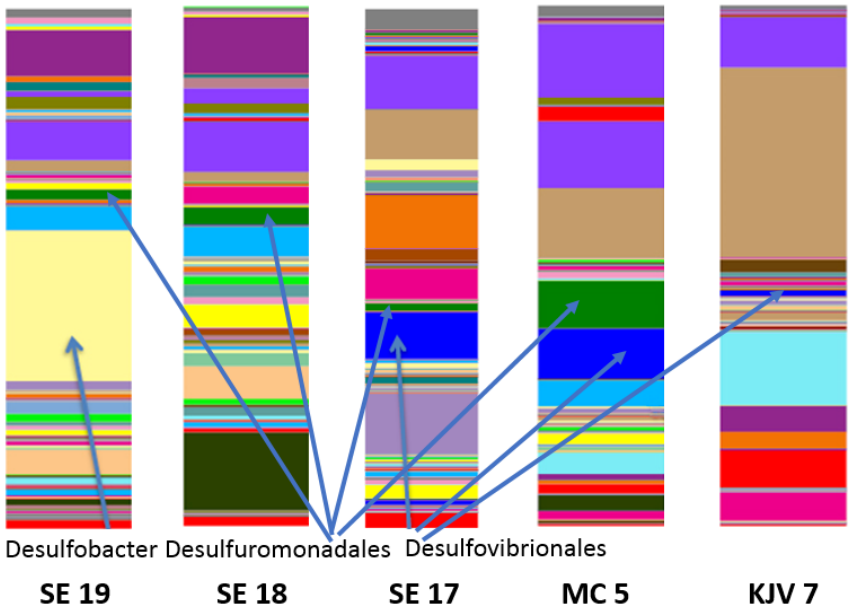

Figure 5- 3 Different combinations/proportions of Deltaproteobacteria in Barnett Shale production water samples*

*: Unpublished microbial diversity was evaluated by 16S rRNA gene sequencing, and numbers of total bacteria, archaea were estimated by qPCR for Barnett Shale production water samples (Duncan *et al.*, 2017). Data collected by Dr. Joseph Suflita's group and Dr. Kathleen Duncan's group from the Department of Microbiology and Plant Biology at the University of Oklahoma, Norman campus.

In the SE 18, SE 17 and MC 5, the pH values were about 0.2 to 1 pH units lower than SE 19 and the dissolved iron concentration was1.2 to 5.5 times higher than the equilibrium iron concentration of $FeCO_{3(S)}$; only 14 to 21% as $FeS_{(S)}$ was found in the particulates embedded in the free-floating biofilm. The sulfate reduction assay showed that SRB presented and were capable of sulfate reduction in the SE 18 and MC 5 and no sulfate reduction was found in SE 17 (Table 5-5); the relative abundance (%) of Deltaproteobacteria ranged from 10.7% to 27.6%; *Desulfovibrionales* and *Desulfuromonadales* which have species that can use both Fe(III) and sulfate as terminal electron acceptor were found in the Deltaproteobacteria (Table 5-5, Figure 5-2 and 5-3) (Lovley, 1993). The above results indicated that SRB presented and sulfate reduction occurred, but the sulfate reduction rate was limited in the SE 17, SE 18 and MC 5. Since the excess dissolved Fe(III) concentration thermodynamically and kinetically favored iron reduction over sulfate reduction. Dependent on the concentration of the organic ligands concentration which controlled the dissolved ferric iron concentration, the function of microorganisms switched between sulfate reduction and iron reduction.

In the KJV 7 and Sucombio samples; no sulfate reduction was found in both samples (Table 5-5). In the KJV 7 sample, the relative abundance (%) of Deltaproteobacteria was only 4.7%. However, the relative abundance (%) of Gammaproteobacteria was 51.5% which include genera that are facultative aerobes and iron reducers (Table 5-5, Figure 5-2 and 5-3 (Duncan & Nanny, 2015).

In the Sucombio, the relative abundance (%) of different genera of bacteria results showed that 30% of microorganisms in the Sucombio production water sample were *Shewanella,* a genus of Gammaproteobacteria, which can use Fe(III) as a terminal electron acceptor (Figure 5-4) (Banfield & Nealson, 1997; Nealson & Saffarini, 1994; Lovley & Phillips, 1988). The pH of KJV 7 was 0.5 pH unit lower than SE 19. The pH of Sucombio was about 1.5 pH unit lower than Loro which had the highest pH in the Putumayo Basin samples (Table 4-1). The dissolved iron concentration and organic ligands concentration in the KJV 7 and Sucombio were higher than the equilibrium iron concentration of $FeCO_{3(S)}$ and $Fe(OH)_{3(S)}$ respectively and no $FeS_{(S)}$ was found in free-floating biofilm embedded with particulates of the KJV 7 (Table 5-5). The above results indicated that no SRB activity in the KJV 7 and Sucombio samples. The high proportion of IRB and the high concentration of dissolved iron suggested that iron respiration thermodynamically and kinetically more favorable than sulfate reduction in the KJV 7 from the Barnett Shale and Sucombio from the Putumayo Basin.

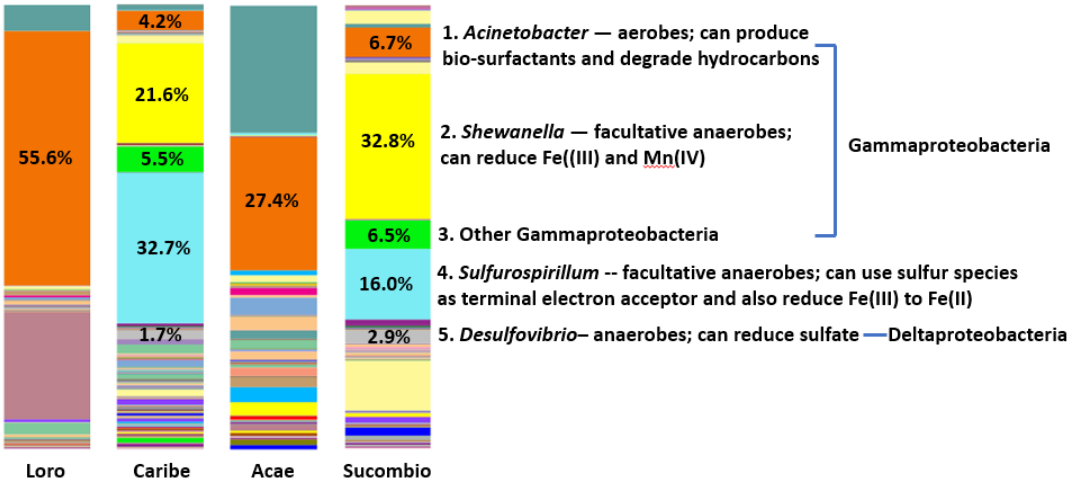

Figure 5- 4 Relative abundance* (%) of different genera of bacteria in Putumayo Basin production water samples*

*: Unpublished microbial diversity was evaluated by 16S rRNA gene sequencing, and numbers of total bacteria, archaea were estimated by qPCR for Putumayo Basin production water samples (Duncan *et al.*, 2017). Data collected by Dr. Stevenson's group from the Department of Microbiology and Plant Biology at the University of Oklahoma, Norman campus.

Overall, the organic ligands concentration controlled the dissolved iron concentration which was supported by the linear relationship between the total peak area of organic ligands and the dissolved iron as shown in Table 5-3 and Figure 5-3. Our second hypothesis was supported that increasing the concentrations of soluble ferric ions through complexation by organic ligands thermodynamically and kinetically makes ferric ions become the preferred terminal electron acceptor over sulfate.

Chapter 6: Conclusions and Future work

When corrosion occurs under aerobic conditions, ferric oxyhydroxide layer forms on the metal surface. More recent studies, using various *in situ* surface analyses, suggest a passive film structure ranging from amorphous to iron hydroxides or oxyhydroxides (Gui & Devine, 1991; Rubim & Dünnwald,1989; O'Grady,1980). The overall goal of this research was to test two hypotheses that 1) the very high concentration of dissolved iron is due to organic ligands that complex iron ions to produce soluble Fe(III)- organic ligands complexes. 2) Increasing the dissolved iron concentration made Fe(III) a more thermodynamically favorable electron acceptor than sulfate, thereby favoring microorganisms capable of using ferric iron as a terminal electron acceptor.

In this work, nine samples from two sites were tested. Four samples are oil production water from the Putumayo Basin and the other five are gas tank production water from the Barnett Shale. Research data supported our hypotheses as concluded below:

1) The dissolved iron in the production water samples in the was oversaturated with respect to the predicted equilibrium $Fe(OH)_{3(s)}$ concentration in the Putumayo production water samples and the predicted equilibrium $FeCO_{3(s)}$ concentration in the Barnett Shale production water storage tanks samples except SE 19 which was undersaturated.

2) The formation of Fe(III)-organic ligands complexes increased Fe(III) solubility leading to the high dissolved iron concentration in the production water samples;

3) Since microorganisms can obtain more energy from iron reduction than sulfate reduction, the high dissolved iron concentration thermodynamically appeared to shift the function of microorganisms from sulfate-reducing to iron-reducing.

Based on the observations, a new microbial induced corrosion mechanism involving IRB is proposed. The overall mechanism proposes that organic ligands adsorb on the ferric oxyhydroxide layer on the corroded steel surface and chelate with Fe(III) from the ferric oxyhydroxide layer. The formation of Fe(III)-ligand complexes solubilizes the insoluble Fe(III) and the Fe(III) in the Fe(III)-ligand complexes is reduced by IRB under anaerobic conditions. Due to the reduction of Fe(III), the Fe(III)-ligand complexes are dissociated, and ligands are released. The organic ligands re-adsorb to the oxidized steel surface to further solubilize Fe(III) and remove ferric oxyhydroxide layer from the steel.

This mechanism is hypothesized from the observed data from the Putumayo Basin and the Barnett Shale samples and will experimentally verify as shown below:

First, it needs to test if organic ligands can chelate with the insoluble Fe(III) from the ferric oxyhydroxide layer on the steel surface and solubilize ferric oxyhydroxide under abiotic conditions.

Second, it needs to test if IRB can reduce the insoluble Fe(III) from the ferric oxyhydroxide layer on the corroded steel surface under anaerobic conditions.

Last, it will test the influence of IRB on the organic ligands removal of insoluble Fe(III) from the ferric oxyhydroxide layer on the steel by forming Fe(III)-ligand complexes as a terminal electron acceptor under anaerobic conditions.

6.1 Research questions

1) Can organic ligands remove ferric oxyhydroxide layer by forming Fe(III)-organic ligands complex?

2) Can the IRB reduce the Fe(III) from the Fe(III)-ligand complexes and release organic ligands to form new Fe(III)-ligands complexes and facilitate the removal of ferric oxyhydroxide layer?

6.2 Hypotheses

1) Organic ligands, dicarboxylic acids, can form Fe(III)-organic ligands complex and solubilize Fe(III) from the iron oxyhydroxide layer under abiotic conditions. The concentration of organic ligands controls the dissolved ferric ion concentration and a positive correlation is expected to find between the concentration of organic ligands and the dissolved iron concentration.

2) When both IRB and organic ligands present under anaerobic conditions, the dissolved ferric and ferrous ions concentration is expected to be higher than only organic ligands present experiment. At the same time, the IRB growth rate and the Fe(III) reduction rate should be measured. A positive correlation between the

concentration of organic ligands and dissolved ferric iron and ferrous iron concentration is expected to be found. And a positive correlation between the amount of IRB and the ferrous iron concentration is expected to be found.

6.3 Objectives

The objectives of the future work are to design and carry out experiments to answer the research questions. *Shewanella oneidensis* MR-1 is chosen as model IRB since *Shewanella* genus has the most abundance of the microbial community found in the Sucombio production water sample which has the highest dissolved iron concentration. Oxalic acid, malonic acid, succinic acid, glycolic acid and diglycolic acid are used as the organic ligands which are detected in the production water samples.

The first objective is to challenge if the organic ligands can cause the dissolution of Fe(III) from the iron oxyhydroxide layer concentration.

- The total dissolved iron ion concentration is determined by AAS;

The second objective is to address if the presence of the organic ligands and IRB can promote the dissolution of Fe(III) from the iron oxyhydroxide layer concentration by the formation of Fe(III)-ligand complexes and the IRB reduction of Fe(III) from the complexes.

- The total dissolved iron ion concentration is determined by AAS;
- The ferrous iron concentration is measured by ferrozine assay;
- Microbes' growth is determined by measuring the OD_{600}.

References

Aktas, D. F., Lee, J. S., Little, B. J., Ray, R. L., Davidova, I. A., Lyles, C. N., & Suflita, J. M. (2010). Anaerobic metabolism of biodiesel and its impact on metal corrosion. *Energy Fuels*, 24(5), 2924-2928.

AlAbbas, F. M., Williamson, C., Bhola, S. M., Spear, J. R., Olson, D. L., Mishra, B., & Kakpovbia, A. E. (2013). Influence of sulfate reducing bacterial biofilm on corrosion behavior of low-alloy, high-strength steel (API-5L X80). *International Biodeterioration & Biodegradation*, 78, 34-42.

Al-Jaroudi, S. S., Ul-Hamid, A., & Al-Gahtani, M. M. (2011). Failure of crude oil pipeline due to microbiologically induced corrosion. *Corrosion Engineering, Science and Technology*, 46(4), 568-579.

Arnold, R. G., DiChristina, T. J., & Hoffmann, M. R. (1988). Reductive dissolution of Fe(III) oxides by *Pseudomonas sp.* 200. *Biotechnology and Bioengineering*, 32(9), 1081-1096.

ASTM Standard G1-03. (2003). Standard Practice for Preparing, Cleaning, and Evaluating Corrosion Test Specimens. West Conshohocken, PA: ASTM International.

ASTM A1010/1018M. (2010). Standard Specification for Steel, Sheet and Strip, Heavy-Thickness Coils, Hot-Rolled,Carbon, Commercial, Drawing, Structural, High-Strength Low-Alloy, High-Strength Low-Alloy with Improved Formability, and Ultra-High Strength. West Conshohocken, PA: ASTM International.

Ayotte, J. D., Nielsen, M. G., Robinson Jr, G. R., & Moore, R. B. (1999). Relation of arsenic, iron, and manganese in ground water to aquifer type, bedrock lithogeochemistry, and land use in the New England Coastal Basins. *Water Resources Investigations Report*, *4162*, 1999.

Beech, I. B., & Sunner, J. (2004). Biocorrosion, towards understanding interactions between biofilms and metals. *Current Opinion in Biotechnology*, 15(3), 181-186.

Beliaev, A. S., & Saffarini, D. A. (1998). *Shewanella putrefaciens* mtrB encodes an outer membrane protein required for Fe (III) and Mn (IV) reduction. *Journal of Bacteriology*, 180(23), 6292-6297.

Beliaev, A. S., Saffarini, D. A., McLaughlin, J. L., & Hunnicutt, D. (2001). MtrC, an outer membrane decahaem c cytochrome required for metal reduction in *Shewanella putrefaciens* MR-1. *Molecular Microbiology*, 39(3), 722-730.

Benjamin, M. M. (2014). *Water Chemistry.* New York: McGraw-Hill.

Bird, L. J., Bonnefoy, V., & Newman, D. K. (2011). Bioenergetic challenges of microbial iron metabolisms. *Trends in Microbiology*, 19(7), 330-340.

Bitton, G. (2005). *Wasterwater Microbiology.* New Jersey, Canada: John Wiley & Sons.

Blais, J. F., Djedidi, Z., Cheikh, R. B., Tyagi, R. D., & Mercier, G. (2008). Metals precipitation from effluents. *Practice Periodical of Hazardous, Toxic, and Radioactive Waste Management*, 12(3), 135-149.

Booth, G. H., & Tiller, A. K. (1968). Cathodic characteristics of mild steel in suspensions of sulphate-reducing bacteria. *Corrosion Science*, 8(8), 583-600.

Bostic, D., Burns, G., & Harvey, S. (1992). Qualitative corrosion monitoring by on-line ion chromatography. *Journal of Chromatography A*, 602(1-2), 163-171.

Brondel, D., Edwards, R., Hayman, A., Hili, D., Mehta, S., & Semerad, T. (1994). Corrosion in the oil industry. *Oilfield Review*, 6(2), 4-18.

Bruno, J., Wersin, P., & Stumm, W. (1992). On the influence of carbonate in mineral dissolution: II. The solubility of $FeCO_{3\,(s)}$ at 25 C and 1 atm total pressure. *Geochimica et Cosmochimica Acta*, 56(3), 1149-1155.

Bruschi, R., Gentile, M., & TorsellettI, E. (2017). Sour Service Challenges. *SPE Abu Dhabi International Petroleum Exhibition & Conference* (pp. SPE-188300-MS). Abu Dhabi, UAE: Society of Petroleum Engineers.

Butterfield, C. N., Soldatova, A. V., Lee, S. W., Spiro, T. G., & Tebo, B. M. (2013). Mn (II, III) oxidation and MnO_2 mineralization by an expressed bacterial multicopper oxidase. *Proceedings of the National Academy of Sciences*, *110*(29), 11731-11735.

Byrne, R. H., & Kester, D. R. (1976). Solubility of hydrous ferric oxide and iron speciation in seawater. *Marine Chemistry*, 4(3), 255-274.

Cheetham, P. S., Blunt, K. W., & Bocke, C. (1979). Physical studies on cell immobilization using calcium alginate gels. *Biotechnology and bioengineering*, *21*(12), 2155-2168

Chemetrics. (2016). *Sulfide CHEMets kits instruction.* Midland, VA: Chemetrics Inc. .

Cohen, M. (1979). Dissolution of Iron. *Corrosion Chemistry*, 126-152.

Coursolle, D., Baron, D. B., Bond, D. R., & Gralnick, J. A. (2010). The Mtr respiratory pathway is essential for reducing flavins and electrodes in *Shewanella oneidensis*. *Journal of Bacteriology*, 192(2), 467-474.

Davison, W. (1979). Soluble inorganic ferrous complexes in natural waters. *Geochimica et Cosmochimica Acta*, 43(10), 1693-1696.

de Moraes, F., Shadley, J. R., Chen, J., & Rybicki, E. F. (2000). Characterization of CO_2 corrosion product scales related to environmental conditions. *Corrosion 2000* (pp. NACE-00030). Orlando, Florida: NACE International.

De Waard, C., & Milliams, D. E. (1975). Carbonic acid corrosion of steel. *Corrosions*, 31(5), 177-181.

DeHaven, C. D., Evans, A. M., Dai, H., & Lawton, K. A. (2010). Organization of GC/MS and LC/MS metabolomics data into chemical libraries. *Journal of Cheminformatics*, 2(1), 9.

Dinh, H. T., Kuever, J., Mußmann, M., Hassel, A. W., Stratmann, M., & Widdel, F. (2004). Iron corrosion by novel anaerobic microorganisms. *Nature*, 427(6977), 829-832.

Drever, J. I., & Stillings, L. L. (1997). The role of organic acids in mineral weathering. *Colloids and Surfaces A: Physicochemical and Engineering Aspects*, 120(1-3), 167-181.

Duckworth, O. W., & Martin, S. T. (2001). Surface complexation and dissolution of hematite by C 1-C 6 dicarboxylic acids at pH= 5.0. *Geochimica et Cosmochimica Acta*, 65(23), 4289-4301.

Duncan, K. E., & Nanny, M. A. (2015). Barnett Shale Production Water Tanks: Sequence analysis of the microbial community and characterization of the

water and metal chemistry. *University of Oklahoma Biocorrosion Center Meeting*, (pp. 14-22). Norman, OK.

Duncan, K. E., Davidova, I. A., Nunn, H. S., Stamps, B. W., Stevenson, B. S., Souquet, P. J., & Suflita, J. M. (2017). Design features of offshore oil production platforms influence their susceptibility to biocorrosion. *Applied Microbiology and Biotechnology*, 1-13.

EcoPetrol. (2014, September). EcoPetrol Data Analysisi Sept 2014. Colombia.

El-Naggar, M. Y., Wanger, G., Leung, K. M., Yuzvinsky, T. D., Southam, G., Yang, J., Laud, W. M., Nealson, K. H., Gorby, Y. A. (2010). Electrical transport along bacterial nanowires from *Shewanella oneidensis* MR-1. Proceedings of the National Academy of Sciences. *Proceedings of the National Academy of Sciences*, 107(42), 18127-18131.

Enning, D., & Garrelfs, J. (2014). Corrosion of iron by sulfate-reducing bacteria: new views of an old problem. *Applied and Environmental Microbiology*, 80(4), 1226-1236.

Enning, D., Venzlaff, H., Garrelfs, J., Dinh, H. T., Meyer, V., Mayrhofer, K. & Widdel, F. (2012). Marine sulfate-reducing bacteria cause serious corrosion of iron under electroconductive biogenic mineral crust. *Environmental microbiology*, *14*(7), 1772-1787.

Esther, J., Sukla, L. B., Pradhan, N., & Panda, S. (2015). Fe (III) reduction strategies of dissimilatory iron reducing bacteria. *Korean Journal of Chemical Engineering*, 32(1), 1-14.

Fennessey, C. M., Jones, M. E., Taillefert, M., & DiChristina, T. J. (2010). Siderophores are not involved in Fe(III) solubilization during anaerobic Fe(III) respiration by *Shewanella oneidensis* MR-1. *Applied and Environmental Microbiology*, 76(8), 2425-2432.

Fitzgerald, L. A., Petersen, E. R., Ray, R. I., Little, B. J., Cooper, C. J., Howard, E. C., Ringeisen, B. R., & Biffinger, J. C. (2012). *Shewanella oneidensis* MR-1 Msh pilin proteins are involved in extracellular electron transfer in microbial fuel cells. *Process BIochemistry*, 47(1), 170-174.

Gao, M., Pang, X., & Gao, K. (2011). The growth mechanism of CO_2 corrosion product films. *Corrosion Science*, 53(2), 557-568.

Garimella, R. (2014). *Coupon cleaning for SEM and dilution for AA protocol.* Norman, Oklahoma: University of Oklahoma.

Garimella, R. (2014). *Polishing & cleaning procedure for 1018 carbon steel circular coupon.* Norman, Oklahoma: University of Oklahoma.

Gayosso, M. H., Olivares, G. Z., Ordaz, N. R., Ramirez, C. J., Esquivel, R. G., & Viveros, A. P. (2004). Microbial consortium influence upon steel corrosion rate, using polarisation resistance and electrochemical noise techniques. *Electrochimica Acta*, 49(25), 4295-430.

Giacomelli, C., Giacomelli, F. C., Baptista, J. A., & Spinelli, A. (2004). The effect of oxalic acid on the corrosion of carbon steel. *Anti-Corrosion Methods and Materials*, 51(2), 105-111.

Gorby, Y. A., Yanina, S., McLean, J. S., Rosso, K. M., Moyles, D., Dohnalkova, A., . . . Fredrickson, J. K. (2006). Electrically conductive bacterial nanowires produced by *Shewanella oneidensis* strain MR-1 and other microorganisms. *Proceedings of the National Academy of Sciences*, 103(30), 11358-11363.

Gram, L. (1994). Siderophore-mediated iron sequestering by *Shewanella putrefaciens*. *Applied and Environmental Microbiology*, 60(6), 2132-2136.

Gui, J., & Devine, T. M. (1991). In situ vibrational spectra of the passive film on iron in buffered borate solution. *Corrosion Science*, 32(10), 1105-1124.

Haas, J. R., & Dichristina, T. J. (2002). Effects of Fe (III) chemical speciation on dissimilatory Fe (III) reduction by *Shewanella putrefaciens*. *Environmental Science & Technology*, 36(3), 373-380.

Hach. (1993). *Digital titration (Model 16900-01) manual.* Loveland, Colorado: Hach Company.

Hach. (1997). *DR/700 colorimeter procedures manual.* Loveland, Colorado: Hach Company.

Handford, R. C., & Kairuz, E. C. (2000). High-frequency sequences and stratigraphic entrapment. In C. V. Formation, *Putumayo Basin.* Colombia.

Harder, E. C. (1919). *Iron-depositing bacteria and their geologic relations.* Washington, D.C.: United States Geological Survey.

Hernandez, M. E., & Newman, D. K. (2001). Extracellular electron transfer. *Cellular and Molecular Life Sciences*, 58(11), 1562-1571.

Hider, R. C., & Kong, X. (2010). Chemistry and biology of siderophores. *Natural Product Reports*, 27(5), 637-657.

Holme, D. E., Chaudhuri, S. K., Nevin, K. P., Mehta, T., Methé, B. A., Liu, A., . . . Lovley, D. R. (2006). Microarray and genetic analysis of electron transfer to electrodes in *Geobacter sulfurreducens*. *Environmental Microbiology*, 8(10), 1805-1815.

Holmén, B. A., Sison, J. D., Nelson, D. C., & Casey, W. H. (1999). Hydroxamate siderophores, cell growth and Fe(III) cycling in two anaerobic iron oxide media containing *Geobacter metallireducens*. *Geochimica et Cosmochimica Acta*, 63(2), 227-239.

Inoue, K., Qian, X., Morgado, L., Kim, B. C., Mester, T., Izallalen, M., Salgueiro, C. A., Lovley, D. R. (2010). Purification and characterization of OmcZ, an outer-surface, octaheme c-type cytochrome essential for optimal current production by *Geobacter sulfurreducens*. *Applied and Environmental Microbiology*, 76(12), 3999-4007.

ISO Standards (ISO 8044). (2015). *Corrosion of metals and alloys- Basic terms and definitions. 2015.*

Jaekel, U., Zedelius, J., Wilkes, H., & Musat, F. (2015). Anaerobic degradation of cyclohexane by sulfate-reducing bacteria from hydrocarbon-contaminated marine sediments. *Frontiers in Microbiology*, 6.

Javaherdashti, R. (2008). *Microbiologically Influenced Corrosion: An Engineering Insight.* Springer-Verlag.

John, W. P., Rughani, J., Green, S. A., & McGinnis, G. D. (1998). Analysis and characterization of naphthenic acids by gas chromatography–electron impact mass spectrometry of tert.-butyldimethylsilyl derivatives. *Journal of Chromatography A*, 807(2), 241-251.

Kato, S. (2016). Microbial extracellular electron transfer and its relevance to iron corrosion. *Microbial Biotechnology*, 9(2), 141-148.

Keiser, J. T., Brown, C. W., & Heidersbach, R. H. (1983). Characterization of the passive film formed on weathering steels. *Corrosion Science*, 23(3), 251-259.

Kermani, M. B., & Harrop, D. (1996). The impact of corrosion on oil and gas industry. *SPE Production & Facilities*, 11(03), 186-190.

Kharaka, Y. K., Ambats, G., & Thordsen, J. J. (1993). Distribution and significance of dicarboxylic acid anions in oil field waters. *Chemical Geology*, 107(3-4), 499-501.

Kim, B. C., Qian, X., Leang, C., Coppi, M. V., & Lovley, D. R. (2006). Two putative c-type multiheme cytochromes required for the expression of OmcB, an outer membrane protein essential for optimal Fe (III) reduction in *Geobacter sulfurreducens*. *Journal of Bacteriology*, 188(8), 3138-3142.

King, R. A., & Miller, J. D. (1971). Corrosion by the sulphate-reducing bacteria. *Nature*, 233(5320), 491-492.

Kopač, J., & Bahor, M. (1999). Interaction of the technological history of a workpiece material and the machining parameters on the desired quality of the surface roughness of a product. *Journal of Materials Processing Technology*, *92*, 381-387.

Kostka, J. E., Haefele, E., Viehweger, R., & Stucki, J. W. (1999). Respiration and Dissolution of iron (III)-containing clay minerals by bacteria. *Environmental Science & Technology*, 33(18), 3127-3133.

Kotloski, N. J., & Gralnick, J. A. (2013). Flavin electron shuttles dominate extracellular electron transfer by *Shewanella oneidensis*. *American Society for Microbiology*, 4(1), e00553-12.

Kraemer, S. M. (2004). Iron oxide dissolution and solubility in the presence of siderophores. *Aquatic Sciences*, 66(1), 3-18.

Lapointe, P. A., Muhsin, M. A., & Maurin, A. F. (1991). Microbial corrosion and biologically induced new products example from a seawater injection system, Umm Shaif Field, UAE. *Middle East Oil Show* (pp. SPE-21367-MS). Bahrain: Society of Petroleum Engineers.

Leang, C., Qian, X., Mester, T., & Lovley, D. R. (2010). Alignment of the c-type cytochrome OmcS along pili of *Geobacter sulfurreducens*. *Applied and Environmental Microbiology*, 76(12), 4080-4084.

Ledyard, K. M., & Butler, A. (1997). Structure of putrebactin, a new dihydroxamate siderophore produced by *Shewanella putrefaciens*. *Journal of Biological Inorganic Chemistry*, 2(1), 93-97.

Lee, A. K., & Newman, D. K. (2003). Microbial iron respiration: impacts on corrosion processes. *Applied Microbiology and Biotechnology*, 62(2-3), 134-139.

Liang, R. (2015). Microbiologically Influenced Corrosion of Carbon Steel in Sulfidogenic Environments: The Link to Thiosulfate Reduction and Biological Stability of Alternative Fuels (Doctoral Dissertation). *University of Oklahoma*. Norman, Oklahoma.

Liang, R., Harvey, B. G., Quintana, R. L., & Suflita, J. M. (2015). Assessing the biological stability of a terpene-based advanced biofuel and its relationship to the corrosion of carbon steel. *Energy & Fuels*, 29(8), 5164-5170.

Little, B. J., Mansfeld, F. B., Arps, P. J., & Earthman, J. C. (2007). *Microbiologically influenced corrosion.* Wiley-VCH Verlag GmbH & Co. KGaA.

Liu, X., & Millero, F. J. (1999). The solubility of iron hydroxide in sodium chloride solutions. *Geochimica et Cosmochimica Acta*, 63(19), 3487-3497.

Lovley, D. R., & Phillips, E. J. (1986). Availability of ferric iron for microbial reduction in bottom sediments of the freshwater tidal Potomac River. *Applied and Environmental Microbiology*, 52(4), 751-757.

Lovley, D. R., & Phillips, E. J. (1988). Novel mode of microbial energy metabolism: organic carbon oxidation coupled to dissimilatory reduction of iron or manganese. *Applied and Environmental Microbiology*, 54(6), 1472-1480.

Lovley, D. R., & Woodward, J. C. (1996). Mechanisms for chelator stimulation of microbial Fe(III) -oxide reduction. *Chemical Geology*, 132(1-4), 19-24.

Lovley, D. R., Phillips, E. J., & Lonergan, D. J. (1991). Enzymic versus nonenzymic mechanisms for iron (III) reduction in aquatic sediments. *Environmental science & technology*, 25(6), 1062-1067.

Macalady, D. L., Langmuir, D., Grundl, T., & Elzerman, A. (1990). Use of model-generated iron($^{3+}$) ion activities to compute Eh and ferric oxyhydroxide solubilities in anaerobic systems. *ACS Symposium Series, 416*, 350-367.

Magot, M., Ravot, G., Campaignolle, X., Ollivier, B., Patel, B. K., Fardeau, M. V., . . . Crolet, J. L. (1997). *Dethiosulfovibrio peptidovorans* gen. nov., sp. nov., a new anaerobic, slightly halophilic, thiosulfate-reducing bacterium from corroding offshore oil wells. *International Journal of Systematic and Evolutionary Microbiology*, 47(3), 818-824.

Malvankar, N. S., & Lovley, D. R. (2014). Microbial nanowires for bioenergy applications. *Current Opinion in Biotechnology*, 27, 88-95.

Marsili, E., Baron, D. B., Shikhare, I. D., Coursolle, D., Gralnick, J. A., & Bond, D. R. (2008). *Shewanella* secretes flavins that mediate extracellular electron transfer. *Proceedings of the National Academy of Sciences*, 105(10), 3968-3973.

Martell, A. E., & Smith, R. M. (1974). *Critical Stability Constants* (Vol. 3). New York: Plenum Press.

Martell, A. E., Motekaitis, R. J., Chen, D., Hancock, R. D., & McManus, D. (1996). Selection of new Fe (III)/Fe (II) chelating agents as catalysts for the oxidation of hydrogen sulfide to sulfur by air. *Canadian journal of chemistry*, *74*(10), 1872-1879.

Mathiassen, O. M. (2003). CO_2 as injection gas for enhanced oil recovery and estimation of the potential on the Norwegian continental shelf. *Trondheim.* Norway.

Malvankar, N. S., & Lovley, D. R. (2012). Microbial nanowires: a new paradigm for biological electron transfer and bioelectronics. *ChemSusChem*, *5*(6), 1039-1046.

Maurice, P. A., Vierkorn, M. A., Hersman, L. E., & Fulghum, J. E. (2001). Dissolution of well and poorly ordered kaolinites by an aerobic bacterium. *Chemical Geology*, 180(1), 81-97.

McNeil, M. B., & Little, B. J. (1990). Mackinawite formation during microbial corrosion. *Corrosion*, 46(7), 599-600.

Mehta, T., Coppi, M. V., Childers, S. E., & Lovley, D. R. (2005). Mehta, T., Coppi, M. V., Childers, S. E., & Lovley, D. R. (2005). Outer membrane c-type cytochromes required for Fe (III) and Mn (IV) oxide reduction in *Geobacter sulfurreducens*. *Applied and Environmental Microbiology*, 71(12), 8634-8641.

Miller, W. P., Zelazny, L. W., & Martens, D. C. (1986). Dissolution of synthetic crystalline and noncrystalline iron oxides by organic acids. *Geoderma*, 37(1), 1-13.

Miranda, E., Bethencourt, M., Botana, F. J., Cano, M. J., Sánchez-Amaya, J. M., Corzo, A., de Lomas, J. G., Fardeau, M. L., Ollivier, B. (2006). Biocorrosion

of carbon steel alloys by an hydrogenotrophic sulfate-reducing bacterium *Desulfovibrio capillatus* isolated from a Mexican oil field separator. *Corrosion Science*, 48(9), 2417-2431.

Misawa, T., Asami, K., Hashimoto, K., & Shimodaira, S. (1974). The mechanism of atmospheric rusting and the protective amorphous rust on low alloy steel. *Corrosion Science*, 14(4), 279-28.

Mohd, M. A. (2012). *Advanced Gas Chromatography - Progress in Agricultural, Biomedical and Industrial Applications,* InTech

Mollar, M., Castro, I., Lloret, F., Julve, F., Faus, J., & Latorre, J. (1991). A solution study of complex formation between iron (III) and oxalate in dimethylsulphoxide. *Transition Metal Chemistry*, 16(1), 31-34.

Montillon, G. H. (1941). Corrosion and cathodic protection. *Journal of American Water Works Association*, 33(2), 302-308.

Munch, J. C., & Ottow, J. C. (1983). Reductive transformation mechanism of ferric oxides in hydromorphic soils. *Ecological Bulletins*, 383-394.

Myers, C. R., & Myers, J. M. (1993). Ferric reductase is associated with the membranes of anaerobically grown *Shewanella putrefaciens* MR-1. *FEMS Microbiology Letters*, 108(1), 15-22.

Myers, J. M., & Myers, C. R. (2001). Role for Outer Membrane Cytochromes OmcA and OmcB of *Shewanella putrefaciens* MR-1 in Reduction of Manganese Dioxide. *Applied and Environmental Microbiology*, 67(1), 260-269.

NACE-TM0194-2014. (2014). Field Monitoring of Bacterial Growth in Oil and Gas Systems. NACE.

Napoli, A. (1972). Complex formation of iron (III) with diglycolic and iminodiacetic acids. *Journal of Inorganic and Nuclear Chemistry*, 34(3), 987-99.

Nealson, K. H., & Saffarini, D. (1994). Iron and manganese in anaerobic respiration: environmental significance, physiology, and regulation. *Annual Reviews in Microbiology*, 48(1), 311-343.

Neilands, J. B. (1995). Siderophores: structure and function of microbial iron transport compounds. *Journal of Biological Chemistry*, 270(45), 26723-26726.

Nevin, K. P., & Lovley, D. R. (2000). Lack of production of electron-shuttling compounds or solubilization of Fe (III) during reduction of insoluble Fe (III) oxide by *Geobacter metallireducens*. *Applied and Environmental Microbiology*, 66(5), 2248-2251.

Nevin, K. P., & Lovley, D. R. (2002a). Mechanisms for Fe(III) oxide reduction in sedimentary environments. *Geomicrobiology Journal*, 19(2), 141-159.

Nevin, K. P., & Lovley, D. R. (2002b). Mechanisms of accessing insoluble Fe(III) oxide during dissimilatory Fe(III) reduction by *Geothrix fermentans*. *Applied and Environmental Microbiology*, 68(5), 2294-2299.

Newbury, D. E. (2009). Mistakes encountered during automatic peak identification of minor and trace constituents in electron-excited energy dispersive X-ray microanalysis. *Scanning*, 31(3), 91-101.

Newman, D. K., & Kolter, R. (2000). A role for excreted quinones in extracellular electron transfer. *Nature*, 405(6782), 94-97.

Obuekwe, C. O., Westlake, D. W., Cook, F. D., & Costerton, J. W. (1981). Surface changes in mild steel coupons from the action of corrosion-causing bacteria. *Applied and Environmental Microbiology*, 41(3), 766-774.

O'Connell, D. (2005). Down to the wire. *Nature Reviews Microbiology*, 3(8), 583-583.

O'Grady, W. E. (1980). Mössbauer study of the passive oxide film on iron. *Journal of the Electrochemical Society*, 127(3), 555-563.

Ogundele, G. I., & White, W. E. (1987). Observations on the influences of dissolved hydrocarbon gases and variable water chemistries on corrosion of an API-L80 steel. *Corrosion*, 43(11),665-673.

Okochi, H., & Brimblecombe, P. (2002). Potential trace metal–organic complexation in the atmosphere. *The Scientific World Journal*, (2),767-786.

Padilla-Viveros, A., Garcia-Ochoa, E., & Alazard, D. (2006). Comparative electrochemical noise study of the corrosion process of carbon steel by the

sulfate-reducing bacterium *Desulfovibrio alaskensis* under nutritionally rich and oligotrophic culture conditions. *Electrochimica Acta*, 51(18), 3841-3847.

Panias, D., Taxiarchou, M., Paspaliaris, I., & Kontopoulos, A. (1996). Mechanisms of dissolution of iron oxides in aqueous oxalic acid solutions. *Hydrometallurgy*, 42(2), 257-265.

Pankhania, I. P., Moosavi, A. N., & Hamilton, W. A. (1986). Utilization of cathodic hydrogen by *Desulfovibrio vulgaris* (Hildenborough). *Microbiology*, 132(12), 3357-3365.

Paris, R., & Desboeufs, K. V. (2013). Effect of atmospheric organic complexation on iron-bearing dust solubility. *Atmospheric Chemistry and Physics*, 13(9), 4895-4905.

Paula, M. S., Gonçalves, M. M., Rola, M. A., Maciel, D. J., Senna, L. F., & Lago, D. C. (2016). Carbon steel corrosion induced by sulphate-reducing bacteria in artificial seawater: electrochemical and morphological characterizations. *Matéria (Rio de Janeiro)*, 21(4), 987-995.

Perrin, D. D. (1959). The stability of iron complexes. Part IV. Ferric complexes with aliphatic acids. *Journal of the Chemical Society*, 1710-1717.

Pietrogrande, M. C., Bacco, D., & Mercuriali, M. (Analytical and Bioanalytical Chemistry). *Pietrogrande, M. C., Bacco, D., & Mercuriali, M. (2010). GC–MS analysis of low-molecular-weight dicarboxylic acids in atmospheric aerosol: comparison between silylation and esterification derivatization procedures.* 2010: 396(2), 877-885.

Poddar, S., & Khurana, S. (2011). *Geobacte*r: the electric microbe! efficient microbial fuel cells to generate clean, cheap electricity. *Indian Journal of Microbiology*, 51(2), 240.

Pollastro, R. M., Jarvie, D. M., Hill, R. J., & Adams, C. V. (2007). Geologic framework of the Mississippian Barnett Shale, Barnett-Paleozoic total petroleum system, Bend arch-Fort Worth Basin, Texas. *AAPG Bulletin*, 91(4), 405-436.

Popoola, L. T., Grema, A. S., Latinwo, G. K., Gutti, B., & Balogun, A. S. (2013). Corrosion problems during oil and gas production and its mitigation. *International Journal of Industrial Chemistry*, 4(1), 35.

Portanova, R., Lajunen, L. H., Tolazzi, M., & Piispanen, J. (2003). Critical evaluation of stability constants for alpha-hydroxycarboxylic acid complexes with protons and metal ions and the accompanying enthalpy changes. Part II. Aliphatic 2-hydroxycarboxylic acids (IUPAC Technical Report). *Pure and Applied Chemistry*, 75(4), 495-540.

Pourbaix, M. (1966). *Atlas of electrochemical equilibria in aqueous solutions.* New York: Pergamon.

Refait, P., Abdelmoula, M., & Génin, J. M. (1998). Mechanisms of formation and structure of green rust one in aqueous corrosion of iron in the presence of chloride ions. . *Corrosion Science*, 40(9), 1547-1560.

Reguera, G., McCarthy, K. D., Mehta, T., Nicoll, J. S., Tuominen, M. T., & Lovley, D. R. (2005). Extracellular electron transfer via microbial nanowires. *Nature*, 435(7045), 1098-1101.

Richardson, D. J., Butt, J. N., Fredrickson, J. K., Fredrickson, J. M., Shi, L., Edwards, M. J.,White, G., Baiden, N., Gates, A.J., Clarke, T. A. (2012). The 'porin–cytochrome'model for microbe-to-mineral electron transfer. *Molecular Microbiology*, 85(2), 201-212.

Roberts, L. D., Souza, A. L., Gerszten, R. E., & Clish, C. B. (2012). Targeted metabolomics. *Current Protocols in Molecular Biology*, 30-32.

Rothery, E. (1998). *Analytical Methods for Graphite Tube Atomizers.* Australia: Varian Techtron Pty. L td.

Rubim, J. C., & Dünnwald, J. (1989). Enhanced Raman scattering from passive films on silver-coated iron electrodes. *Journal of Electroanalytical Chemistry and Interfacial Electrochemistry*, 258(2), 327-344.

Rütschlin, S., Gunesch, S., & Böttcher, T. (2017). One enzyme, three metabolites: *Shewanella algae* controls siderophore production via the cellular substrate pool. *Cell Chemical Biology*, 24(5), 598-604.

Schmitt, G. H., & Horstemeier, M. (2006). Fundamental aspects of CO_2 metal loss corrosion - Part II: influence of different parameters on CO_2 corrosion mechanisms. *Corrosion 2006* (pp. NACE-06112). San Diego, California: NACE International.

Schwenk, W. (1974). Korrosion von unlegiertem Stahl in sauerstoffreier Kohlensäurelösung. *Materials and Corrosion*, 25(9), 643-646.

Scott, D. T., McKnight, D. M., Blunt-Harris, E. L., Kolesar, S. E., & Lovley, D. R. (1998). Quinone moieties act as electron acceptors in the reduction of humic substances by humics-reducing microorganisms. *Environmental Science & Technology*, 32(19), 2984-2989.

Shi, L., Squier, T. C., Zachara, J. M., & Fredrickson, J. K. (2007). Respiration of metal (hydr) oxides by *Shewanella* and *Geobacter*: a key role for multihaem c-type cytochromes. *Molecular Microbiology*, *65*(1), 12-20.

Simons, M. R. (2008). Report of offshore technology conference presentation. *NACE International oil and gas production*.

Singer, P. C., & Stumm, W. (1970). The solubility of ferrous iron in carbonate-bearing waters. *Journal of American Water Works Association*, 6(2),198-202.

Snoeyink, V. L., & Jenkins, D. (1980). *Water Chemistry.* New York, N.Y.: John Wiley & Sons.

Soe, C. Z., Telfer, T. J., Levina, A., Lay, P. A., & Codd, R. (2016). Simultaneous biosynthesis of putrebactin, avaroferrin and bisucaberin by *Shewanella putrefaciens* and characterisation of complexes with iron(III), molybdenum(VI) or chromium(V). *Journal of Inorganic Biochemistry*, 162, 207-215.

Spruit, C. J., & Wanklyn, J. N. (1952). Iron sulphide ratios in corrosion by sulphate-reducing bacteria. *Nature*, 168(4283), 951-952.

Stams, A. J., De Bok, F. A., Plugge, C. M., Eekert, V., Miriam, H. A., Dolfing, J., & Schraa, G. (2006). Potential for nonenzymatic reduction of Fe(III) via electron shuttling in subsurface sediments. *Environmental Microbiology*, 8(3), 371-382.

Starosvetsky, J. (2016). Rust dissolution and removal by iron-reducing bacteria: A potential rehabilitation of rusted equipment. *Corrosion Science*, 446-454.

Stefánsson, A. (2007). Iron(III) Hydrolysis and Solubility at 25 °C. *Environmental Science & Technology*, 41(17), 6117-6123.

Stumm, W., & Lee, G. F. (1961). Oxygenation of ferrous iron. *Industrial & Engineering Chemistry*, 53(2), 143-146.

Morgan, J. J., & Stumm, W. (1970). *Aquatic chemistry*. Wiley-interscience, New York.

Swain, H. A., Lee, C., & Rozelle, R. B. (1975). Determination of the solubility of manganese hydroxide and manganese dioxide at 25. deg. by atomic absorption spectrometry. *Analytical Chemistry*, *47*(7), 1135-113

Tawancy, H. M., Al-Hadhrami, L. M., & Al-Yousef, F. K. (2013). Analysis of corroded elbow section of carbon steel piping system of an oil–gas separator vessel. *Case Studies in Engineering Failure Analysis*, 1(1), 6-14.

Thamdrup, B. (2000). Bacterial manganese and iron reduction in aquatic sediments. *Advances in microbial ecology,* 41-84

Thomas, S. (2008). Enhanced oil recovery-an overview. *Oil & Gas Science and Technology-Revue de l'IFP*, 63(1), 9-19.

Thrasher, J., & Fleet, A. J. (1995). Predicting the risk of carbon dioxide pollution in petroleum reservoirs. *Organic Geochemistry: Developments and Applications to Energy, Climate, Environment and Human History, Proceedings of the 17th International Meeting on Organic Geochemistry*, (pp. 1086-1088). San Sebastian, Spain.

TM0194-94. (1994). *Field Monitoring of Bacterial Growth in Oilfield Systems.* Houston: NACE Standard.

Tremblay, P. L., Aklujkar, M., Leang, C., Nevin,, K. P., & Lovley, D. R. (2012). A genetic system for *Geobacter metallireducens*: role of the flagellin and pilin in the reduction of Fe (III) oxide. *Environmental Microbiology Reports*, 4(1), 82-8.

Trolard, F., & Tardy, Y. (1987). The stabilities of gibbsite, boehmite, aluminous goethites and aluminous hematites in bauxites, ferricretes and laterites as a function of water activity, temperature and particle size. *Geochimica et Cosmochimica Acta*, 51(4), 945-957.

Turick, C. E., Tisa, L. S., & Caccavo, J. F. (2002). Melanin production and use as a soluble electron shuttle for Fe (III) oxide reduction and as a terminal electron acceptor by *Shewanella algae* BrY. *Applied and Environmental Microbiology*, 68(5), 2436-2444.

Uhlig, H. H. (1947). Fundamental factors in corrosion control. *Corrosion*, 3(4), 173-184.

Ulrich, G. A., Krumholz, L. R., & Suflita, J. N. (1997). A rapid and simple method for estimating sulfate reduction activity and quantifying inorganic sulfides. *Applied and Environmental Microbiology*, 63(4), 1627-1630.

van Nuland, Y. M., de Vogel, F. A., Scott, E. L., Eggink, G., & Weusthuis, R. A. (2017). Biocatalytic, one-pot dterminal oxidation and esterification of n-alkanes for production of α, ω-diol and α, ω-dicarboxylic acid esters. *Metabolic Engineering*, (44),134-142.

Videla, H. A., Le Borgne, S., Panter, C., & Singh Raman, R. K. (2008). MIC of steels by iron reducing bacteria. *Corrosion 2008* (pp. NACE-08505). New Orleans, Louisiana: NACE International.

Villarreal, J., Laverde, D., & Fuentes, C. (2006). Carbon-steel corrosion in multiphase slug flow and CO_2. *Corrosion Science*, 2363-2379.

Von Canstein, H., Ogawa, J., Shimizu, S., & Lloyd, J. R. (2008). Secretion of flavins by *Shewanella* species and their role in extracellular electron transfer. *Applied and Environmental Microbiology*, 74(3), 615-623.

von Wolzogen Kühr, C. A., & van der Vlugt, L. S. (1934). Graphication of cast iron as an electrochemical process in anaerobic. *Water*, 18, 147-165.

Wang, H., & Liang, C. (2007). Effect of sulfate reduced bacterium on corrosion behavior of 10CrMoAl steel. *Journal of Iron and Steel Research, International*, 14(1), 74-78.

Wang, W., Wang, J., Xu, H., & Li, X. (2006). Electrochemical techniques used in MIC studies. *Materials and Corrosion*, 57(10), 800-804.

Wang, Z., Fu, H., Zhang, L., Song, W., & Chen, J. (2017). Ligand-promoted photoreductive dissolution of goethite by atmospheric low-molecular dicarboxylates. *The Journal of Physical Chemistry A*, 121(8), 1647-1656.

Westall, J. C. (1976). *MINEQL: A computer program for the calculation of chemical equilibrium composition of aqueous.* Cambridge, MA: MIT.

Westbrook, A. M., & Nanny, M. A. (2013). *Characterization of Polar Organic Acids and Alcohols Extracted from Four Petroleum Process Water Samples from the Putumayo Oil Field, Colombia, South America.* Norman, Oklahoma: University of Oklahoma.

Wingender, J., Neu, T. R., & Flemming, H. C. (1999). *Microbial extracellular polymeric substances.* Berlin, Germany: Springer-Verlag Berlin Heidelberg.

Winkelmann, G. (1997). *Transition metals in microbial metabolism.* CRC Press.

Wranglen, G. (1974). Pitting and sulphide inclusions in steel. *Corrosion Science*, 14(5), 331-349.

Yamashita, M., Miyuki, H., Matsuda, Y., Nagano, H., & Misawa, T. (1994). The long term growth of the protective rust layer formed on weathering steel by atmospheric corrosion during a quarter of a century. *Corrosion Science*, 36(2), 283-299.

Yamashita, M., Miyuki, H., Nagano, H., & Misawa, T. (1994). Stabilizing process of rust layer formed on weathering steels by atmospheric corrosion for a long period. *Zairyo-to-Kankyo*, 43(1), 26-32.

Yang, L. (2013). *Scanning electron microscopy.* Weinheim, Germany: John Wiley & Sons, Inc.

Yumoto, H., Nagamine, Y., Nagahama, J., & Shimotomai, M. (2002). Corrosion and stability of cementite films prepared by electron shower. *Vacuum*, *65*(3-4), 527-531.

Zhang, J., Xue, Q., Gao, H., Lai, H., & Wang, P. (2016). Zhang, J., Xue, Q., Gao, H., Lai, H., & Wang, P. (2016). Bacterial degradation of crude oil using solid formulations of Bacillus strains isolated from oil-contaminated soil towards microbial enhanced oil recovery application. *RSC Advances*, 6(7), 5566-5574.

Zheng, Y., Brown, B., & Nešić, S. (2013). Electrochemical study and modeling of H_2S corrosion of mild steel. *Corrosion*, 70(4), 351-365.